Towards understanding the mechanisms of allostery: the investigation of the relationship between dynamics, structure and function in the model allosteric protein CheY

Leanna Rose McDonald

A dissertation submitted to the faculty of the University of North Carolina at Chapel Hill in partial fulfillment of the requirements for the degree of Doctor of Philosophy in the Department of Biochemistry and Biophysics

Chapel Hill
2013

Approved by:

Andrew Lee

Sharon Campbell

Robert Bourret

Brian Kuhlman

Edward Collins

ABSTRACT

LEANNA ROSE MCDONALD: Towards understanding the mechanisms of allostery: the investigation of the relationship between dynamics, structure and function in the model allosteric protein CheY
(Under the direction of Andrew Lee)

Allosteric proteins are extremely important in signaling, yet the mechanism(s) of the switch between inactive and active conformations is not clearly understood. It is now widely recognized that dynamics are important to consider for understanding allosteric protein function. *Escherichia coli* CheY, a response regulator protein from the two-component signal transduction system that regulates bacterial chemotaxis, is an ideal protein for the study of allosteric mechanisms. Here, we report an NMR relaxation study of dynamics over multiple timescales at both backbone and side-chain sites upon an allosteric response to phosphorylation. By utilizing ^{15}N CPMG relaxation dispersion experiments, we monitored the inherent dynamic switching of unphosphorylated CheY. We show that unphosphorylated CheY does *not* undergo a two-state concerted switch between the inactive and active conformations. Interestingly, partial saturation of Mg^{2+} enhances the intrinsic allosteric motions. Taken together with chemical shift perturbations, these data indicate that the μs-ms timescale motions underlying CheY allostery are segmental in nature. Upon phosphorylation, CheY allosterically responds with a change in dynamics on both the μs-ms and ps-ns timescale. We observe an apparent decrease and redistribution of μs-ms dynamics upon phosphorylation of CheY. Additionally, methyl groups with the largest changes in ps-ns dynamics localize to the regions of conformational change measured by μs-ms dynamics. The limited spread of changes in ps-ns dynamics suggests a distinct

relationship between motions on the μs-ms and ps-ns timescales in CheY. Analysis of an activating mutant A113P yields a similar pattern of side-chain ps-ns dynamic changes as upon phosphorylation. This relationship between an activating mutant and an activating pattern of dynamic changes is further evidence for a distinct relationship between the dynamics on multiple timescales and the function of the protein. The allosteric mechanism utilized by CheY highlights the diversity of roles dynamics play in protein function and the complex mechanisms proteins utilize for allostery.

For my parents, who showed me nothing could stand in the way of getting where I love.

For my husband, who joined me on the journey and made it remarkable.

ACKNOWLEDGEMENTS

This work would not have been possible without the support and encouragement from a large number of people. First I would like to thank my advisor, Andrew Lee for giving me the opportunity to train in his lab. His constant teaching and enthusiasm continuously developed me into a better scientist. Additionally, the members of the Lee lab, past and present have been there over the years offering their support, friendship, and providing an environment that allowed me to grow into the scientist I am today. Josh, Matthew, Chad, Tony, Randy, Mary, Jun, Tina, and Paul each have made significant contributions that have meant the world to me.

I would not be here had I not spent a summer working in Kevin Gardner's lab as an undergraduate. The spark lit that summer has only burned brighter. I also need to thank Barry Lentz who not only allowed me to study in the biophysics program, but covered my stipend with the biophysics training grant for two years.

I would like to thank my committee members, Drs. Sharon Campbell, Brian Kuhlman, Bob Bourret and Ed Collins for their always insightful comments and suggestions at each year's meeting. A special thanks to Bob Bourret and his lab including Ruth Silversmith and Bob Immormino for always being available to discuss CheY. Karl Koshlap and Greg Young were a tremendous help throughout the years giving technical NMR help. Thank you to Qi Zhang and Jan Hermans for their insightful comments and suggestions.

Finally I would like to thank my family and friends who have been there along the way, however incomprehensible this work is to them. My parents always pushed me to do my best and to figure out my passion. Their unending encouragement gave me the courage to follow this road. And for my husband, who moved across the country and has never blinked an eye at this crazy journey we've been on. For his unending support and enthusiasm I will forever be thankful.

TABLE OF CONTENTS

LIST OF TABLES

LIST OF FIGURES

LIST OF ABBREVIATIONS AND SYMBOLS

A	active conformation
A113P-P	phosphorylated A113P CheY; typically BeF_x-bound CheY
A113P-unP	unphosphorylated A113P CheY
AIC	Akiake information criteria
BIC	Bayesian information criteria
CheA	Chemotaxis protein A; histidine kinase
CheY	Chemotaxis protein Y; response regulator
CheY-P	phosphorylated CheY; typically BeF_x-bound CheY
CheY-unP	unphosphorylated CheY
CheZ	Chemotaxis protein Z; phosphatase
$\chi 1$	first side-chain torsion angle
$\chi 2$	measure of goodness of fit
CSA	chemical shift anisotropy
CPMG	Carr-Purcell-Meiboom-Gill
DHFR	dihydrofolate reductase
D_y	quadrupolar transverse relaxation
D_z	quadrupolar longitudinal relaxation
$\Delta\delta$	difference in chemical shift
FliM	flagellar mtor protein; CheY's target binding partner
GdnHCl	Guanidinium hydrochloride
HSQC	heteronuclear single quantum coherence
HX	hydrogen exchange
I	inactive conformations
KNF	Koshland-Nemethy-Filmer

μs-ms	microsecond to millisecond
MWC	Monod-Wyman-Changeux
NMR	nuclear magnetic resonance
NtrC	nitrogen regulatory protein C
NOE	nuclear Overhauser enhancement
PDB	Protein Data Bank
ps-ns	picosecond to nanosecond
R_1	spin-lattice (longitudinal) relaxation
R_2	spin-spin (transverse) relaxation
R_{ex}	transverse relaxation due to conformational exchange
$R_{2,eff}$	effective R_2
R_2^0	intrinsic R_2
rms	root mean square
RR	response regulator
S^2	order parameter
S^2_{axis}	order parameter of the methyl symmetry axis
τ_e	effective internal correlation time
$\tau_{e,axis}$	effective internal correlation time of the methyl symmetry axis
τ_{cp}	time between consecutive refocusing pulses in a CPMG train
τ_m	rotational correlation time
WT	wild type

CHAPTER 1

INTRODUCTION

1.1 Background

1.1.1 Overview of Protein Allostery

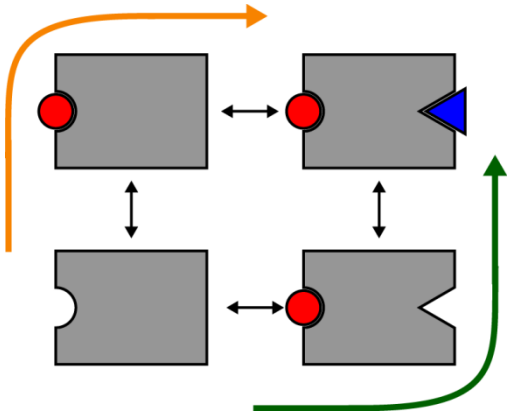

Figure 1.1. Allosteric conformational change by multiple mechanisms. The pathway for KNF and MWC allosteric conformational change is indicated by the orange and green arrows, respectively.

Reliable and efficient molecular signaling is an essential function for cellular survival. Signal propagation requires translation and transmission of a signal event into the correct response. In many cases, the signal event is allosteric: a signaling protein receives a signal at a distal effector site that is transmitted to a second site via long-range intramolecular communication. Allostery typically occurs by an initial perturbation to a protein such as ligand binding or chemical modification which usually causes a change in the conformation and leads to a change in function (e.g. catalytic efficiency or binding affinity) at a distal site.

Despite the widespread nature and crucial function of allostery, the mechanisms by which the long-range communication occur are still not well understood. Classically,

allostery has been described by two competing theories in which both have been shown to be accurate descriptions in separate specific cases. In the Koshland-Nemethy-Filmer (KNF) model, a conformational change only occurs upon the initial perturbation in an induced-fit manner (Figure 1.1, orange arrow).[1] Conversely, in the Monod-Wyman-Changeux (MWC) model, the protein exists as an equilibrium of conformations in which allosteric perturbation selects a new major conformation in a population shift manner (Figure 1.1, green arrow).[2] Furthermore, the KNF model typically describes a sequential pathway between effector and allosteric sites while the MWC model is linked to a concerted conformational change. Recent studies of allosteric proteins have started to support mechanisms which have aspects of both the KNF and MWC model.[3-5] This mixed mechanism has been described as an asynchronous population shift for trp RNA-binding attenuation protein (TRAP)[3], a "molecular slide bearing" which allows a range of conformational states in hemoglobin[4], and conformational spread in the FliM ring of the flagellar motor.[5]

1.1.2 Dynamics as a basis for protein function

Understanding allostery at the molecular level continues to be a challenge. The study of allosteric protein function has been dominated by the use of x-ray crystallography and therefore has been limited to the static structures of proteins. These structures mostly give only time-averaged information about a protein, effectively yielding a "snapshot". However, in general, proteins are not static molecules and this is especially true for allosteric molecules that dynamically switch between conformations. Therefore, together with the static structural information, dynamics data should give valuable insights into the function of proteins.

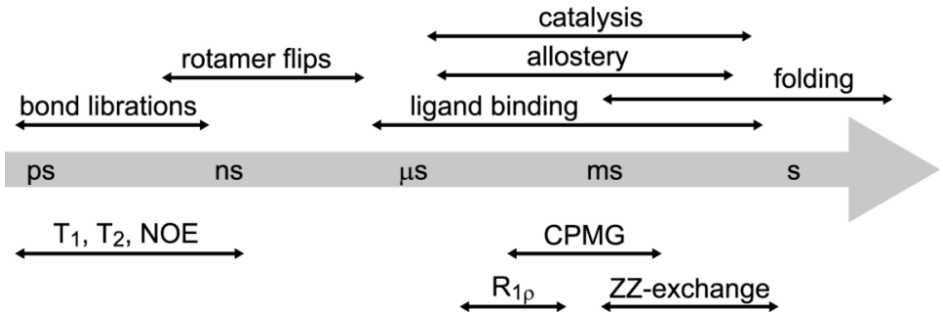

Figure 1.2. Common protein motions and NMR experiments to measure dynamics.

Proteins undergo dynamics over a range of timescales (Figure 1.2), ranging from faster than picoseconds to slower than a second. The motions over every timescale can contribute to a protein's function. The fastest motions are bond vibrations and librations, and these dynamics are considered to have a large contribution to the entropy of the system.[6-10] Motions on a slower timescale (microsecond-millisecond; μs-ms) are those involving conformational change (e.g. caused by allosteric signaling), ligand binding, and catalysis.[11, 12] The slowest motions are typically due to large scale conformational changes such as domain motions and folding/unfolding.

It has been shown that entropic changes to the protein measured by changes in motions on the ps-ns timescale can cause a change in the function of the protein.[6, 13, 14] The thermodynamics of every process in a protein is made up of two components: enthalpic and entropic. While the enthalpic contribution is usually straightforward to calculate, the entropic contribution is a challenge and difficult to predict. However, conformational entropy can be measured by NMR techniques[7-9] (described below) and has been shown to contribute to ligand binding for calmodulin[6], catabolite activator protein[14], and a pdz domain.[13]

Conformational changes in a protein occur on a slower, μs-ms timescale. These dynamics, often related to a protein's function, have been monitored for a number of

proteins. For example, the conformations and dynamics of the enzyme dihydrofolate reductase (DHFR) have been well studied.[15-18] Wright and coworkers have monitored the switching between the ground and excited state for every step in the catalytic cycle.[15, 16] The conformational switching directly correlates with the kinetics measured by other methods. DHFR is only a single example of the numerous proteins that have dynamics on this timescale essential for their function. Specifically, a few allosteric proteins have studies utilizing NMR techniques to monitor dynamics at atomic level resolution including catabolite activator protein[19], the KIX domain of the CREB binding protein[20], and the PBX1 homeodomain[21].

1.2 CheY as a Model System

1.2.1 Overview of CheY Function

We have chosen the chemotaxis signaling protein CheY for use as a model protein for the study of structural dynamics in allostery. CheY is a response regulator (RR) of a two-component signal transduction system that regulates chemotaxis in *Escherichia coli*.[22, 23] Upon phosphorylation at D57[24], CheY has an increased affinity for the flagellar motor protein, FliM (Figure 1.3). These two events occur at a significant distance making this signaling event classically allosteric.

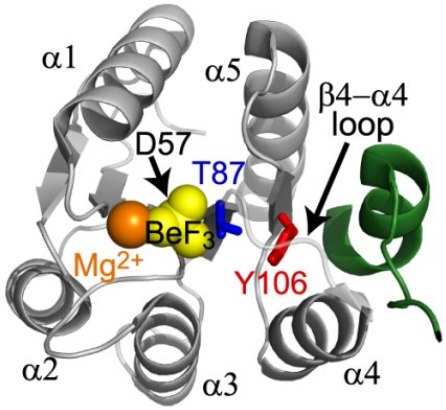

Figure 1.3. Crystal structure of active CheY. BeF_x (phosphoryl mimic, yellow)-bound at the site of phosphorylation, D57 and FliM peptide (green)-bound CheY.

Two component systems are prevalent in bacteria and comprise an RR and a sensor kinase. The majority of RRs include both a receiver domain, which contains the site of phosphorylation, and an output domain which contains the target binding site or catalytic region.[25, 26] CheY is a RR that is only a single domain homologous to the receiver domains. It is phosphorylated by the histidine kinase, CheA which induces a conformational change and enables CheY to bind the flagellar motor protein FliM.[27] The binding of CheY to the flagellar motor causes conformational changes throughout the motor and results in a switch in the flagellar rotation from counterclockwise to clockwise.[28]

CheY is an important protein in the signaling of *E. coli* chemotaxis, which allows the bacteria to sense and respond to changes in the chemical environment.[29] Through this signaling pathway a bacterium is able to move towards an attractant or away from a repellent. Counterclockwise flagellar rotation results in the bacteria's ability to swim smoothly while clockwise flagellar rotation causes tumbling behavior. Tumbling allows the bacterium to randomly reorient before switching to smooth swimming. For example, reorientation towards an attractant will cause an increase in phosphorylated CheY resulting in a higher likelihood

to continue counterclockwise rotation and therefore smooth swimming. The signaling cascade begins with a receptor sensing the external environment and causing an increase in phosphorylated CheA. CheA then phosphorylates CheY which binds the flagellar motor. The flagellar motor is composed of numerous proteins in a large complex. The portion protruding furthest in the intracellular direction is the C-ring, composed of 35 FliM, 140 FliN, and 25 FliG molecules. The main interaction of CheY is with FliM, but FliN has been shown to have lesser interactions.[30] Binding of CheY to FliM is thought to disrupt FliM's interaction with FliG and cause an important conformational transition to switch flagellar rotation.[31] The ability of a cell to quickly signal to change direction is extremely important. It is for this reason that CheY has a rapid autodephosphorylation rate of 2.5 min^{-1}.[32] This means it is difficult to study the phosphorylated state and it has become common to utilize BeFx as a phosphoryl mimic.[27, 33-35] Lastly, CheY can also be dephosphorylated by the phosphatase CheZ. For both phosphorylation and dephosphorylation, the presence of Mg^{2+} is required.[36]

Upon phosphorylation at D57, CheY undergoes a conformational change which allows binding to FliM.[27] The largest regions of change in the backbone localize to the β4-α4 and β5-α5 loops (Figure 1.4). The β4-α4 loop moves in an "upward" manner to create space for the rotation of Y106 to an inward position. This rotation of Y106 is an extremely important switch to the binding-competent conformation since Y106 sterically hinders the binding of FliM when in the "out" position. It has been proposed that the β4-α4 loop motions are coupled with rotation of Y106 to enable the conformational switch.[37, 38] A second proposed mechanism of allosteric conformational switch in CheY is the "Y-T coupling mechanism" in which the signal from the site of phosphorylation is propagated through T87 to Y106 as the central switching in the protein.[27] The conformational switch also includes a

number of changes in side-chain positioning and rotation noted by comparing the respective crystal structures including K109, F14, E89, W58, and others.

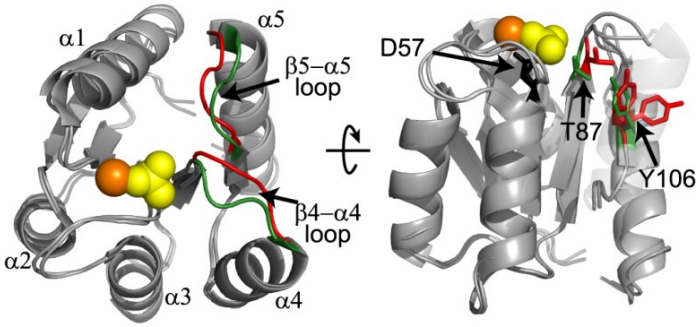

Figure 1.4. Conformational change upon phosphorylation in CheY. Overlay of apo-CheY (red) and phosphoryl mimic BeF_x-bound CheY (green).

1.2.2 Using CheY as a Model Allosteric Protein

Response regulator receiver domains have been widely studied for their role in two-component signal transduction systems in bacteria. Because of this breadth of knowledge and their small size, they have become a popular structural and dynamical model for the study of protein allostery. The receiver domain from nitrogen regulator protein C (NtrC) has been shown to display a two-state dynamic equilibrium between inactive and active conformations with a proposed allosteric mechanism in line with the MWC model.[39, 40] NtrC, like CheY, becomes phosphorylated in its receiver domain, but unlike CheY, its signaling pathway is complicated by the necessity of NtrC to form a homodimer (and subsequent hexamer) and signal to its output domains. The studies on NtrC have played a major role in forming the current paradigm for understanding the allosteric mechanisms in RRs. However, study of a simpler system such as CheY could lead to large insights not available through study of NtrC.

Other than the comparison to NtrC, currently the allosteric mechanism in CheY is understood through inspections of its conformation by x-ray crystallography and mutational and biochemical characterization. CheY is thought to exist in a pre-existing equilibrium in the unphosphorylated state between the binding-incompetent (inactive; I) and binding competent (active; A) conformations. The ability of unphosphorylated CheY to reach the active conformation is supported by CheY's ability to bind FliM in the absence of phosphorylation[41] and Y106 found both in the solvent exposed and buried conformations[42] in the unphosphorylated crystal structure (Figure 1.4). Additionally, binding of FliM, CheA, and CheZ to CheY affect its auotphosphorylation rate which is hypothesized to be caused by a shift in the equilibrium between I and A.[43] Together these data suggest a simple two-state population shift mechanism for the allosteric conformational change in CheY. However, recent results have complicated this simple idea. The crystal structure of FliM bound to the unphosphorylated CheY reveals an intermediate CheY conformation.[44] Some single site mutations in CheY also yield a conformation not corresponding with either I or A.[37, 45] Additionally, molecular dynamics simulations suggest that Y106 rotamer orientation and the formation of a hydrogen bond between T87 and the phosphoryl group are independent of one another.[38] This suggests that CheY is able to access multiple conformations, not just I and A. Therefore, the simple two-state switch between I and A may not be as straightforward as previously thought.

1.3 Methods for Measuring Protein Dynamics

1.3.1 Spin Relaxation and Molecular Dynamics

Fundamental to nuclear magnetic resonance (NMR) spectroscopy is the perturbation of a nuclear spin away from the ground state by a radio frequency pulse. Subsequently, the nuclear spin seeks to return to equilibrium. The rate of spontaneous transition back to the ground state is very slow and therefore these transitions rely on external stimulation. It is this key fact that connects spin relaxation to molecular dynamics; motions at specific frequency are responsible for the relaxation of excited spin states.

The NMR-active nuclei for which spin relaxation is typically measured in biomolecules are ^{15}N, ^{13}C and ^{2}H. For these, there are two main mechanisms by which relaxation is induced: dipole-dipole interactions and chemical shift anisotropy (CSA). The dipole-dipole mechanism results from the reorientation of a bond vector in relation to the static magnetic field. If the reorientation is at the appropriate frequency, relaxation will occur. The second mechanism, CSA, results from the fluctuations in the spatially oriented shielding of a nuclei. Both mechanisms have contributions from overall molecular tumbling and/or local fluctuations of a molecule.

In this work, we measure ^{15}N and ^{2}H relaxation rates, which are for the measure of backbone and methyl side-chain protein dynamics, respectively. For the backbone, spin-lattice (longitudinal) relaxation (R_1), spin-spin (transverse) relaxation (R_2) with the addition of the ^{1}H-^{15}N nuclear Overhauser enhancement (NOE) are measured utilizing a heteronuclear single quantum coherence (HSQC) type experiment. Similarly, for the side-chains, we measure quadrupolar transverse relaxation (D_y) and quadrupolar longitudinal relaxation (D_z).

The connection between spin relaxation and molecular motions are clear and their relationship is described by the spectral density function, J(ω). The spectral density function describes the probability to excite transitions at a certain frequency, ω, or more precisely, the density of fluctuation for that ω for a given bond vector. If we assume a rigid molecule tumbling isotropically, the spectral density is expressed as

$$J(\omega) = \frac{\tau_m}{1+\omega^2\tau_m^2}, \quad (1.1)$$

where τ_m is the characteristic global tumbling time for the molecule. The faster a protein tumbles in solution, the wider the frequency range available to relax the excited nucleus. Since we know molecules are not completely rigid, we must use a more complex spectral density function and the most common is the Lipari-Szabo "model free" formalism.[46, 47] Model-free only assumes that $\tau_m >> \tau_e$, in which τ_e is the effective internal correlation time, and the internal and global motions are independent of one another. The model-free spectral density is

$$J(\omega) = \frac{2}{5}\left(\frac{S^2\tau_m}{1+\omega^2\tau_m^2} - \frac{(1-S^2)\tau_m}{1+\omega^2\tau_e^2}\right) \quad (1.2)$$

where S^2 is the amplitude of local fluctuations called the order parameter. The value of S^2 can vary between 0, no spatial preference and 1, completely rigid. This function can be modified to account for transverse relaxation due to chemical exchange (R_{ex}) and internal motions occurring on two different timescales (S^2_f and S^2_s, fast and slow, respectively).

1.3.2 Characterizing ps-ns backbone dynamics using ^{15}N relaxation

Motions of the protein backbone on the ps-ns timescale are monitored by measuring ^{15}N relaxation rates (Figure 1.2) which account for the ^{15}N-^{1}H amide bond vector. As mentioned above, to get a full picture of the dynamics more than one relaxation rate must be

measured. The three ^{15}N relaxation parameters (R_1, R_2, and $\{^1H\}$-^{15}N NOE) can be written in terms of the spectral density function:

$$R_1 = d^2[J(\omega_H - \omega_N) + 3J(\omega_N) + 6J(\omega_H + \omega_N)] + c^2 J(\omega_N)$$

$$R_2 = \frac{d^2}{2}[4J(0) + J(\omega_H - \omega_N) + 3J(\omega_N) + 6J(\omega_H) + 6J(\omega_H + \omega_N)] + \frac{c^2}{6}[3J(\omega_N) + 4J(0)] + R_{ex} \quad (1.3)$$

$$NOE = 1 + (\gamma_H/\gamma_N)d^2[6J(\omega_H + \omega_N) - J(\omega_H - \omega_N)]\frac{1}{R_1}$$

where $d^2 = \frac{1}{10}\gamma_N^2\gamma_H^2\hbar^2\langle 1/r_{NH}^3\rangle^2$ and $c^2 = \frac{2}{15}\gamma_N^2 H_0^2 \Delta\sigma^2$ which are the strength of the dipole interaction and a scaling factor related to including the contribution of CSA, respectively; γ_x is the gyromagnetic ratio for x, r_{NH}^3 is the N-H bond distance, H_0 is the strength of the static magnetic field, and $\Delta\sigma$ is the anisotropy of the ^{15}N chemical shift tensor. Backbone dynamics parameters are calculated by a search for a minimal difference between experimental and theoretical relaxation values. The backbone is generally very rigid with S^2 values between 0.8 and 0.9 with lower values often observed in long loops or termini (Figure 1.5, black circles).

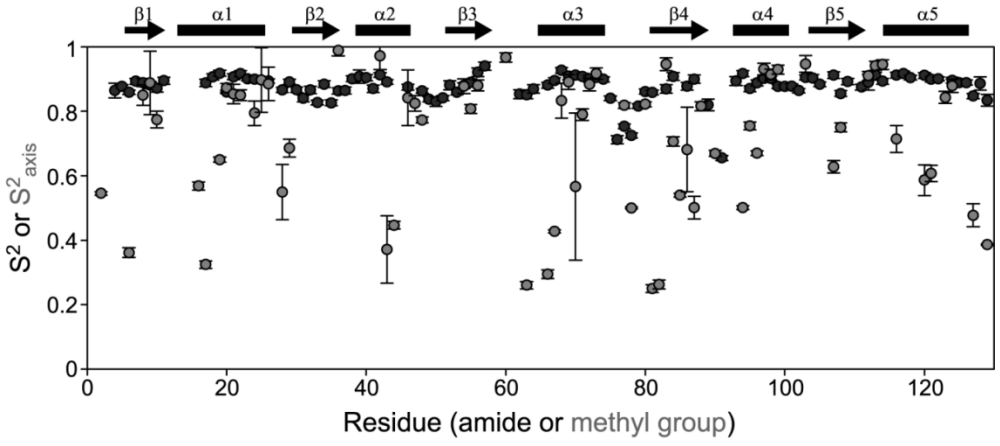

Figure 1.5. Order parameter comparison for backbone and side chains. S^2 (black) and S^2_{axis} (grey) are displayed for unphosphorylated CheY.

1.3.3 Characterizing ps-ns side-chain dynamics using ^2H relaxation

To measure dynamics of side-chain methyl groups, ^2H relaxation of CH_2D groups are made. D_z (longitudinal) and D_y (transverse) relaxation rates are given by

$$D_z = \frac{3}{16}\left(\frac{e^2qQ}{\hbar^2}[J(\omega_D) + 4J(2\omega_D)]\right)$$
$$D_y = \frac{1}{32}\left(\frac{e^2qQ}{\hbar^2}[9J(0) + 15J(\omega_D) + 6J(2\omega_D)]\right), \quad (1.4)$$

where e^2qQ is the quadrupolar coupling constant. Measurement of the D_y and D_z relaxation rates is possible for the lone ^2H of the $^{13}CH_2D$ isotopomer. Knowledge of these rates allow dynamics parameters of the methyl symmetry axis to be obtained: S^2_{axis} and $\tau_{e,axis}$. The meaning of these parameters and the fitting is the same as for the backbone. These experiments are only able to characterize terminal methyl groups and therefore, are limited in which amino acids can be measured. In contrast to the backbone, side-chains have a much larger range of order parameter values (Figure 1.5, grey circles) and are very sensitive to perturbation of the protein.

1.3.4 Characterizing μs-ms backbone dynamics using ^{15}N relaxation dispersion

The previous experiments characterize motions on the ps-ns timescale, however slower motions are often critical for protein function. The R_2 relaxation is a combination of the intrinsic relaxation rate R_2^0 and the relaxation due to exchange:

$$R_2 = R_2^0 + R_{ex}. \quad (1.5)$$

While there are multiple experiments designed for the measure of slower timescale motions in proteins such as ZZ-exchange and $R_{1\rho}$, here we use Carr-Purcell-Meiboom-Gill (CPMG) relaxation dispersion experiments (Figure 1.2).[48] These experiments monitor chemical

exchange on the μs-ms timescale by utilizing HSQC-based experiments. By varying the spacing between 180° pulses (τ_{cp}) in the CPMG pulse train, we are to monitor the effect on peak intensity by the dephasing of nuclear magnetization during this period caused by chemical exchange. For a given τ_{cp}, the effective R_2 ($R_{2,\text{eff}}$) can be calculated by

$$R_{2,eff} = -\frac{1}{T}\ln\frac{I}{I_0}$$

where I and I_0 are the peak intensity with and without the CPMG period, respectively and T is the total time of the relaxation period which is kept constant.

In the simplest case, exchange occurs between two states:

$$A \underset{k_{-1}}{\overset{k_1}{\rightleftharpoons}} B. \tag{1.6}$$

Assuming this simple case, $R_{2,\text{eff}}$ is dependent on τ_{cp} according to the Carver-Richards equation to relate R_{ex} to the kinetic and thermodynamic properties of the chemical exchange:

$$R_{2.eff}(1/\tau_{cp}) = \frac{1}{2}\left(R_{2A}^0 + R_{2B}^0 + k_{ex} - \frac{1}{\tau_{cp}}\cosh^{-1}[D_+\cosh(\eta_+) - D_-\cosh(\eta_-)]\right)$$

$$D_\pm = \frac{1}{2}\left[\pm 1 + \frac{\Psi + 2\Delta\omega^2}{(\Psi^2 + \zeta^2)^{1/2}}\right]$$

$$\eta_\pm = \frac{\tau_{cp}}{\sqrt{2}}\left[\pm\Psi + (\Psi^2 + \zeta^2)^{1/2}\right]^{1/2} \tag{1.7}$$

$$\Psi = (R_{2A}^0 - R_{2B}^0 - p_A k_{ex} + p_B k_{ex})^2 - \Delta\omega^2 + 4p_A p_B k_{ex}^2$$

$$\zeta = 2\Delta\omega(R_{2A}^0 - R_{2B}^0 - p_A k_{ex} + p_B k_{ex})$$

where k_{ex} is the exchange rate ($k_{ex} = k_1 + k_{-1}$), p_A (p_B) is the population of state A (B), R_{2A}^0 (R_{2B}^0) is the intrinsic R_2 of A (B), and Δω is the chemical shift difference between A and B. In the limit of fast exchange, this equation simplifies to

$$R_{2,eff}(1/\tau_{cp}) = R_2(1/\tau_{cp} \to \infty) +$$

$$(p_A p_B \Delta\omega^2/k_{ex})\left[1 - 2\tanh(k_{ex}\tau_{cp}/2)/(k_{ex}\tau_{cp})\right] \quad (1.8)$$

It is important to remember that the Carver-Richards equation and the fast approximation assume the simple case of two site exchange. For more complicated cases, it is simpler to use the Bloch-McConnell equations for fitting to exchange parameters. In principle these experiments can be applied to any NMR active nuclei, here we solely use ^{15}N relaxation dispersion experiments. For the more complicated case of 3+ state exchange, it is necessary to collect additional experiments for accurate fitting.

1.4 Overview of This Work

In this work, we utilize CheY as a model allosteric protein to increase understanding of the allosteric mechanisms proteins use. While allosteric signaling mechanisms have been studied for decades, there is a lack of information about the molecular dynamics associated with the signaling event. Here we aim to close that gap by studying CheY on a range of timescales while utilizing the immense structural and biochemical information already available for the protein.

Chapter 2 focuses on the molecular dynamics on the timescale of the conformational switch, μs-ms. We find that unphosphorylated CheY does not change conformations in a simple two state switch but in a segmental manner. These results led to follow-up studies on this timescale described in Chapters 3 and 4 of the phosphorylated CheY and activating mutant A113P CheY. Furthermore, in Chapter 3, we investigate how the dynamics on a faster timescale (ps-ns) change upon phosphorylation of CheY. Together with results described in Chapter 4 of the fast timescale dynamics of A113P CheY, we suggest that the

dynamics on multiple timescale in CheY are correlated and this correlation is important for the allosteric signaling. Lastly, Chapter 5 deals with discovery of long range communication within an allosteric protein. The results are preliminary, but further experiments could lead to great insights in combination with the preceding dynamics results.

CHAPTER 2

SEGMENTAL MOTIONS, NOT A TWO-STATE CONCERTED SWITCH UNDERLIE ALLOSTERY IN CHEY[A]

2.1 Introduction

Allosteric conformational change is critical for the function of many proteins. At the present time, it is not generally understood how allosteric conformational changes are executed or how many different execution strategies exist. As a simpler alternative to defining precise conformational change trajectories, there has been intense focus directed at the "selected fit" versus "induced fit" paradigms[49-53], as well as at concerted vs. propagated conformational changes.[54, 55] The pairing of selected fit with a concerted conformational change – that is, a simple "switch" – has been particularly popular. It is widely recognized that dynamics are central to these processes, yet there are few experiments that have been carried out to directly assess some of the basic assumptions of allostery. Hence there is a need for experimental dynamics data on the timescale of conformational equilibria in allosteric proteins.

Receiver domains from response regulator (RR) proteins have been studied extensively and, because of their small size, have become favored as models for understanding conformational allostery. RRs, along with sensor kinases, comprise the two-component system ubiquitous in prokaryotes. RRs usually consist of an input receiver domain that is activated by phosphorylation, and an output domain that transmits the signal

[A] Published as: McDonald, L. R., Boyer, J. A. & Lee, A. L. (2012). Segmental Motions, Not a Two-State Concerted Switch, Underlie Allostery in CheY. *Structure* 20, 1363-1373.

into various activities such as DNA binding.[25, 26] Accordingly, the ability of the receiver domain to undergo a well-defined conformational change is a vital component of RR function.[27, 56] The chemotaxis protein Y (CheY) from *Escherichia coli* is a RR that regulates chemotactic flagellar rotation.[22, 23] Because it lacks an output domain, the CheY receiver domain must both accept a phosphoryl group and directly activate its downstream effector; in response to phosphorylation at D57[24], which requires the presence of Mg^{2+} [36], CheY undergoes a conformational change that enables it to directly bind the flagellar motor switch protein FliM at a surface distal to D57. CheY binding to FliM promotes a change in the flagellar rotation from counterclockwise to clockwise.[28] Unphosphorylated CheY also interacts with FliM, though with considerably reduced affinity.[41, 57]

As is common in allosteric signaling molecules, CheY samples an active conformation ("A", FliM binding competent) and an inactive conformation ("I", FliM binding incompetent). In the I conformation, FliM binding is sterically hindered by the location of Y106 in a solvent exposed or "out" position (Figure 2.1A). Upon activation by phosphorylation, Y106 (~11 Å away from the phosphoaspartate) rotates to the "in", buried position, relieving the hindrance. T87 hydrogen bonds with the phosphoryl group and has been shown to be an important link for Y106 rotation.[27, 58] Motion of the β4-α4 loop, consisting of residues 88-91, facilitates burial of Y106[37, 38], leading to the possibility that residues in the loop (in addition to T87) may be involved in the signaling. Together with small changes in the β5-α5 loop and side-chain motions of K109 and F14, the I and A conformations differ mainly in the Y106 rotation and the location of the β4-α4 loop.[27]

The prevailing conceptual framework for receiver domain activation/allostery has been that the protein exists in a dynamic equilibrium that accesses both the I and A

conformations, in line with the Monod-Wyman-Changeux (MWC) model of allostery. The following findings provide evidence of an I-to-A state conformational equilibrium: (1) in the absence of phosphorylation, CheY still has the ability to stimulate clockwise flagellar rotation;[41] (2) in the crystal structure of unphosphorylated, Mg^{2+}-free CheY, both "out" and "in" conformations of the Y106 side chain were observed;[42] (3) binding of FliM, CheA, and CheZ peptides to CheY affect its ability to phosphorylate and can be explained by a ligand-induced shift of the I-to-A equilibrium;[43] (4) NMR studies of the receiver domains of Spo0F and NtrC showed that in regions where structural changes upon phosphorylation were observed, there was enhanced transverse relaxation due to conformational exchange on the μs-ms time scale;[39, 59] and (5) mutant NtrC proteins revealed a correlation between activity/inactivity and a two-state equilibrium between active and inactive conformations.[39, 40] While these data are consistent with a two-state switch of RRs, direct detection of a two-state dynamic process between active and inactive conformations has been elusive.

Complicating the simple idea of a pre-existing equilibrium between I and A conformations are several crystal structures of CheY that show intermediate conformations.[37, 44, 45] Additionally, molecular dynamics simulations indicated that Y106 rotation and the formation of a hydrogen bond between T87 and the phosphoryl group are independent of one another.[38] These studies showed that CheY is not restricted to the two end states and taken together suggest that it can be trapped in metastable states that presumably are sampled along the allosteric conformational change trajectory. It is unknown, however, whether such trapped states are functionally relevant or are merely artifacts from crystallization; it also remains unknown what the relevant timescales are for conformational switching in CheY.

In order to further understand the allosteric switch CheY undergoes upon phosphorylation, we investigated the conformational equilibrium that occurs in the unphosphorylated protein. NMR relaxation dispersion was used to measure the dynamics of CheY switching to test for consistency with a two-state model. We found that a physiological level of Mg^{2+} likely plays a critical role in promoting allosteric conformational changes. Nevertheless, whether Mg^{2+} is present or absent, unphosphorylated CheY appears *not* to undergo two-state concerted switching between I and A conformations. Rather, the data are more suggestive of a model in which CheY switches in a non-concerted, segmental fashion. Local sites may occupy their active conformations at different times utilizing a previously undescribed signaling network consisting of A88 with T87 and the quartet of W58, M85, E89, and Y106.

2.2 Materials and Methods

2.2.1 Protein expression and purification

E. coli CheY DNA (provided by Dr. Bob Bourret, University of North Carolina at Chapel Hill) was subcloned into the pET28a plasmid (Novagen). Mutants were made by site-directed mutagenesis PCR. The CheY vector was transformed into BL21 Star (DE3) cells (Invitrogen) and grown in minimal media with the appropriate isotope(s): $^{15}NH_4Cl$ (99%) and/or D-glucose (U-$^{13}C_6$-99%) as the sole nitrogen and carbon sources, respectively). Samples for relaxation dispersion were grown to yield high (>80%) ^2H incorporation. Cells were grown at 37 °C until A_{600} reached 0.6. Isopropyl 1-thio-β-D-galactopyranoside was added to a final concentration of 1 mM and cells were grown for an additional 22-26 hours

(32-36 hours if ^2H_2O used) at 20 °C. The cells were harvested by centrifugation, resuspended in buffer A (25 mM Tris, 10 mM $MgCl_2$, pH 8.0), and stored at -20 °C until needed.

Resuspended cells underwent three freeze/thaw cycles and sonication. The lysate was then centrifuged at 6000 rpm and dialyzed overnight into buffer A at 4 °C. The protein was purified on a Q Sepharose Fast Flow column equilibrated with buffer A. CheY eluted approximately halfway along a gradient of buffer B (buffer A with the addition of 1.5 M NaCl) from 10 to 55% buffer B over 135 mL. The eluent was passed over either a G-50 or G-75 gel-filtration column equilibrated with NMR buffer (50 mM NaP_i, 0.02% NaN_3, pH 7.0 and an appropriate amount of $MgCl_2$ and/or EDTA). Pure CheY was concentrated to between 1.2 and 3 mM and stored at 4 °C. Concentrations were determined using the extinction coefficient of 10.3 cm^{-1}/mM[60] and 14.3 cm^{-1}/mM for wild-type and Y106W CheY, respectively.

2.2.2 NMR Spectroscopy

All NMR spectra were collected on 1 mM CheY with NMR buffer and 10% ^2H_2O. The appropriate amount of $MgCl_2$ or EDTA was present in the NMR buffer, depending on the experiment. NMR experiments were collected at 15 °C on Varian INOVA spectrometers equipped with room-temperature (500 and 600 MHz) or cryogenic (700 MHz) probes. Assignments for wild-type CheY in the presence of 10 mM Mg^{2+} were made from triple resonance experiments, supplemented by previously published assignments.[61] We made use of both triple resonance experiments and assignments of wild-type CheY to assign mutant and BeF_x-bound wild-type CheY (both in the presence of 10 mM Mg^{2+}). Assignments of CheY in the presence of 1 mM EDTA were made based on following peak shifts during

titration with Mg^{2+}. All NMR data were processed using NMRPipe[62] and visualized with NMRDraw and NMRView.[63]

2.2.3 Preparation of BeF_x-bound CheY

NMR samples of BeF_x-bound CheY were prepared with high enough concentrations of $BeCl_2$ and NaF to ensure saturation of CheY and in an ideal ratio for a BeF_3^- complex. The samples were prepared by first combining all components of a typical unphosphorylated CheY sample (e.g. 1 mM CheY protein, 10 mM $MgCl_2$, 10% D_2O). Then $BeCl_2$ and lastly NaF were added to a final concentration of 4 mM and 25 mM, respectively. The samples were then left at room temperature overnight and centrifuged briefly before transferring to an NMR tube.

2.2.4 ^{15}N CPMG Relaxation Dispersion

Relaxation dispersion experiments were carried out using relaxation-compensated CPMG experiments.[64] Most experiments were collected with a 40 ms total CPMG period and one with 20 ms. 12 or 13 τ_{cp} values with 2 duplicates and a reference experiment were collected interleaved. $R_{2,eff}$ was calculated from peak intensities as previously described.[65]

NMR relaxation dispersion experiments measuring motions on the μs-ms timescale were fit assuming a two-state model. Residues were considered to have significant motions and worth analyzing if $R_{ex} > 2\ s^{-1}$. These residues were analyzed as previously described.[17] Briefly, using an F-test ($\alpha_{critical} = 0.01$), the data were fit to both a model that assumes no exchange and a simple two-state model to determine which residues exhibited a significant dependence of $R_{2,eff}$ on $1/\tau_{cp}$. These residues were then fit to the Carver-Richards equation.[48]

By fitting the dependence of $R_{2,eff}$ on $1/\tau_{cp}$, the exchange rate (k_{ex}), populations (p_I, p_A), and chemical shifts ($\Delta\omega$) were determined. Data from two and three field strengths were fit simultaneously for 1 mM EDTA and 10 mM Mg^{2+}, respectively, using the in-house program exrate2.0. Errors were estimated by Monte Carlo simulation.

In the limit of fast exchange, equation 2.3 can be used to fit dispersion curves.[48] Residues were also fit to this equation to assess appropriateness of the Carver-Richards equation. For many of the slower residues, the simplified fast equation did not give the same fit as the Carver-Richards equation and therefore we decided the latter was needed to distinguish the best parameters.

Fitting all of the residues together to the same k_{ex} and p_I or "group fitting" was done in the same manner as previously described.[17, 65] In order to justify group fitting, $\chi^2_{group}/\chi^2_{local} \leq 2$ where χ^2_{local} is the χ^2 when a residue is locally fit and χ^2_{group} is the χ^2 of the same residue when group fit. If necessary, the residue with the highest ratio is removed and the group fitting is attempted again. For CheY, the attempt to group fit resulted in elimination of all residues partly due to the high quality of data.

After all fitting was complete, two residues (G39 in 10 mM Mg^{2+} and D13 in 1 mM EDTA) were determined to have errors that were too large to be accurately fit. Visual inspection revealed both of the peaks to be extremely broad in the ^1H-^{15}N HSQC. Therefore, these residues undergo motions but are unable to be fit due to high error in the intensity measurements. These residues were removed from any further quantitative interpretation of the data.

Utilizing cpmg_fit (provided by Dmitry Korzhnev and Lewis Kay), curves from each residue were fit to a three-state model; however, the fits were not robust due to the limited

data. These preliminary fits yielded individual three-state parameters that were diverse. Nevertheless, using an F-test ($\alpha_{critical} = 0.05$), three residues (A36, T87, and E89) in 10 mM Mg^{2+} fit better to a three-state model than a two-state model. In 1mM EDTA, no residues showed improvement with a three-state fit. Additionally, group fitting to a three-state model did not provide significant statistical improvement. This suggests that CheY is not functioning as a three-state concerted switch.

The sign of $\Delta\omega$ was determined from comparison of peak positions in the HSQC and HMQC spectra.[66]

2.2.5 Determination of approximate R_{ex} by relaxation dispersion

An estimate of R_{ex} can be obtained by using a very low and a very high $1/\tau_{cp}$, as long as the rate of exchange is less than ~5000 s^{-1}. We used the same experimental set-up as used for measuring full relaxation dispersion curves (as described above) except only two τ_{cp} values, 10.0 ms and 0.556 ms were employed. A 40 ms total relaxation time (T) was used and all R_{ex} estimates were made at 15 °C. R_{ex} was calculated from the peak intensities for each plane using

$$R_{ex} = \frac{1}{T} \ln \frac{I_{\tau_{cp}=0.556ms}}{I_{\tau_{cp}=10ms}}, \quad (2.1)$$

in which I is the peak intensity for the given τ_{cp} value.

2.2.6 Binding affinity determination of Mg^{2+}

The K_d for CheY and Mg^{2+} was calculated using chemical shift perturbations of ^{1}H-^{15}N HSQC spectra using a titration of 8 concentrations ranging from 0 to 12 mM $MgCl_2$. To be consistent with the NMR CPMG experiments, the titrations were carried out in NMR buffer (50mM NaP_i, pH 7.0) at 15 °C. To ensure removal of any residual Mg^{2+}, CheY was

buffer exchanged into NMR Buffer with 1 mM EDTA and then buffer exchanged into NMR buffer without EDTA or Mg^{2+}. Residues were only included in the analysis if the change in chemical shift between the highest and lowest Mg^{2+} concentrations was greater than one standard deviation above the average. Therefore, 10 and 9 residues were used for the K_d calculation of wild-type and Y106W CheY, respectively. Residues were individually fit assuming a single binding site, and the reported K_d is the average. Error was estimated from Monte Carlo simulations. We measured the wild-type K_d to be 1.5 ± 0.3 mM which is near to other reported values of 1.0 ± 0.2 mM[67] and 0.45 ± 0.03 mM.[36] The binding affinity of Mg^{2+} to the CheY mutant Y106W was measured in the same manner and was also found to be 1.5 ± 0.3 mM.

2.2.7 Binding affinity determination of FliM

Binding of CheY to the FliM peptide (MGDSILSQAEIDALLN) was measured by fluorescence similar to the procedure previously described.[43] CheY in NMR buffer at 10 μM was titrated with concentrated FliM peptide in NMR buffer. Phosphorylated CheY was measured using CheY in the presence of 10 mM $MgCl_2$ and approximately 50 mM Phosphoramidate. All binding experiments were performed at 15 °C.

2.3 Results

2.3.1 Microsecond-millisecond motions are along the allosteric path

Large scale conformational changes in proteins frequently occur on the slow, or μs-ms, timescale.[11, 12] In an attempt to measure the dynamic switching between the I and A conformations of unphosphorylated CheY, we used ^{15}N Carr-Purcell-Meiboom-Gill (CPMG)

relaxation dispersion experiments to measure motions on this timescale.[48] These experiments elucidate processes on the μs-ms timescale that contribute to broadening (or "width") of NMR peaks. Specifically, the NMR line width is proportional to the transverse relaxation rate, R_2, which is comprised of an "intrinsic" rate, $R_2°$, and a rate that arises from conformational exchange processes on the μs-ms timescale, R_{ex}:

$$R_2 = R_2^o + R_{ex} . \tag{2.2}$$

The CPMG relaxation dispersion experiment measures the suppression of R_{ex} contributions to R_2 as a function of spacing between 180° pulses in the CPMG train, τ_{cp}.[64] For a two-state exchange process in the limit of fast exchange on the NMR timescale,

$$R_{2,\text{eff}}\left(\frac{1}{\tau_{cp}}\right) = R_2^o + \left(\frac{p_I p_A \Delta\omega^2}{k_{ex}}\right)\left[1 - \frac{2\tanh\left(\frac{k_{ex}\tau_{cp}}{2}\right)}{k_{ex}\tau_{cp}}\right] , \tag{2.3}$$

where p_I and p_A are populations of the major and minor states, $\Delta\omega$ is the difference in chemical shift between the two states, and k_{ex} is the rate of exchange between I and A (= k_1 + k_{-1}). A longer expression (the Carver-Richards equation) exists for the general case.[48] A particular residue's R_{ex} value is considered to be non-zero (i.e. affected by conformational exchange) if $R_{ex} > 2\ s^{-1}$, as described in the Materials and Methods.

Pilot relaxation dispersion experiments indicated that the dispersion curves were more pronounced at lower temperatures, and 15 °C was determined to be a good compromise between pronounced dispersion curves and signal-to-noise. Under the standard conditions of 10 mM Mg^{2+}, ^{15}N CPMG relaxation dispersion data were collected at 500, 600, and 700 MHz for CheY. Residues with non-zero R_{ex} values localized to the active site and FliM binding interface, which includes residues T87, A88, and E89 (in the β4-α4 loop), as well as

Y106 and V107 (Figure 2.1A). This was not surprising since all substantial conformational differences between the I and A states are limited to this region.[27] There were no non-zero R_{ex} values elsewhere in the protein, detected either by CPMG relaxation dispersion or by model-free analysis of T_1, T_2, and $\{^1H\}$-^{15}N NOE data. Therefore, at a qualitative level, these data are consistent with motion corresponding to the I-to-A transition.

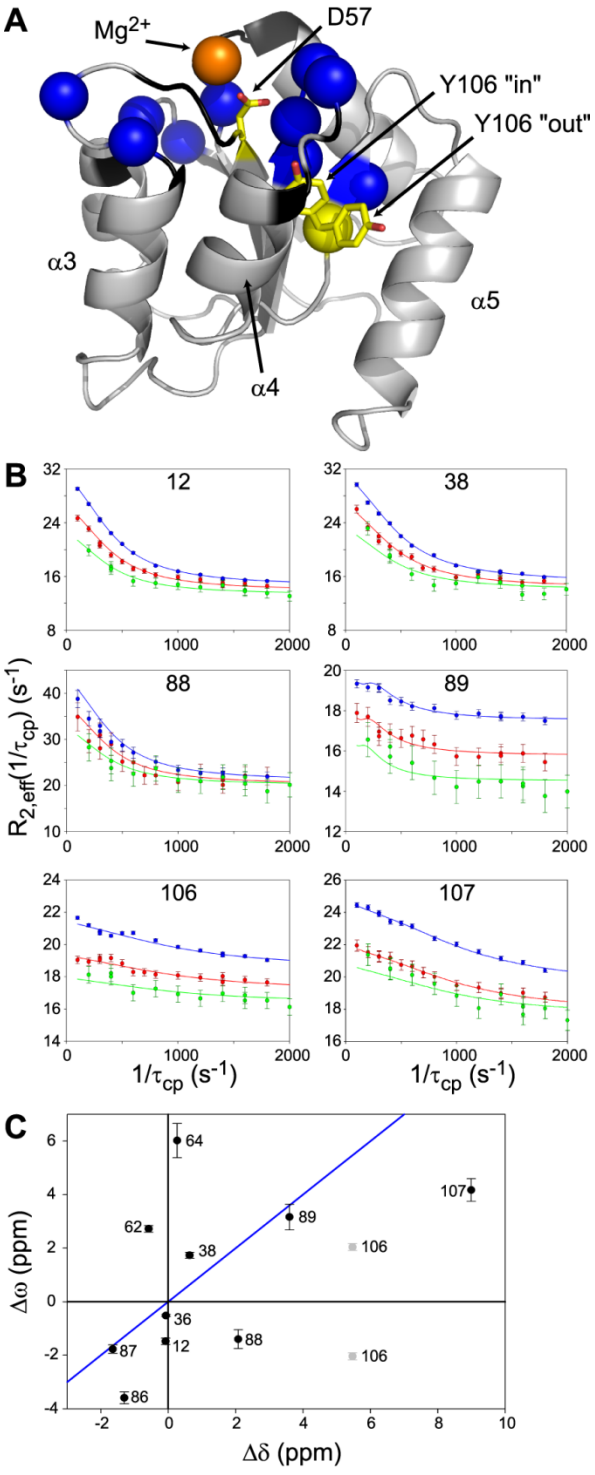

Figure 2.1. ^{15}N CPMG Relaxation dispersion data from unphosphorylated CheY in the presence of 10 mM Mg^{2+}. (A) Structure of unphosphorylated CheY using 3CHY with the side-chain orientation of D57 and Mg^{2+} location from 2CHE. Residues with non-zero R_{ex} values at 10 mM Mg^{2+} are displayed as blue spheres. Black indicates residues that are too broad to be measured. Highlighted in yellow are Y106 and the site of phosphorylation, D57. For Y106, the "in" rotamer indicates active and "out" indicates inactive CheY. (B) Raw CPMG dispersion curves are displayed for 6 example residues at 700 MHz (blue), 600 MHz (red) and 500 MHz (green). Lines are local fits to the Carver-Richards equation with parameters given in Table 1. (C) Δω values from local fits of relaxation dispersion are plotted against Δδ using the difference between unphosphorylated CheY and BeF_x-bound CheY both with 10 mM Mg^{2+}. Δδ was determined using $\Delta\delta' = N^{10mM\ Mg^{2+}} - N^{BeF_x}$, where to get the final Δδ value we made an additional adjustment. Since unphosphorylated CheY is not completely inactive and BeF_x-bound CheY is not completely active, we used $\Delta\delta = 1.05\Delta\delta'$. The blue line has a slope of 1.

Table 2.1. Local fits of ^{15}N CPMG relaxation dispersion for CheY in the presence of 10 mM Mg^{2+}.

Residue	k_{ex} (s^{-1})	Δω (ppm)	p_I	$R_2°$ (s^{-1}) 500 MHz	$R_2°$ (s^{-1}) 600 MHz	$R_2°$ (s^{-1}) 700 MHz	χ^2
12	1220 ± 50	1.5 ± 0.1	0.94 ± 0.01	13.3 ± 0.3	13.9 ± 0.2	14.6 ± 0.1	4.0
36	1910 ± 300	0.52 ± 0.04	0.91 ± 0.02	13.1 ± 0.2	13.2 ± 0.1	14.1 ± 0.1	2.6
38	1370 ± 70	1.7 ± 0.1	0.95 ± 0.01	14.0 ± 0.4	14.3 ± 0.2	15.1 ± 0.2	46
62	2060 ± 180	2.7 ± 0.1	0.99 ± 0.01	12.0 ± 0.1	12.2 ± 0.1	13.1 ± 0.1	0.75
64	3620 ± 460	6.0 ± 0.6	0.99 ± 0.01	13.7 ± 0.5	13.0 ± 0.6	13.8 ± 0.7	5.3
86	2100 ± 330	3.6 ± 0.2	0.99 ± 0.01	15.1 ± 0.3	15.5 ± 0.2	16.9 ± 0.2	13
87	1370 ± 180	1.8 ± 0.2	0.98 ± 0.01	15.3 ± 0.4	14.8 ± 0.3	16.6 ± 0.2	3.6
88	1230 ± 280	1.4 ± 0.4	0.91 ± 0.04	20.1 ± 1	20.2 ± 0.9	21.0 ± 0.8	14
89	246 ± 31	3.2 ± 0.5	0.99 ± 0.01	14.5 ± 0.3	15.8 ± 0.2	17.5 ± 0.1	2.9
106	3100 ± 410	2.0 ± 0.1	0.99 ± 0.01	16.4 ± 0.2	17.1 ± 0.2	18.5 ± 0.2	4.5
107	2840 ± 380	4.2 ± 0.4	0.99 ± 0.01	17.6 ± 0.3	17.7 ± 0.3	19.3 ± 0.4	5.5

2.3.2 Motions measured by relaxation dispersion do not result from a single conformational switch event

The relaxation dispersion curves (Figure 2.1B) were quantitatively analyzed using the general Carver-Richards equation[48] to fit each residue individually (i.e., "local fits", see Materials and Methods). A total of 11 residues could be fit with reasonable precision. If CheY switches concertedly in a simple two-state manner between I and A conformations, we would expect to measure the same exchange rate and populations for all residues. However, the fits yielded a range of kinetic and thermodynamic parameters (Table 2.1). Exchange rates varied from slow (~1300 s^{-1} for residues 12 and 38) to fast (~3000 s^{-1} for residues 106 and 107) and populations varied from 90% - 99% of I. The different exchange rates were also evident in the raw dispersion curves (compare rows of Figure 2.1B). In addition, two-state or three-state concerted switching could not be rationalized based on attempts to group fit the data (see Materials and Methods for details).

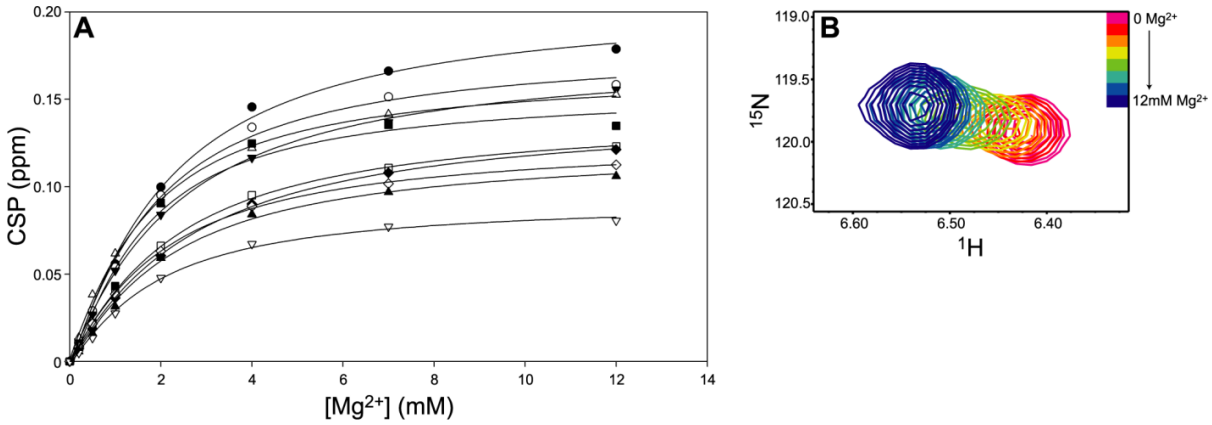

Figure 2.2. ^{1}H and ^{15}N Chemical shift perturbations (CSPs) were used to determine the dissociation constant of Mg^{2+} with CheY in the presence of 50 mM NaP_i at 15 °C. (A) The 10 residues (11, 17, 21, 36, 38, 64, 86, 87, 88, 107) considered for analysis are plotted with their individual fit. CSPs were calculated using $CSP = \sqrt{\Delta HN^2 + \left(\frac{\Delta N}{5}\right)^2}$. (B) An example residue, 17, displays a perturbation due to the Mg^{2+} binding.

Yet another test for two-state behavior is to compare the dispersion-based differences in chemical shifts to known differences in chemical shifts for two defined structural states. Accordingly, we compared Δω from the local fits of relaxation dispersions to Δδ from the chemical shift perturbations between unphosphorylated and BeF_x-bound (phosphoryl mimic[33]) CheY. A poor correlation between Δω and Δδ was obtained (Figure 2.1C), further indicating that the I-to-A transition cannot be described by a simple two-state transition.

Taken together, the non-uniform values of the individual exchange parameters, the inability to group fit, and poor correlation of Δω and Δδ indicates that CheY does not undergo concerted, two-state switching in the presence of 10 mM Mg^{2+} at 15 °C.

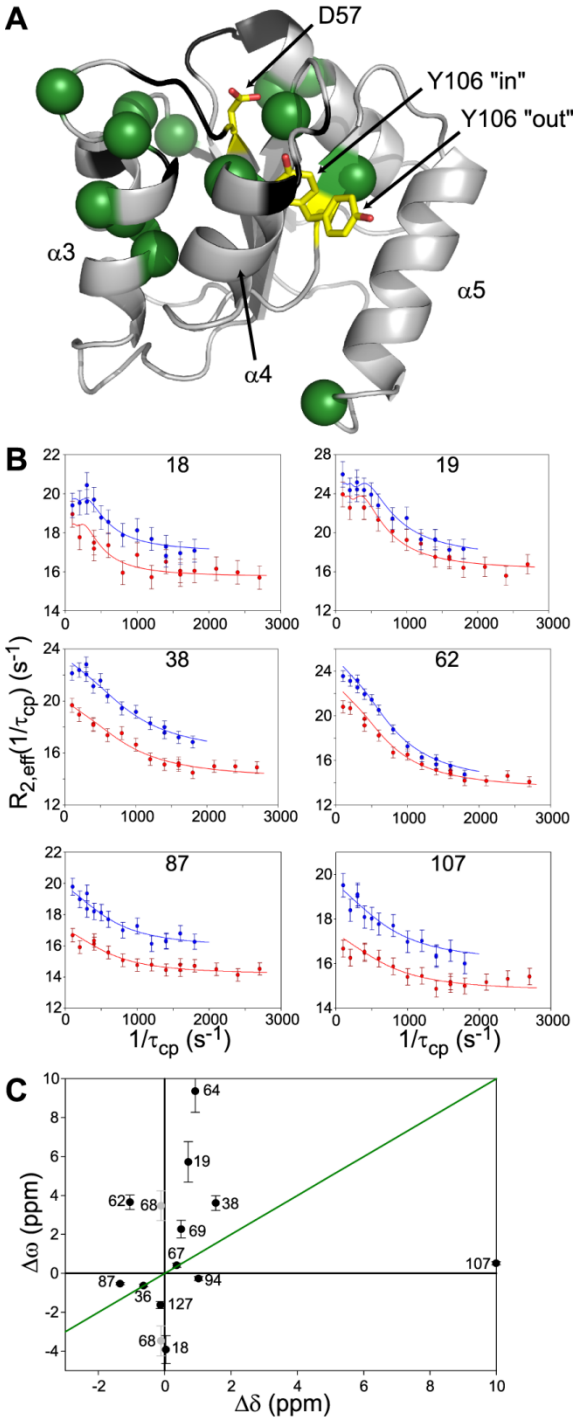

Figure 2.3. ^{15}N CPMG Relaxation dispersion data from unphosphorylated CheY in the absence of Mg^{2+} and presence of 1 mM EDTA. (A) Similar to Figure 2.1, residues with non-zero R_{ex} values at 1 mM EDTA are displayed as green spheres. (B) At 700 MHz (blue) and 600 MHz (red), data are displayed with local fits using the Carver-Richards equation with parameters given in Table 2. (C) Plot of Δω vs. Δδ using Δδ between CheY with 1 mM EDTA and CheY with saturating BeF_x and 10 mM Mg^{2+}.

Table 2.2. Local fits of ^{15}N CPMG relaxation dispersion for CheY in the presence of 1 mM EDTA

Residue	k_{ex} (s^{-1})	Δω (ppm)	p_I	$R_2°$ (s^{-1}) 600 MHz	$R_2°$ (s^{-1}) 700 MHz	χ^2
18	288 ± 57	3.9 ± 0.7	0.99 ± 0.01	15.7 ± 0.3	17.0 ± 0.3	2.9
19	180 ± 30	5.7 ± 1	0.96 ± 0.01	16.1 ± 0.7	17.4 ± 0.9	7.6
36	2400 ± 500	0.6 ± 0.1	0.86 ± 0.04	13.3 ± 0.2	14.1 ± 0.3	2.6
38	2360 ± 640	3.6 ± 0.4	0.99 ± 0.01	14.0 ± 0.5	15.8 ± 0.7	4.3
62	1820 ± 520	3.7 ± 0.4	0.99 ± 0.01	13.4 ± 0.4	13.8 ± 0.7	11
64	96 ± 16	9.4 ± 1	0.80 ± 0.04	20.0 ± 1	22.2 ± 2	13
67	1860 ± 920	0.4 ± 0.1	0.73 ± 0.1	15.2 ± 0.4	16.3 ± 0.6	3.5
68	1400 ± 790	3.5 ± 0.8	0.99 ± 0.01	16.1 ± 0.4	15.9 ± 0.6	1.5
69	2400 ± 1100	2.3 ± 0.5	0.99 ± 0.01	15.0 ± 0.5	15.0 ± 0.8	1.1
87	2130 ± 540	0.53 ± 0.1	0.81 ± 0.05	14.2 ± 0.3	15.9 ± 0.4	2.3
94	1330 ± 800	0.27 ± 0.1	0.67 ± 0.2	15.4 ± 0.2	16.1 ± 0.3	3.3
107	2440 ± 570	0.52 ± 0.1	0.80 ± 0.08	14.8 ± 0.2	16.1 ± 0.4	2.6
127	1980 ± 550	1.6 ± 0.2	0.98 ± 0.01	15.8 ± 0.3	16.5 ± 0.5	2.5

2.3.3 Removal of Mg^{2+} alters dynamics of unphosphorylated CheY

Another possible source of non-zero R_{ex} values in CheY and other RRs is the reversible binding of Mg^{2+}. A divalent metal ion is necessary for all RR phosphorylation and dephosphorylation.[36] In the experiments described in the previous section, near physiological concentrations of Mg^{2+} (10 mM) were used to characterize CheY in an environment similar to inside of cells and to have consistency with previous biochemical and NMR work on CheY.[61, 68] Because the binding affinity of Mg^{2+} to CheY is 1.5 ± 0.3 mM under our conditions (determined by NMR ^{1}H-^{15}N HSQC peak shifts, Figure 2.2), at 10 mM Mg^{2+} and 1 mM CheY, 86% of CheY is bound by the ion. Thus, if the Mg^{2+} binding kinetics are on the appropriate timescale, the binding of Mg^{2+} and associated side-chain rearrangements could be detected by relaxation dispersion and this could complicate the interpretation in terms of conformational exchange.

To separate motions associated with Mg^{2+} binding and release from those intrinsic to CheY, we carried out relaxation dispersion experiments without Mg^{2+} present (i.e., with 1

mM ethylenediaminetetraacetic acid, EDTA). In the absence of Mg^{2+}, 13 residues displayed non-zero R_{ex} values for CheY, compared to 11 when Mg^{2+} is present at 10 mM. These residues are localized to the FliM binding interface or the active site (Figure 2.3A) just as when Mg^{2+} is present (Figure 2.1A). The locally fit parameters, when assuming a two-state mechanism, are diverse (Figure 2.3B and Table 2.2). In comparison with dynamics in the presence of Mg^{2+}, many of the same residues display significant dispersion, including T87 and V107. The locally fit parameters of the common residues differ significantly between the Mg^{2+}-free and Mg^{2+}-present conditions (Tables 2.1 and 2.2). Additionally, $\Delta\omega$ and $\Delta\delta$ do not correlate (Figure 2.3C), as was the case with Mg^{2+} (Figure 2.1C). Therefore, even without the potentially complicating effects of Mg^{2+}, CheY appears not to undergo two-state switching.

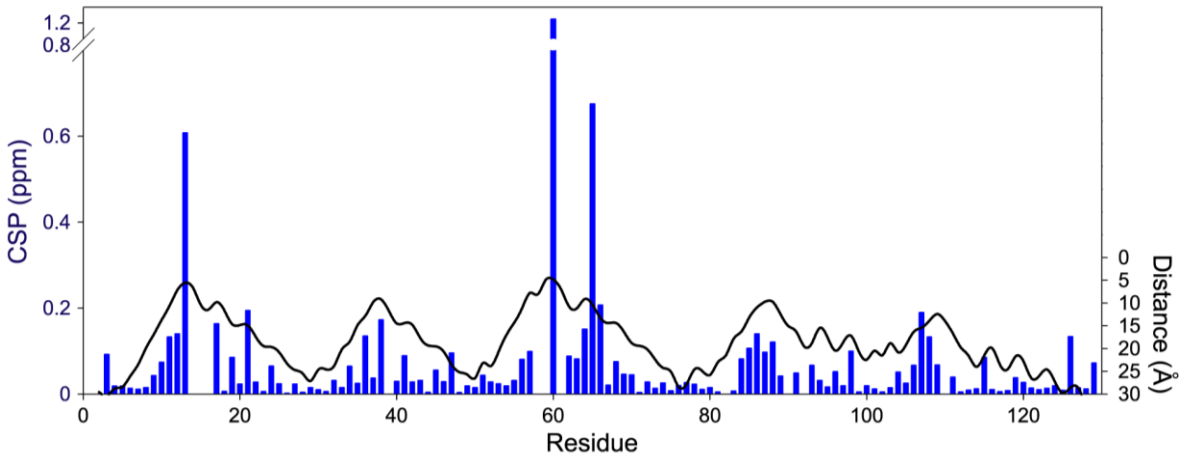

Figure 2.4. CSPs upon Mg^{2+} binding are compared to the distance from Mg^{2+}. The distance indicated by the black line is from the Mg^{2+} ion bound to CheY (location from 2CHE) to the backbone C_α of the specified residue. The CSP indicated by blue bars was calculated with the same equation as figure 2.2 using ΔHN and ΔN between CheY in the absence of Mg^{2+} (i.e. 1 mM EDTA) and CheY in the presence of 75 mM Mg^{2+}.

It is possible that bound Mg^{2+} induces a conformational change in CheY. The crystal structure of Mg^{2+}-bound *E. coli* CheY reveals a conformational difference from Mg^{2+}-free CheY that localizes to α4 and the β4-α4 loop.[69] However, chemical shift perturbations of CheY upon the addition of Mg^{2+} are strongly correlated with closeness to the ion and in

general are small in regions of allosteric conformational change (Figure 2.4), suggesting no significant structural rearrangements. In addition, the crystal structure of *Salmonella typhimurium* CheY[70] (which differs by 3 amino acids from *E. coli*) and the NMR structure of *E. coli* CheY[61], both with Mg^{2+} present, have no indication of any large structural rearrangement. For these reasons, the different CheY dynamics observed with or without Mg^{2+} do not appear to be the direct result of Mg^{2+}-induced conformational change.

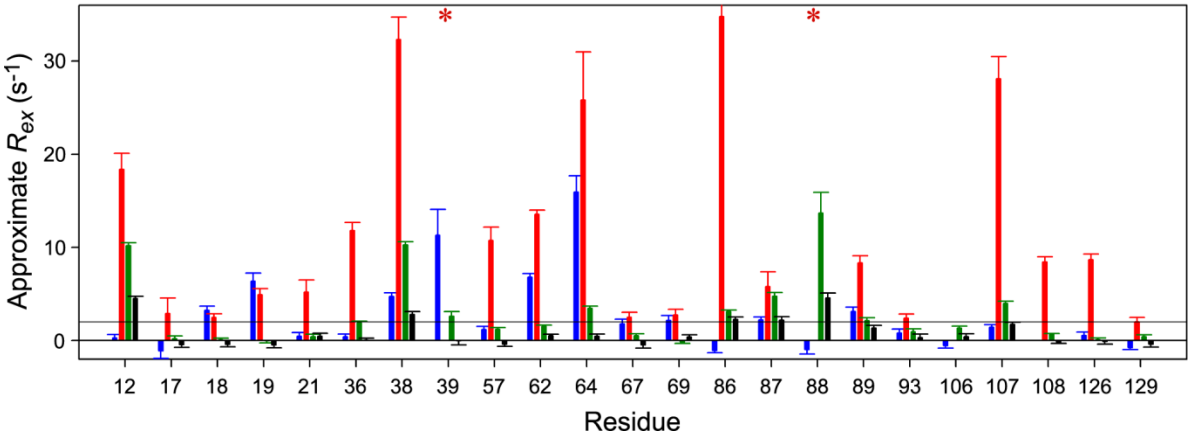

Figure 2.5. Effect of Mg^{2+} concentration on R_{ex}. R_{ex} is approximated by the change in $R_{2,eff}$ of two CPMG relaxation dispersion planes. Approximate R_{ex} is shown for CheY in the presence of 1 mM EDTA (blue), 1 mM Mg^{2+} (red), 10 mM Mg^{2+} (green), and 75 mM Mg^{2+} (black) for all residues with non-zero R_{ex} values at 1 mM Mg^{2+}. Residues G39 and A88 are broadened away at 1 mM Mg^{2+} presumably from exchange, indicated by *. Also, there are no data for Y106 at 1 mM Mg^{2+} and V108 at 1 mM EDTA because of peak overlap.

2.3.4 Physiological Mg^{2+} concentrations enhance allosteric dynamics

To gain greater insight into the effect of Mg^{2+} on CheY dynamics, we obtained estimates of R_{ex} at additional Mg^{2+} concentrations of 1 mM and 75 mM (Figure 2.5). Thus, assuming a single binding site, 1 mM CheY was calculated (based on the K_d of 1.5 mM) to be bound by Mg^{2+} at a level of 0%, 31%, 86%, and 98% for 0 mM, 1 mM, 10 mM, and 75 mM concentrations of Mg^{2+}, respectively. For all concentrations of Mg^{2+}, estimates of R_{ex} were obtained as the difference of $R_{2,eff}$ values at the lowest and highest values of τ_{cp} used for

dispersion measurements. Overall, the dependence of R_{ex} on the concentration of Mg^{2+} is immediately apparent: R_{ex} in the presence of no Mg^{2+} or very high concentration of Mg^{2+} (75 mM) is relatively low, and R_{ex} at intermediate levels of Mg^{2+} (1 mM) is very high (Figure 2.5). Furthermore, peak broadening was evident in many residues at intermediate Mg^{2+} concentrations, implying increased motion. While high R_{ex} levels at intermediate concentrations of Mg^{2+} are expected for residues in close proximity to the bound ion (assuming appropriate line-broadening kinetics), high R_{ex} levels are not expected at residues distal to Mg^{2+} that are not structurally affected by the ion, such as on the FliM binding interface. Yet, R_{ex} at V107 is quite pronounced (28 s^{-1}) at 1 mM Mg^{2+}. We note that Mg^{2+} binding induces a small chemical shift change of 0.52 ppm for the amide nitrogen of V107 (Figure 2.4), especially compared to the large chemical shift change of 8.6 ppm brought about by binding of BeF_x. Furthermore, A88 experiences extreme line broadening at intermediate concentrations of Mg^{2+}. The dispersion experienced at this position is larger than expected when compared to neighboring residues. Thus, there is something particular about partial Mg^{2+} saturation that increases conformational dynamics at A88 and even further at the FliM binding interface more than 10 Å away.

To probe the coupling between Mg^{2+} binding and Y106 dynamics using an alternate approach, we elected to make R_{ex} measurements on the Y106W mutant. The primary structural difference between crystallized wild-type and Y106W CheY is the orientation of the side chain at position 106, which was found to solely adopt the "in" orientation for unphosphorylated Y106W.[71] We hypothesized that changing the side-chain dynamics at position 106 will alter the allosteric coupling with Mg^{2+} binding. To test this idea, we measured R_{ex} values for Y106W CheY and observed a similar overall R_{ex} dependence on

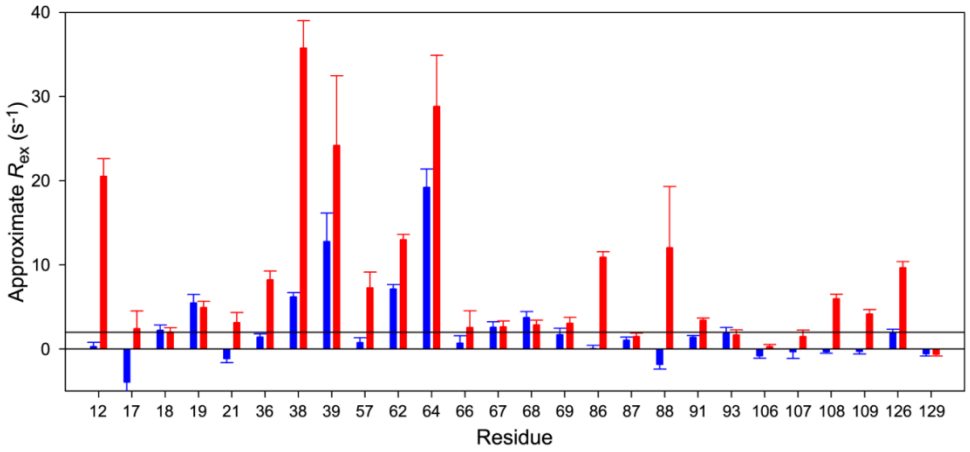

Figure 2.6. Approximate R_{ex} for CheY mutant Y106W. Shown in blue is approximate R_{ex} in the absence of Mg^{2+} (1 mM EDTA) and in red is in the presence of 1 mM Mg^{2+}. R_{ex} is approximated in the same manner as Figure 2.5. Additionally, residues are the same as in Figure 2.5 with two additional residues, L68 and K109, that have $R_{ex} > 2\ s^{-1}$ for Y106W but not wild-type CheY. Furthermore, E89 is not displayed because of overlap in the Y106W spectra and L66 is displayed even though it was not in the wild-type because of overlap in the wild-type spectra.

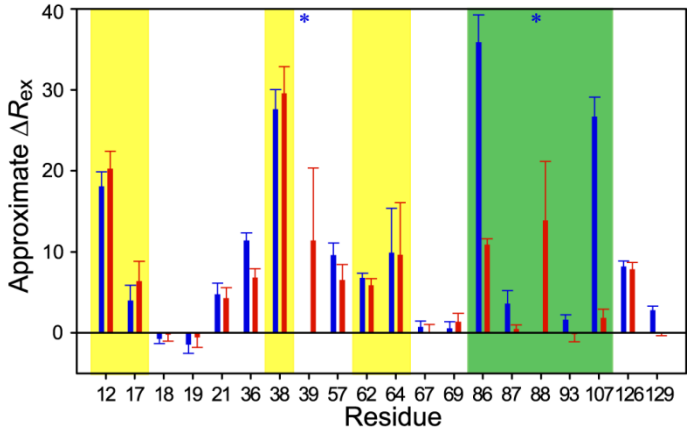

Figure 2.7. Comparison of the difference between R_{ex} without Mg^{2+} present (1 mM EDTA) and addition of 1 mM Mg^{2+} for wild-type and Y106W CheY. The change in approximate R_{ex} upon addition of Mg^{2+} ($\Delta R_{ex} = R_{ex}^{1mM\ Mg2+} - R_{ex}^{1mM\ EDTA}$) is shown for wild-type (blue) and Y106W (red) CheY. Shaded in yellow are residues with their amides near to bound Mg^{2+} and shaded in green are residues associated with the allosteric transition. For G39 and A88, the peaks are broadened away upon addition of Mg^{2+} indicated by *. The same residues are displayed as in Figure 2.5 except Y106 and V108 were eliminated due to lack of data from peak overlap.

Mg^{2+} to wild-type (Figure 2.6). In comparing the quantitative effect Mg^{2+} has on wild-type and Y106W CheY, we notice a significant difference. Residues that are close to the Mg^{2+} binding site are extremely similar in their R_{ex} dependence on Mg^{2+} for wild-type and Y106W (Figure 2.7, shaded yellow). However, residues that are far from the bound Mg^{2+} ion and are involved in the allosteric transition depend differently on Mg^{2+} for wild-type and Y106W (Figure 2.7, shaded green). Since the effect due to Mg^{2+} is the same for wild-type and Y106W CheY at residues near to the bound ion, the difference in R_{ex} far from Mg^{2+} must be due to a change in the I-to-A transition. Therefore, enhanced R_{ex} at intermediate concentrations of Mg^{2+} are not merely caused by Mg^{2+} binding and release but due to a change in the motions associated with the I-to-A transition.

Importantly, the difference in R_{ex} far from Mg^{2+} is due to a change in the I-to-A transition without significant changes to the structure of the ground state (see above), even though phosphorylation – which occurs at nearly the same location as Mg^{2+} binding – induces a large structural change. The Mg^{2+} concentration's effect on the I-to-A transition is likely biologically relevant since R_{ex} is largest at intermediate concentrations of Mg^{2+} (1 mM); this concentration is close to the K_d for Mg^{2+} and CheY (1.5 mM), and also close to the concentration of Mg^{2+} in *E. coli* (~1-2 mM Mg^{2+} [72]).

2.3.5 Key residues display linear chemical shifts in response to Mg^{2+} binding

We observed that, for Y106, V107, and E89, the NH chemical shifts move along a line for various states of CheY, which include apo, BeF_x-bound, inactive mutant T87I CheY[73], and activated mutant A113P CheY[74] (Figures 2.8A, 2.8B, and 2.8C). Linear chemical shifts are indicative of a classic, two-state, I-to-A switch, as was described for the

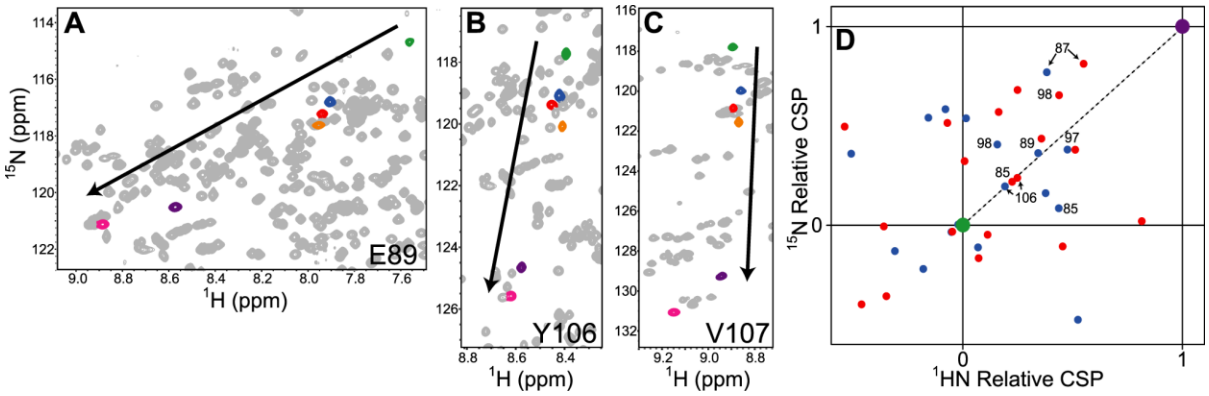

Figure 2.8. Chemical shift perturbations (CSP) from inactive to BeF_x activated CheY. Overlaid ^{1}H-^{15}N HSQCs are shown with peaks highlighted for (A) E89, (B) Y106, and (C) V107 from various conditions and mutants of CheY: inactivating mutant T87I with 10 mM Mg^{2+} (green), wild-type with 1 mM EDTA (blue), wild-type with 10 mM Mg^{2+} (red), activating mutant A113P with 10 mM Mg^{2+} (orange), BeF_x-bound wild-type with 10 mM Mg^{2+} (purple) and BeF_x-bound A113P with 10 mM Mg^{2+} (pink). (D) To display all residues, CSP is normalized according to inactivating mutant T87I with 10mM Mg^{2+} (green) and BeF_x-bound wild-type CheY (purple). Each circle represents the normalized CSP of each residue of wild-type CheY in the presence of 10 mM Mg^{2+} (red) and 1mM EDTA (blue). Residues are only shown if $CSP = \sqrt{\Delta HN^2 + \left(\frac{\Delta N}{5}\right)^2}$ was greater than 0.20 where ΔHN and ΔN are between T87I and wild-type BeF_x-bound CheY. If $\Delta HN < 0.06$ ppm or $\Delta N < 0.25$ ppm, the chemical shifts are considered within error in that dimension and the residues were removed. Therefore, while V107 appears linear, it is not shown in (D) since the proton shift is < 0.06 ppm.

receiver domain of the NtrC RR.[39] To test whether linear shifts were observed throughout CheY, we plotted all Mg^{2+}-induced CSPs on a normalized vector scale (Figure 2.8D). If Mg^{2+} shifts this equilibrium, all chemical shifts should fall along the dotted line from inactive mutant T87I to BeF_x-bound wild-type CheY. However, with a few exceptions, the CSPs distribute essentially randomly, with no apparent preferred "direction". Thus, it appears that, overall, Mg^{2+} binding elicits either a new conformational state(s) that has only subtle differences from the I state and bears no resemblance to A-like chemical shifts, or Mg^{2+} has essentially no significant effect on CheY conformation. This is further supported by no significant change in the affinity of binding of FliM to unphosphorylated CheY with the addition of Mg^{2+} (Figure 2.9). Nevertheless, there are a few key residues (e.g. Y106, E89) that display the linear chemical shifts suggestive of an equilibrium shift (Figure 2.8).

Interestingly, additional residues that fall near the line (Figure 2.8D, M85, A97 and A98) lie in the pocket surrounding W58. These residues, along with Y106 and E89, may experience a shift in conformation due to the presence of Mg^{2+} (discussed below).

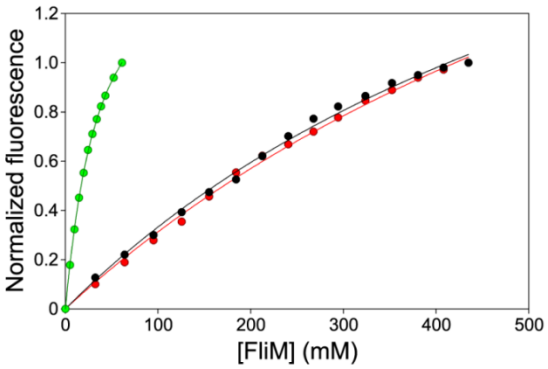

Figure 2.9. Binding of FliM peptide to CheY. Intrinsic fluorescence was monitored upon addition of FliM under conditions of no Mg^{2+} (red), 10 mM Mg^{2+} (black) and 10 mM Mg^{2+} with 50 mM small molecule phosphodonor, phosphoramidate (green).

2.4 Discussion

For half a century now, allosteric conformational change has been revealed to be an extremely successful mechanism for regulating protein function. Yet, key specific questions regarding allostery have yet to be answered. Is the conformational change concerted? Are there structural intermediates? What are those intermediates? What is the dynamic process that allows conversion between the end conformations and how is it triggered? In summary, we still have a poor understanding of how allosteric conformational changes actually happen. By conducting in-depth NMR experiments on the small allosteric protein CheY, we hoped to gain new insights into the mechanism(s) of allostery. CheY is an excellent system for probing allostery because numerous crystal structures have been solved in a variety of liganded states and it is highly amenable to NMR relaxation experiments. It also exhibits a

rich complement of residues with μs-ms motion at residues that connect the physically separated upstream and downstream effector sites.

2.4.1 Allostery in CheY does not operate by a simple shift of a two-state equilibrium

From previous crystallographic, NMR, and functional data[39, 40, 59, 75], the evidence suggests that receiver domains primarily adopt two conformations and hence allostery is achieved by shifting a pre-existing dynamic equilibrium between these two states, consistent with the MWC model of allostery. Based on this previous work on NtrC, FixJ, and Spo0F, and our initial observation here of R_{ex} in the allosteric network of residues, the simplest expectation would be that CheY undergoes a concerted switch between I (inactive) and A (active) conformations. Here, we show using NMR relaxation dispersion that intrinsic allostery in CheY does *not* appear to operate by a simple shift of a two-state equilibrium. This conclusion rests, in part, on the ability of relaxation dispersion experiments to accurately identify conformational exchange rates and populations.

It is possible that unphosphorylated CheY does not completely switch to the A state but rather samples a conformational intermediate between the I and A states, and this may account for the lack of correlation in $\Delta\delta$ and $\Delta\omega$ values. However, this cannot be confirmed experimentally without having accurate chemical shifts for the intermediate state, which has yet to be isolated in solution. Alternatively, if a structural model for the intermediate exists, the chemical shifts can be calculated using SHIFTX[76]; then $\Delta\delta$ can be calculated between the inactive and intermediate states and compared with $\Delta\omega$ from relaxation dispersion fits. This was carried out using the partially switched structure of CheY bound to FliM without phosphorylation (2B1J[44]) as the intermediate, but the $\Delta\omega$ values did not correlate. In any

case, if the observed R_{ex} values result only from unphosphorylated CheY switching concertedly to an intermediate state, one would still expect k_{ex} and populations to be uniform, yet they are not.

2.4.2 Distal quartet of residues directs allosteric conformational change

In order for CheY to undergo its allosteric transition it must primarily do two things: (1) reposition the β4-α4 loop, and (2) swing Y106 into the pocket just under the β4-α4 loop. We measured three residues, Y106, V107, and E89, that appeared to approach two-state behavior, although this is apparent only in the chemical shift data (Figure 2.8) and not in the relaxation dispersion data (Figures 2.1 and 2.3). One possible explanation for the linear chemical shifts is that because Y106 is at the solvent interface and presumably under less structural constraint, its position is to a reasonable approximation either "out" or "in", yielding a bimodal distribution of possible chemical shift values for the amide of Y106. The strong ring currents dominate the chemical shifts of both Y106 and V107 amides. The amide chemical shift of E89, located in the β4-α4 loop, likely monitors the remodeling of this loop. We utilized SHIFTX[76] to calculate the effect on chemical shift from a conformational change. Y106 and V107 amide chemical shifts are very sensitive to the rotation of Y106, with minimal effects from the location of the β4-α4 loop. By contrast, the amide shift of E89 is very sensitive to movement of the β4-α4 loop, but not to Y106. Therefore, E89 monitors the β4-α4 loop motion, and Y106 and V107 likely monitor the rotation of Y106. Taken together, the chemical shift data reveal a localized shift to active-like states.

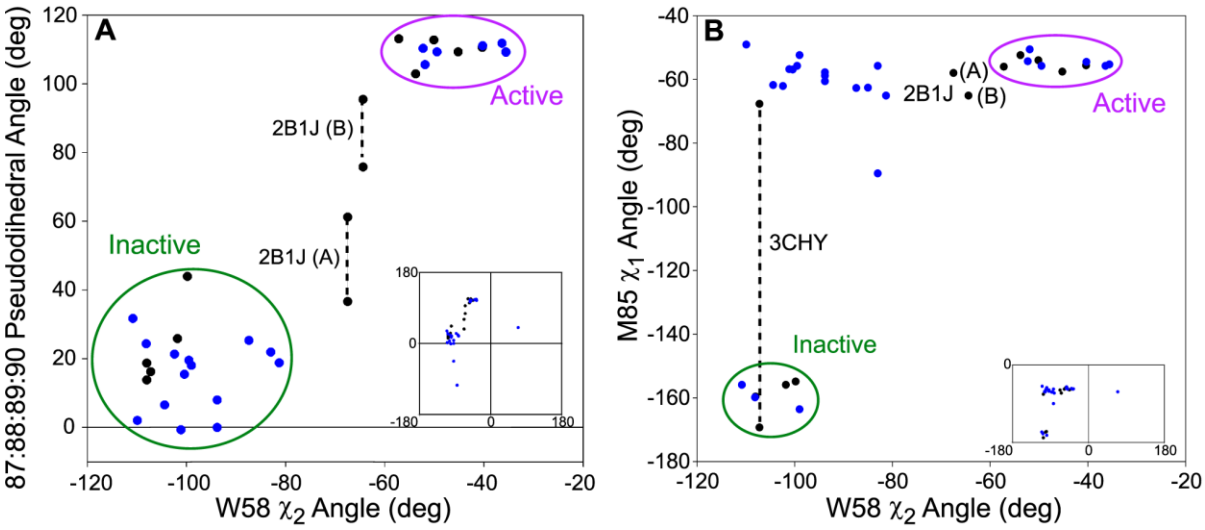

Figure 2.10. Comparison of dihedral angles in crystal structures of CheY. (A) Comparison of the 87:88:89:90 pseudodihedral angle with the rotation of W58 and (B) comparison of M85 χ_1 angle with the rotation of W58. The pseudodihedral angle was measured using C_α coordinates. In black are wild-type CheY crystal structures (1FQW, 1F4V, 2B1J, 1JBE, 3CHY, 2CHE, and 1C4W) and in blue are mutant or CheA-bound CheY crystal structures (only single site mutations and >2.5 Å resolution, full list is provided in Table 2.3). Insets are the full range of angles occupied while large plots are zoomed on the majority of crystal structures.

While E89, Y106, and V107 have the most linear chemical shifts, a few residues are nearly linear (M85, A97, and A98) while all others show no semblance of linearity. M85, A97, and A98 have not been discussed previously as part of the allosteric mechanism. Yet, these residues line the pocket occupied by W58 and are proximal to the β4-α4 loop and Y106. Examination of CheY in its inactive (3CHY[42]), active (1FQW[27]), and intermediate conformations (2B1J[44]) reveals an extended set of conformational interactions. Upon activation, the hydroxyl of Y106 hydrogen bonds to the backbone carbonyl of E89, which is allowed by movement of the β4-α4 loop. What appears to further stabilize this interaction is a large movement of the E89 side chain towards the side chain of W58, resulting in hydrophobic contacts between the methylene groups of E89 and the tryptophan indole. Interestingly, superimposition of inactive and active CheY structures shows that the tryptophan indole group reorients by ~55° and the intermediate state (when CheY is bound

only to FliM peptide) shows the indole at an intermediate angle. Although tryptophan at position 58 is not conserved amongst RRs, the receiver domain from PhoB displays a similar rotation of ~60° upon binding BeF_x.[77, 78] When analyzing a range of crystal structures, we find that the angle of the W58 indole correlates with the pseudodihedral angle 87:88:89:90 (Figure 2.10A). This pseudodihedral angle has been used to indicate the location of the β4-α4 loop[44]. In order to contact E89, W58 increases its distance from M85, which is associated with W58 in the inactive conformation. Thus, M85 and E89 appear to be in competition for W58, with E89 making contact only in the active conformation. In further support of this extended mechanism, we note that in 3CHY, M85 was found to occupy two conformations (similar to Y106), of which only one is adopted in the intermediate and active conformations and the other is adopted in other crystal structures of the inactive state (Figure 2.10B). Additional crystal structures reveal that M85 often occupies the "active" rotamer even though W58 has not rotated to the active state (Figure 2.10B). This indicates that W58 is not as robustly coupled to M85 as the β4-α4 loop. However, one should be cautioned not to overinterpret the lack of coupling between M85 and W58; since the two M85 side-chain conformations have similar electron density, this leads to the possibility that the crystal structures did not accurately account for multiple conformations. We also note that the amide of W58 could not be assigned, which is consistent with its indole sampling at least two conformations prior to full activation. We propose here that the quartet of W58, M85, E89, and Y106 are coupled, as a key component of the allosteric signaling process from phosphorylation.

Table 2.3. List of crystal structures and angle measurements used for Figure 2.10.

PDB Code	Mutation and/or ligand bound	87:88:89:90 Pseudodihedral (deg)	M85 Chi1 (deg)	W58 Chi2 (deg)
1JBE (A)[37]	WT	18.7	-159.6	-108
1JBE (B)	WT	13.8	-159.6	-108
3CHY (A)[42]	WT	16.2	-67.7	-107.2
3CHY (B)	WT	16.2	-169.3	-107.2
2CHE[70]	WT Mg^{2+} *S. typhimurium*	25.8	-155.9	-101.8
1C4W[79]	Phospho - WT	43.9	-154.9	-99.8
1F4V (A)[34]	WT BeF_3^-, FliM & Mg^{2+}	112.8	-54	-50.13
1F4V (B)	WT BeF_3^-, FliM & Mg^{2+}	102.9	-52.4	-53.8
1F4V (C)	WT BeF_3^-, FliM & Mg^{2+}	113.1	-56	-57.2
1FQW (A)[27]	WT BeF_3^- & Mn^{2+}	109.3	-57.6	-45.22
1FQW (B)	WT BeF_3^- & Mn^{2+}	110.6	-55.6	-40.35
2B1J (A-A)[44]	WT FliM & Mg^{2+}	61.2	-58	-67.5
2B1J (A-B)	WT FliM & Mg^{2+}	36.6	-58	-67.5
2B1J (B-A)	WT FliM & Mg^{2+}	95.5	-65.1	-64.4
2B1J (B-B)	WT FliM & Mg^{2+}	75.8	-65.1	-64.4
1D4Z[80]	I95V	24.3	-159.9	-108.1
5CHY[71]	Y106W & Ca^{2+}	31.7	-155.9	-110.8
1EHC (A)[81]	D13K	18	-163.6	-99
1EHC (B)	D13K	18	-52.4	-99
3OO1 (A)	A113P & Mg^{2+}	19.5	-55.8	-99.5
3OO1 (B)	A113P & Mg^{2+}	7.95	-57.8	-93.8
1E6M[82]	D57A	18.8	-65.1	-81.3
2ID7 (A)[83]	Phospho - T87I	21.9	-89.5	-83
2ID7 (B)	Phospho - T87I	21.9	-55.8	-83
1VLZ (A)[73]	T87I	21.3	-62.1	-102.4
1VLZ (B)	T87I	2.03	-49.1	-109.9
1E6L[82]	D13A	40.3	-62	69.8
1E6K[82]	D12A	-105.9	-62.6	-85
3OO0 (A-A)	A113P SO_4 & Mn^{2+}	110.3	-54.3	-52.3
3OO0 (A-B)	A113P SO_4 & Mn^{2+}	-0.05	-60.6	-93.8
3OO0 (A-C)	A113P SO_4 & Mn^{2+}	-45.1	-58.8	-93.8
3OO0 (B)	A113P SO_4 & Mn^{2+}	109.3	-55.8	-49.5
3OLV (A)	A88V BeF_3^- & Mg^{2+}	105.6	-50.6	-51.9
3OLV (B-A)	A88V BeF_3^- & Mg^{2+}	109.2	-55.3	-35.6
3OLV (B-B)	A88V BeF_3^- & Mg^{2+}	109.3	-55.3	-35.6
3MYY (A)	A113P BeF_3^- & Mn^{2+}	111.1	-54.5	-40.3
3MYY (B)	A113P BeF_3^- & Mn^{2+}	111.8	-55.8	-36.4
1FFG (A)[84]	WT CheA & Mn^{2+}	15.4	-56.9	-100.4
1FFG (C)	WT CheA & Mn^{2+}	-0.7	-56.8	-101.1
1FFS (A)	WT CheA, PO_4 & Mn^{2+}	25.3	-62.7	-87.4
1FFS (C)	WT CheA, PO_4 & Mn^{2+}	6.5	-61.8	-104.4

2.4.3 A88 links Mg^{2+} binding to the allosteric quartet

Upon Mg^{2+} binding to CheY, intrinsic fluorescence of W58 is quenched[36], indicating that Mg^{2+} may play an additional role in this signaling cascade. T87 is considered to be the initial "sensor" of phosphorylation and triggers the allosteric response.[58] However, it is

unclear whether additional residues play a crucial role and which residues may sense Mg^{2+}. A88, in addition to T87, also hydrogen bonds with the phosphoryl group via its backbone amide. Perhaps most importantly, from the relaxation dispersion data in 10 mM Mg^{2+}, A88 fit to parameters unlike any other residue. While most residues fit to populations (p_I) of 0.98-0.99, A88 fit to 0.91. Furthermore, its dispersion curve visually resembles residues 12 and 38, which are near to the bound Mg^{2+} ion, more than the allosteric residues 87, 89, 106, and 107 (Figure 2.1B). Careful inspection of the fit to A88 indicates that its $R_2°$ values are anomalously high and the quality of the fits is significantly lower than the other residues (Table 2.1). Thus, we suspect that in addition to the motion that gives rise to the main part of A88's dispersion curve, there is a separate, faster motion on the μs timescale. Only A88 appears to have this more complex combination of motions. Furthermore, A88 experiences line broadening severely affected by the concentration of Mg^{2+}. At 1 mM Mg^{2+}, A88 is completely broadened away in the ^{1}H-^{15}N HSQC. Given its behavior at different Mg^{2+} concentrations, A88 may be especially sensitive to Mg^{2+} binding and release.

We therefore hypothesize that A88 acts as a crucial monitor of ion binding and/or phosphorylation at the active site. It is important to note that, even though they are adjacent, residues 86-89 have different exchange parameters. Therefore, at face value these residues appear largely independent. Nevertheless, because these residues lie within the allosteric pathway and all show motion on the μs-ms timescale, we suggest that in addition to T87, A88 provides a linkage to E89, and that the recruitment of W58 by E89 represents a key step in switching the β4-α4 loop. Given these considerations, we propose that the allosteric network in CheY is facilitated by several distinct behaviors that extend from D57, to T87 and A88, and ultimately to the distal quartet of W58, M85, E89, and Y106 (Figure 2.11).

2.4.4 Effects of Mg^{2+} on the allosteric dynamics

Mg^{2+} binding to the active site in CheY has a distinct effect on the dynamics measured by relaxation dispersion experiments. Addition of Mg^{2+} causes a significant change in the μs-ms dynamics; residues that have significant dynamics in both cases have a change in the dispersion curves (Figures 2.1 and 2.3) causing a large change in the fit parameters to the Carver-Richards equation (Table 2.1 and 2.2). Therefore, the binding of Mg^{2+} does not merely cause a shift in a simple equilibrium. Furthermore, as mentioned above, the binding of Mg^{2+} does not cause a large change in structure of the protein as seen by both chemical shift and crystal structures. The effect of Mg^{2+} on the allosteric transition in CheY is best observed at an intermediate (1 mM) Mg^{2+} concentration. This enhanced R_{ex} at intermediate concentrations of Mg^{2+} is not merely caused by Mg^{2+} binding and release but due to a change in the motions associated with the I-to-A transition. However, in order to understand how exactly Mg^{2+} affects the allosteric switch, we must first understand the transition without Mg^{2+}.

A second metal binding site has been proposed for the RR Spo0F[85] and is therefore also possible for CheY. We have measured only small ($\Delta\delta < 0.5$ ppm where $\Delta\delta = N^{10\ mM\ MgCl2} - N^{200\ mM\ MgCl2}$) chemical shift changes that could be due to a second binding site and a $K_d > 50$ mM. This indicates that it is highly unlikely that we would be able to detect the binding and release of Mg^{2+} at a second site by relaxation dispersion. If R_{ex} values are affected due to binding at a second site, we would expect R_{ex} to increase near to the K_d due to an increase in $p_A p_B$. However, every residue with non-zero R_{ex} at 10 mM Mg^{2+} has a decrease

in R_{ex} upon an increase in Mg^{2+} to 75 mM (Figure 2.5). This provides strong evidence that Mg^{2+} binding to a second site does not affect our relaxation dispersion experiments.

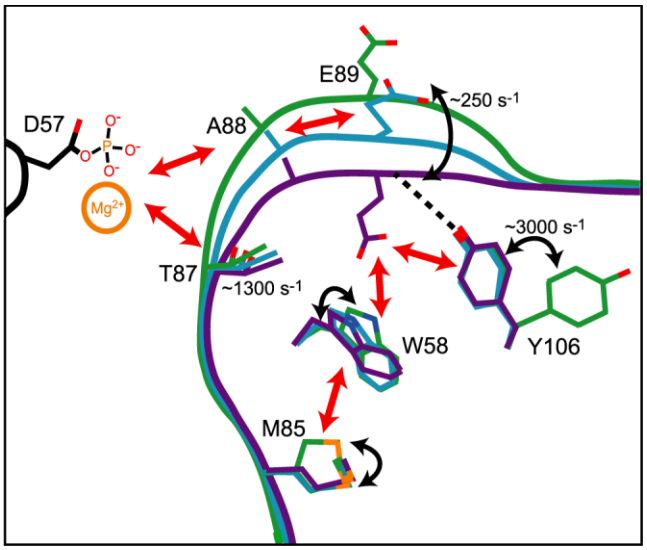

Figure 2.11. Cartoon model of the allosteric signaling mechanism in CheY. Representations of inactive (green), intermediate (blue) and active (purple) CheY with important signaling residues displayed.

2.4.5 Evidence for segmental allosteric dynamics

Considering the chemical shift and relaxation dispersion data together leads inexorably to a paradox. How can there be linear chemical shifts in key allosteric residues when switching appears not to be concerted by relaxation dispersion? A distribution of 2D chemical shifts along a line is typically considered to indicate a rapid exchange between two states[39], with the spread of positions resulting from a shifting of the equilibrium. While this is indeed highly likely to be the case at the spin probes' "site" (amide H and N could be considered as one site), if two probes show this behavior at significant distances from one another, they need not result from the same conformational exchange process. Thus, we consider if the observed linearity can result from *local* two-state switching. Specifically, the

switching of W58 can be sensed by residues 85, 97 and 98, but the switching of Y106 appears independent of W58. It is possible that some groups of residues switch concertedly, yet with some independence from other switching events. Even though such a group appears to switch independently, there could be coupling with a time lag or interference effects. This situation could give rise to linear chemical shifts, yet show dispersion curves that cannot be fitted together, as was the case for CheY here. Thus, we propose that CheY's allosteric switching is segmental in nature. It is not truly two-state, but there are several groupings of coupled residues that move with some independence and perhaps in a preferred sequential order. This rough model also suggests that CheY shares features of both conformational selection and induced fit. It does not appear that the A-state is fully formed in the absence of phosphorylation, since there is a poor correlation of $\Delta\omega$ and $\Delta\delta$. Yet, some residues may sample "active-like" *local* conformations. We speculate that binding and release of Mg^{2+} actuates conformational transitions along the allosteric pathway, from T87 and A88 to the W58-M85-E89-Y106 quartet (Figure 2.11). This is highlighted by maximal R_{ex} at Y106 occurring at the intermediate Mg^{2+} concentration of 1 mM.

The segmental nature of CheY's allosteric dynamics is perhaps best supported by the behavior of Y106. The rate of dynamic switching as observed by CPMG relaxation dispersion is clearly faster than the other switching residues, as evidenced by visual inspection of the dispersion curve (Figure 2.1B), as well as the fitted k_{ex} of 3100 s^{-1} (Table 2.1). Assuming that this observed motion corresponds to the allosteric conformational change, Y106 must be moving with at least partial independence from the other residues. That Y106 switches rapidly and with relative ease is supported by the significantly populated active-like inward position in 3CHY[42], as well as its low activation barrier for switching, as

determined from a computational study.[38] Even from the linear chemical shift data (Figure 2.8), it is seen that in 10 mM Mg^{2+}, Y106 is only ~20% toward the active state chemical shift, whereas the other linear shift data appear to be in a range of ~20-60% toward the active state (Figure 2.8D). Thus, neither relaxation dispersion nor chemical shift data fully support a model for pre-existing, concerted, two-state switching dynamics.

2.4.6 Comparison to other systems

Most of our knowledge of allosteric dynamics in RRs derives from NMR work on the nitrogen regulatory protein C (NtrC) receiver domain. A combination of chemical shift analysis (particularly of mutants) and transverse relaxation measurements led to the proposal of a two-state dynamic equilibrium between I and A conformations in NtrC.[39] The recent CPMG relaxation dispersion study on NtrC reported that those data are consistent with a two-state pre-existing equilibrium and that unphosphorylated NtrC populates the active state at the ~14% level;[40] interestingly, it appears that that study was carried out in the absence of Mg^{2+}. By contrast, because CheY does not appear two-state (even in the absence of Mg^{2+}) we cannot currently estimate the population of the active state. Even when considering residues locally, the populations of "excited states" from relaxation dispersion (Table 2.1) are typically much lower than those deduced from chemical shift plots (Figure 2.8), assuming that T87I populates only the inactive state. Unfortunately, relaxation dispersion data have not been reported for any other RR to the best of our knowledge. CPMG relaxation dispersion is an excellent approach to studying allosteric mechanisms if the conformational switching occurs on the timescale between a few hundred s^{-1} to ~3000 s^{-1}. Application of this method to other allosteric proteins holds the promise of revealing allosteric mechanisms. This has been

done successfully for the KIX domain of the CREB binding protein[20], catabolite activator protein (CAP)[19], and the PBX1 homeodomain[21], each of which exhibited two-state allosteric switching. Additionally, a study on the *trp* RNA-binding attenuation protein (TRAP) revealed allosteric motions as a series of localized conformational changes.[3] TRAP's behavior is similar to CheY's segmental dynamics and shed light on the diverse mechanisms proteins may employ to achieve allostery. These results imply that a protein may not solely employ a MWC or Koshland-Nemethy-Filmer (KNF) allosteric mechanism, but may combine them to form a complicated switching event.

CHAPTER 3

COLOCALIZATION OF FAST AND SLOW TIMESCALE DYNAMICS IN THE ALLOSTERIC SIGNALING PROTEIN CHEY[B]

3.1 Introduction

Allostery is widespread in biology as an effective means for regulating protein activity. While the existence of protein dynamics over a range of timescales is well established, how these dynamics contribute to allosteric protein function is poorly understood. The mechanism(s) underlying long-range communication necessary for allostery may include not only large changes in the conformation but also changes in the dynamic fluctuations about a mean conformation.[54, 86] Allosteric mechanisms have been shown to utilize the now familiar conformational change,[20, 21, 39] but more recent cases have been shown to solely use fast (i.e. ps-ns) internal dynamics.[6, 13, 14] It has been suggested that fast fluctuations are involved in facilitating the slower motions.[87] This connection between different timescales of motion and relation to function may be an important mechanism in allostery. However, to our knowledge, only for adenylate kinase has there been any discussion of the relationship between timescales.[87] Allosteric proteins often possess both slow and fast dynamics, but the relationship between the two remains unclear.

Escherichia coli CheY is an ideal protein for the study of protein motions as they relate to function since it is an allosteric signaling protein that displays significant motions on

[B] Published as: McDonald, L. R., Whitley, M. J., Boyer, J. A. & Lee, A. L. (2013). Colocalization of Fast and Slow Timescale Dynamics in the Allosteric Signaling Protein CheY. *J Mol Biol* 425, 2372-81.

multiple timescales. CheY is a response regulator (RR) from the two-component system that regulates chemotaxis.[22, 23] Upon phosphorylation at D57[24], CheY undergoes a conformational change that enables tight binding to the flagellar motor protein FliM (and minor interactions with FliN[30]) at a distal surface. CheY binding to FliM and FliN promotes a conformational change in the flagellar protein FliG that results in a switch from counterclockwise to clockwise flagellar rotation.[28, 88] Because of the necessity for a quick chemotactic response, the autodephosphorylation rate of CheY is 2.5 min^{-1}.[32] Therefore, the ability to study the phosphorylated state of CheY is difficult and it has become common to use the phosphoryl mimic BeF_x.[27, 33-35]

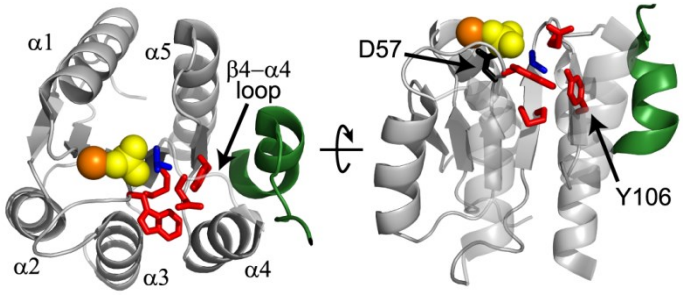

Figure 3.1. Crystal structure of CheY displaying residues involved in the conformational switch. FliM (green), BeF_x (yellow), and Mg^{2+}(orange)-bound CheY (1F4V[34]). The site of phosphorylation, D57, is highlighted in black. Allosteric signaling quartet, W58, M85, E89, and Y106, are shown as red sticks and T87 as blue sticks.

The CheY conformational switch has been extensively studied as a model RR for understanding phosphorylation induced activation. Phosphorylation in CheY is initially sensed by T87, A88 and K109 which form hydrogen bonds with the phosphoryl group and are important in the initial allosteric signaling.[35, 58] The phosphorylation-induced conformational change in CheY includes motion of the β4-α4 loop and a quartet of residues (E89, W58, M85, Y106)[89] whose motions result in the rotation of Y106 from an "out" solvent exposed rotamer to an "in" buried one (Figure 3.1).[27, 35]

Not only is CheY an excellent model RR for conformational change due to phosphorylation, RRs have become favored models for understanding conformational allostery. Previous studies of RRs focused on the conformational switch between inactive and active conformations on the slow timescale by monitoring the inherent equilibrium in the unphosphorylated protein.[39, 40, 59, 89] While fast backbone dynamics have also been reported, they have not been shown to be involved in the allosteric transition.[39, 59, 90] Here, we report the first multi-timescale study of both an unphosphorylated and phosphorylated RR including measurement of fast side-chain dynamics.

We previously reported motions on the μs-ms timescale that correlate with the intrinsic switching between inactive and active-like conformations in CheY in the absence of the activating phosphoryl group.[89] Here we observe the slow dynamics dampen and shift to the FliM binding interface upon phosphorylation (and accompanying Mg^{2+} saturation) of CheY. Additionally, we show large changes in methyl dynamics on the ps-ns timescale upon phosphorylation of CheY correlate with areas that undergo conformational change. Additional small significant changes are located in other regions known to affect CheY function. The dynamics on the slow and fast timescales localize to the same areas indicating a possible connection between timescales that may be necessary for the allosteric transition in CheY.

3.2 Materials and Methods

3.2.1 Protein expression and purification

E. coli CheY was overexpressed and purified as described previously.[89] The CheY plasmid was transformed into BL21 Star (DE3) cells (Invitrogen) and grown in minimal

media supplemented with the appropriate isotopes for the desired labeling utilizing $^{15}NH_4Cl$ [99%] and/or D-glucose [U-$^{13}C_6$-99%]. Samples for relaxation dispersion and ^2H relaxation were grown to yield > 80% and ~60% ^2H incorporation, respectively. Pure CheY was concentrated and stored in NMR buffer (50 mM NaP_i, 10 mM $MgCl_2$, 0.02% NaN_3, pH 7.0) at 4 °C.

3.2.2 Preparation of BeF_x-bound CheY

As previously described[89], BeF_x-bound CheY was prepared with 4 mM $BeCl_2$ and 25 mM NaF to ensure saturation of 1 mM CheY and in an ideal ratio for a BeF_3 complex. Assuming a K_d of 7.7 μM for BeF_x and CheY[43], 99.7% of CheY is bound by BeF_x. The NMR samples were prepared by starting with a typical CheY-unP sample (1 mM CheY and 10% ^2H_2O in NMR buffer) and adding the $BeCl_2$ and lastly NaF. Samples were left at room temperature overnight and centrifuged briefly before transferring to an NMR tube.

3.2.3 NMR Spectroscopy

All NMR spectra were collected on 1 mM CheY in NMR buffer and 10% ^2H_2O at 25 °C except for relaxation dispersion experiments, which were collected at 15 °C. NMR experiments were collected on Varian INOVA spectrometers equipped with room-temperature (500 and 600 MHz) or cryogenic (700 MHz) probes. Side-chain methyl assignments were made by utilizing previously assigned C^α and C^β chemical shifts and a three-dimensional $HCCH_3$ total correlated spectroscopy spectrum.[91] Resonances from methionine methyl groups were assigned using a combination of a three-dimensional methyl-

methyl NOESY spectrum[92] and mutation of methionine residues. All NMR data were processed using NMRPipe[62] and visualized with NMRDraw and NMRView[63].

3.2.4 ^{15}N CPMG relaxation dispersion

^{15}N relaxation dispersion of CheY-P was performed using a relaxation-compensated CPMG experiment[64] utilizing a 20 ms total CPMG period. Ten τ_{cp} values with two duplicates and a reference experiment were collected interleaved at 700 MHz. $R_{2,eff}$ was calculated from peak intensities as described previously[65]. Approximate R_{ex} was calculated by using $R_{2,eff}$ values from this experiment: Approximate $R_{ex} = R_{2,eff}(\tau_{cp} = 5\text{ ms}) - R_{2,eff}(\tau_{cp} = 0.556\text{ ms})$. Error in approximate R_{ex} was propagated from peak intensity analysis of duplicate τ_{cp} values. Relaxation dispersion of CheY-unP was previously published[89] and approximate R_{ex} values were calculated in the same manner as CheY-P for data collected at 700 MHz.

3.2.5 ^{15}N backbone and ^{2}H methyl relaxation

Standard backbone ^{15}N relaxation experiments were used to collect the T_1, T_2, and $\{^1H\}$-^{15}N NOE data at 500 MHz for CheY-unP and at 500 and 600 MHz for CheY-P[93]. For T_1 and T_2 experiments, 9 or 10 relaxation time points along with 3 duplicates were collected. For the $\{^1H\}$-^{15}N NOE, the recycle delay was a combination of a ^1H saturation time of 5.5 or 6 s and a pre-delay of 100 ms. ^2H T_1 and $T_1\rho$ experiments[94] to measure $I_zC_zD_y$ and $I_zC_zD_z$ relaxation[95] for side-chain ps-ns dynamics were collected at 500 and 700 MHz for CheY-unP and at 500 and 600 MHz for CheY-P. For each experiment, 9 relaxation time points along with 3 duplicate points were collected.

3.2.6 Relaxation analysis

Relaxation decays were best fit to single exponentials using in-house programs. Motions on the ps-ns timescale were characterized using the model-free formalism.[46, 47] Global correlation times for both CheY-unP and CheY-P were determined to be 8.1 ns from global analysis of the data. Backbone relaxation rates were fitted to the five standard model-free models and the Akaike information criterion[96] was used for model selection utilizing the in-house program relxn2.2.[97] Determination of side-chain methyl dynamics parameters (order parameter, S^2_{axis} and effective correlation time, τ_e) was carried out as previously described.[98]

Table 3.1. Local fits of ^{15}N CPMG relaxation dispersion for CheY-P.

Residue	k_{ex} (s^{-1})	Δω (ppm)	p_A	$R_2°$ (700 MHz)	χ^2
8	260 ± 40	7.2 ± 0.9	0.99 ± 0.01	17.2 ± 0.4	12
38	220 ± 50	5.3 ± 0.7	0.98 ± 0.01	14.5 ± 0.3	3.8
60	250 ± 30	7.4 ± 0.8	0.99 ± 0.01	16.3 ± 0.3	16
87	200 ± 40	2.9 ± 0.7	0.99 ± 0.01	18.7 ± 0.3	0.23
88	270 ± 90	4.2 ± 1	0.99 ± 0.01	18.3 ± 0.6	1.2
89	190 ± 30	5.2 ± 1	0.99 ± 0.01	18.5 ± 0.3	0.32
91	320 ± 80	7.1 ± 2	0.99 ± 0.01	14.4 ± 0.5	1.2
93	3100 ± 1000	4.4 ± 0.9	0.99 ± 0.01	21.2 ± 0.9	0.62
104	240 ± 60	2.5 ± 0.5	0.99 ± 0.01	20.7 ± 0.3	3.5
106	2800 ± 1000	0.43 ± 0.08	0.85 ± 0.05	20.7 ± 0.3	0.17
107	840 ± 100	8.5 ± 1	0.99 ± 0.01	18.5 ± 0.6	48
117	300 ± 40	3.1 ± 0.6	0.99 ± 0.01	18.4 ± 0.2	0.40
119	230 ± 20	7.6 ± 0.9	0.99 ± 0.01	17.1 ± 0.3	0.21
124	2100 ± 1000	0.28 ± 0.06	0.81 ± 0.09	18.3 ± 0.2	0.13

^{15}N CPMG relaxation dispersion at 700 MHz were locally fit to the Carver-Richards equation with curves shown in Figure S1. Since only one field of data is used, the fits are not quantitatively reliable and strict interpretation of the fitted parameters is not recommended.

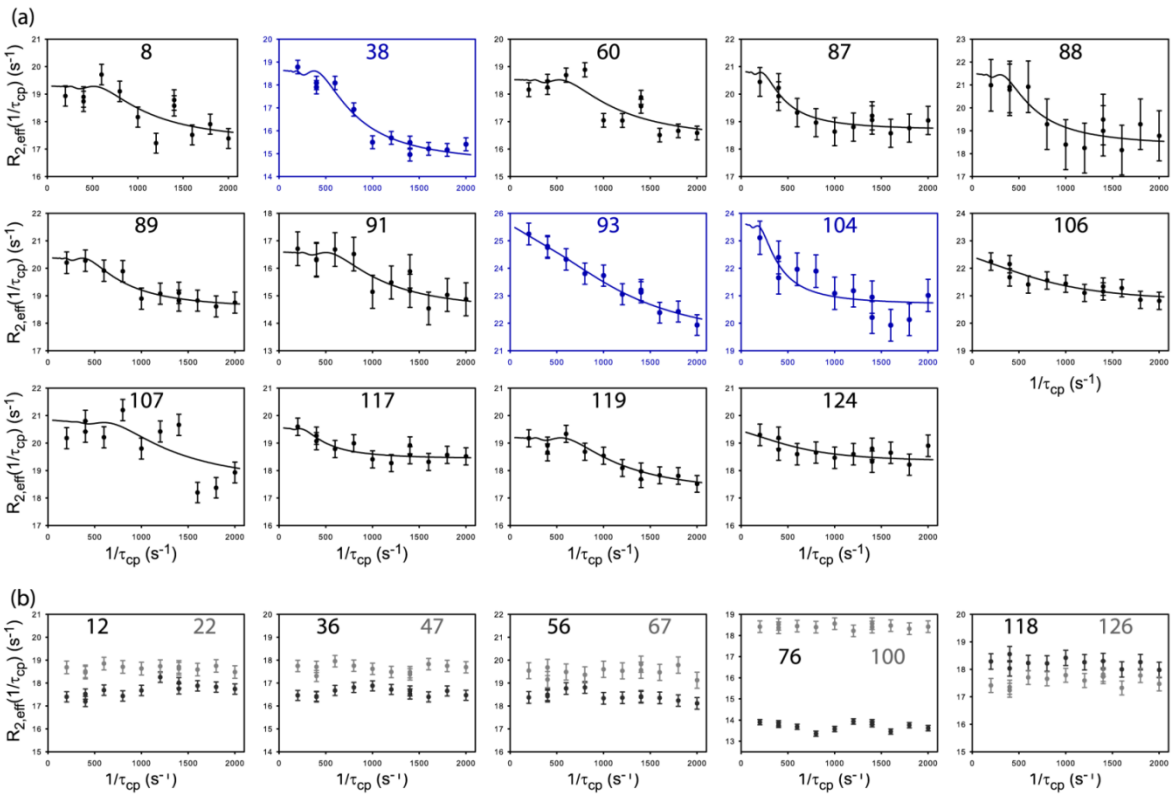

Figure 3.2. ^{15}N CPMG relaxation dispersion of BeF_x-bound CheY at 700 MHz. (a) Curves are displayed for all residues with R_{ex} > 1 s^{-1} shown in Figure 3.3 with lines displaying local fits to the Carver-Richards equation (Table 3.1). However, because only one field of data was used, these fits are not quantitatively reliable and strict interpretation of the fitted parameters is not recommended. (b) Example residues (12, 22, 36, 47, 56, 67, 76, 100, 118, & 126) that do not have significant R_{ex}. A few of these (12, 36, 56, & 126) display significant dynamics in CheY-unP, but not CheY-P.

3.3 Results and discussion

3.3.1 µs-ms dynamics are dampened and shift toward the FliM binding interface upon phosphorylation of CheY

^{15}N Carr-Purcell-Meiboom-Gill (CPMG) relaxation dispersion experiments[48] were used to measure motions on the µs-ms timescale for unphosphorylated CheY (CheY-unP)[89] and BeF_x-bound CheY (CheY-P). This experiment measures the contribution from a conformational exchange process on the µs-ms timescale (R_{ex}) to the effective transverse relaxation rate ($R_{2,eff}$) as a function of the spacing between 180° pulses in the CPMG train (τ_{cp}),

$$R_{2,eff} = R_2^\circ + R_{ex}(1/\tau_{cp}), \quad (3.1)$$

where $R_2°$ is the intrinsic relaxation rate.[64] Full relaxation dispersion experiments can be fit to reveal the kinetic and thermodynamic parameters of the exchange. For CheY-P, full relaxation dispersion experiments were carried out, but only a few residues have a high enough R_{ex} (> 2 s^{-1}) to enable accurate fitting and it is therefore more beneficial to only consider the level of R_{ex} in each CheY state (details in Materials and Methods). The complete curves and fits for these residues (R_{ex} > 2 s^{-1}) can be seen in Figure 3.2a and Table 3.1.

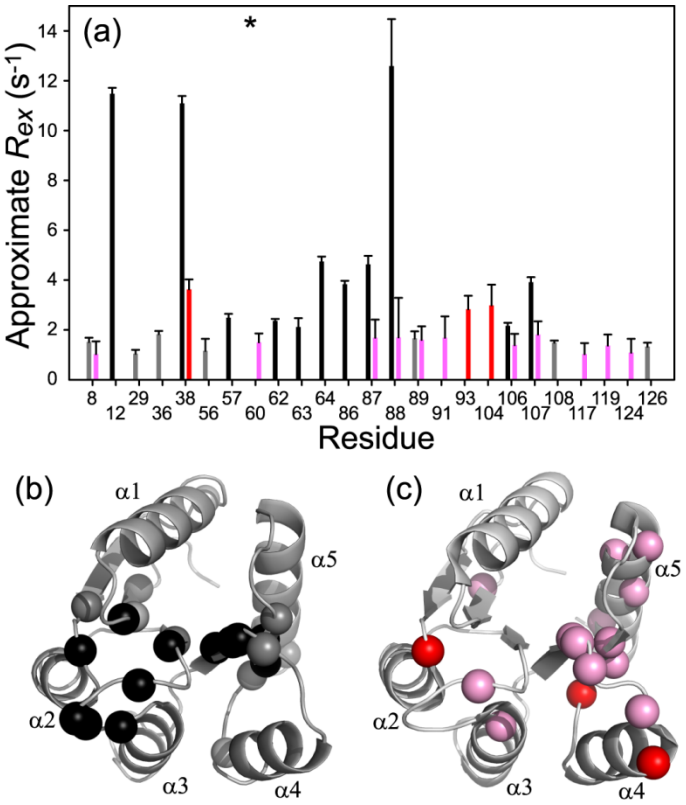

Figure 3.3. Comparison of µs-ms motions between CheY-unP and CheY-P. Approximate R_{ex} is shown as bars (a) and displayed on the crystal structure of CheY-unP (black/grey) (b) and CheY-P (red/pink) (c). Black or red indicates R_{ex} > 2 s^{-1} and grey or pink indicates 2 s^{-1} > R_{ex} > 1 s^{-1}. R_{ex} below 1 s^{-1} is considered zero and not shown. Residues are displayed if R_{ex} is greater than 1 s^{-1} for either CheY-unP or CheY-P. Approximate R_{ex} = R_{2eff}(τ_{cp} = 5 ms) – R_{2eff}(τ_{cp} = 0.556 ms) at 700 MHz. For both CheY-unP and CheY-P, an F-test ($\alpha_{critical}$ = 0.10) was used to remove any residues with unreliable R_{ex} values by fitting to both a straight line and a simple two-state model. M60 failed the F-test indicated by an asterisk for CheY-unP.

Here, we compare μs-ms dynamics in CheY-P to CheY-unP. CheY sample buffers with 10 mM Mg^{2+} were used, even though CheY-unP is not fully saturated with Mg^{2+} at this concentration[89] (CheY-P is), as partial saturation is expected under normal cellular conditions. Overall, there is a decrease in R_{ex} upon phosphorylation of CheY (Figure 3.3a) compared to CheY-unP in the presence of 10 mM Mg^{2+}. Surprisingly, R_{ex} is not zero for CheY-P. In CheY-unP, dynamics on this timescale report on the switch between inactive and active states (Figure 2.3b).[89] We would expect phosphorylated CheY to be fully switched to the active state and therefore have zero R_{ex}. However, we see small amounts of R_{ex} throughout the protein and much of it localized to the β4-α4 loop and near to Y106 (Figure 3.3c). This indicates that CheY-P may be primarily in the active conformation but is able to switch to another conformation(s), such as the inactive state.

In CheY-unP, residues with dynamics on this timescale localize to the active site and allosteric pathways (Figure 3.3b). Upon phosphorylation, residues with dynamics are shifted towards the FliM binding interface (Figure 3.3c). While the allosteric pathway continues to have a small amount of R_{ex}, many active site residues are diminished (Figure 3.3b) and a new low level of R_{ex} appears near to the FliM binding interface. The slow dynamics in CheY-P are indicative of its ability to access more than one conformation on the μs-ms timescale. Since CheY does not switch to the active state in a two-state concerted manner[89], it is not surprising that a different selection of residues show motions in the phosphorylated state. CheY-P is likely locally accessing the inactive conformation in the regions of the allosteric pathway. By contrast, the new dynamics of CheY-P at the FliM-binding interface are monitoring motions not present in CheY-unP and may be indicative of CheY-P's dynamics between multiple active-like states. It is possible that these are not new motions, but the timescale of the

motions has shifted. If this were the case, motions in CheY-unP may have been too fast to monitor by these experiments, but upon phosphorylation the motions become slow enough to be detectable.

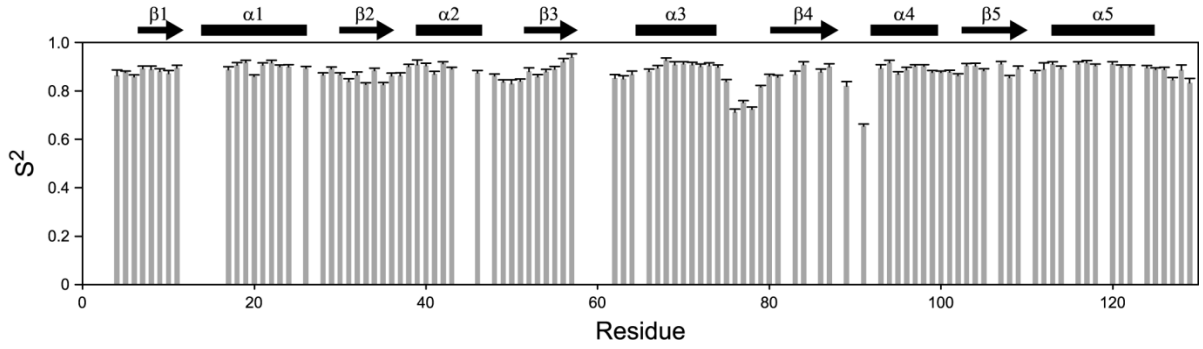

Figure 3.4. Backbone order parameters of CheY-unP. Residues with no data are due to no assignment, proline, or overlapped resonances. Error bars were determined by peak intensity analysis of duplicate experiments. The CheY secondary structure is displayed above.

3.3.2 Ps-ns dynamics become both more rigid and more flexible upon phosphorylation of CheY

NMR ^{15}N and ^{2}H relaxation experiments were collected for CheY-P and CheY-unP to measure dynamic fluctuations on the ps-ns timescale. The dynamics report on the N-H bond vector for ^{15}N relaxation and the methyl symmetry axis of a CH_2D methyl isotopomer for ^{2}H relaxation. Model free analysis of the relaxation parameters yields the order parameter (S^2) for the bond vector which ranges from 0 (no orientational bias) to 1 (completely rigid).[46, 47] In addition to the order parameter, the effective correlation time (τ_e) for the internal motion of the bond vector is obtained.

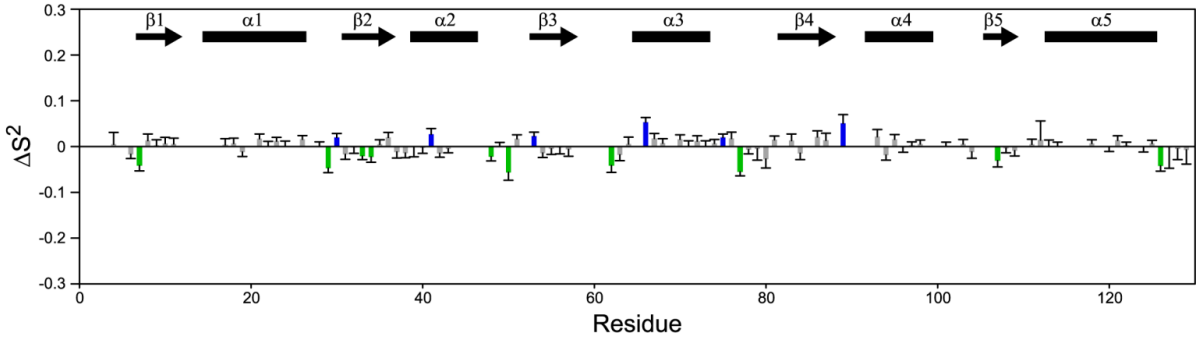

Figure 3.5. Changes in backbone order parameter upon phosphorylation of CheY. Colored bars indicate the difference is more than twice the error where blue is a rigidification and green becomes more flexible upon phosphorylation: $\Delta S^2 = S^2_{BeFbound} - S^2_{free}$. The CheY secondary structure is displayed above.

The backbone dynamics were measured utilizing ^{15}N T_1, T_2, and $\{^1H\}$–^{15}N NOE relaxation experiments. We found the CheY backbone to be rigid on the ps-ns timescale in areas of secondary structure. The order parameters for CheY-unP ranged from 0.66 to 0.94 with an average of 0.88 (Figure 3.4) which is consistent with previously reported values.[61] Upon phosphorylation, backbone dynamics only change slightly throughout the protein (Figure 3.5). The small changes occur in both directions: some residues become more rigid and others become more flexible upon phosphorylation.

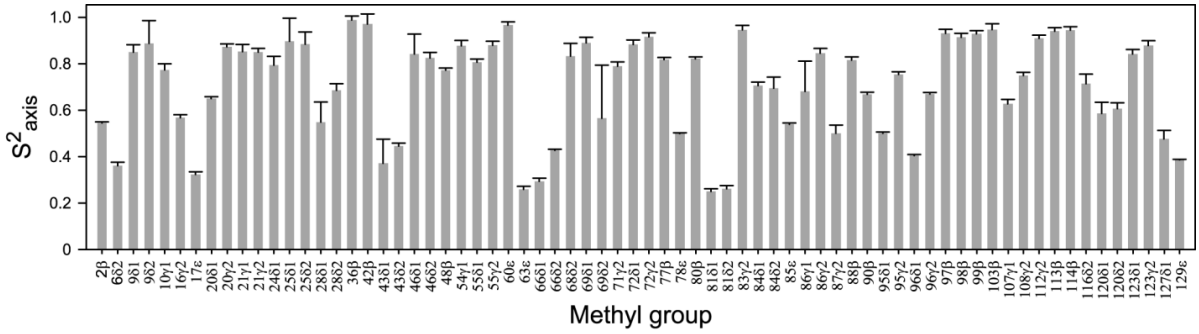

Figure 3.6. Methyl side-chain order parameters of CheY-unP. Error bars were determined by peak intensity analysis of duplicate experiments.

It is becoming increasingly clear that side-chain dynamics can reveal functional dynamics that are invisible to the backbone since side-chain dynamics are more heterogeneous and more sensitive to perturbation.[99] ^{2}H relaxation experiments[94] were collected to measure the ps-ns dynamics of the methyl side chains of CheY-unP and CheY-P. The methyl order parameters (S^2_{axis}) ranged from 0.25 to 0.99 with an average of 0.71 for CheY-unP (Figure 3.6) Comparison of CheY-unP and CheY-P order parameters show larger changes in order parameter than the backbone, with some methyl groups with increased flexibility and some with increased rigidity upon phosphorylation (Figure 3.7a). Overall, it appears phosphorylation induces an slight increase in flexibility in CheY.

T87 and A88, which are located very close to the bound BeF_x, have increased rigidity upon phosphorylation. This is to be expected since binding pockets typically become more rigid upon ligand binding. Furthermore, the hydroxyl group of T87 and backbone of A88 form hydrogen bonds with the phosphate group. Therefore, it is not surprising that these particular methyl groups become more rigid. Other than at the active site, most changes in dynamics correspond to increases in flexibility upon phosphorylation. This is commonly seen and thought to compensate for the entropic penalty incurred by the rigidification of the active site residues.[100, 101] Many other residues exhibit changes in dynamics, although it is clear that much of the protein is silent (Figure 3.7c).

Furthermore, some methyl groups have a change in the correlation time as measured by τ_e (Fig. 3.7b) and many are not accompanied by a change in S^2_{axis}. Methyl groups with a change in τ_e are distributed throughout the protein with many near to the active site and FliM binding interface (Fig. 3.7d). The methyl groups with the largest change in τ_e, L28, L43, and A113 do not undergo changes in S^2_{axis} and are located far from the active site. This

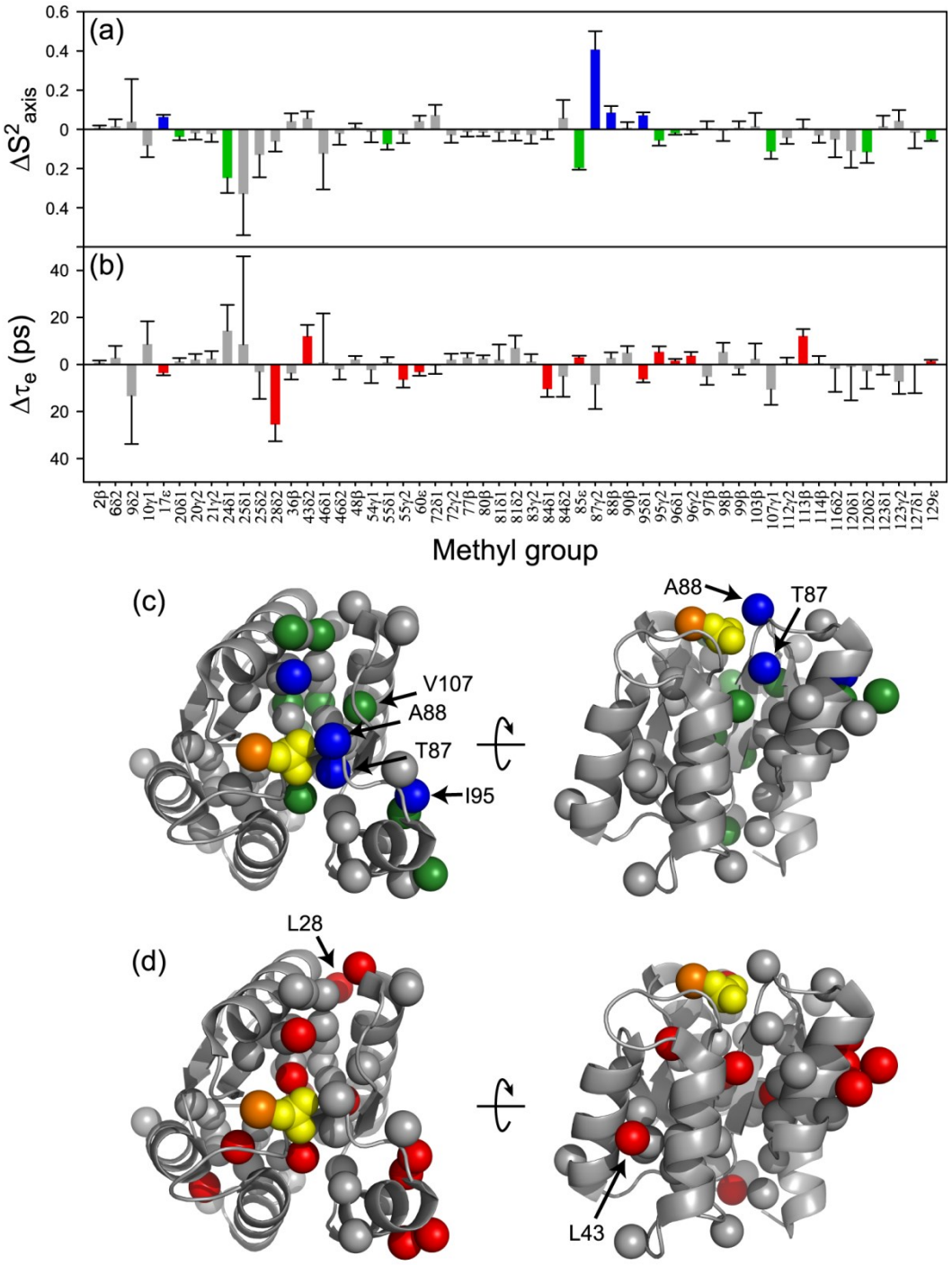

Figure 3.7. Difference in ps-ns motions between CheY-unP and CheY-P. Change in the order parameter (a) and correlation time (b) upon phosphorylation with colored bars shown as colored spheres in (c) and (d), respectively. $\Delta S^2_{axis} = S^2_{axis}$(CheY-P) – S^2_{axis}(CheY-unP) and $\Delta\tau_e = \tau_e$ (CheY-P) – τ_e (CheY-unP). Blue indicates an increase in rigidity upon phosphorylation, green is an increase in flexibility, and red is a change in τ_e. Colored bars indicate a significant change determined by $\Delta S^2_{axis} > 2\sigma$ or $\tau_e > 2\sigma$.

phenomenon was also observed upon mutation in eglin c.[97] A large change in τ_e without a change in S^2_{axis} indicates a large change in the rate of rotation of the methyl group about the symmetry axis. Further interpretation of changes in τ_e is unclear, yet it remains a reliable measure of the changes in dynamics on this timescale.

3.3.3 The largest changes in ps-ns side-chain dynamics are along the allosteric pathway

The allosteric switch in CheY and other RRs has been well characterized as a conformational change between inactive and active states.[27, 35, 39, 40, 59, 89] It is this conformational switch (which is triggered by phosphorylation) that allows increased activity at a distal site. In CheY, the location of the conformational change as seen in numerous crystal structures[27, 37, 44] and confirmed by numerous mutational studies[32, 74, 102] centers around the initial sensing by T87 and A88. These residues couple to the movement of the β4-α4 loop (especially E89), rotation of W58 about χ_2, rotation of M85 about χ_1 and, most importantly, inward rotamer selection of Y106. This conformational switch can be monitored by NMR relaxation experiments (above).

The largest changes in side-chain methyl ps-ns dynamics upon phosphorylation occur in this region (indicated by the oval in Fig. 3.8). Not only are there changes at T87 and V107 (adjacent to Y106 motion), but also large changes at M85 and A88. In addition to V107, there are significant changes to I95 which contacts Y106, is involved in FliM binding, and alters CheY's activity when mutated.[80] This further confirms the involvement of T87, A88, M85, Y106, and I95 in the conformational change and allosteric signaling upon phosphorylation.

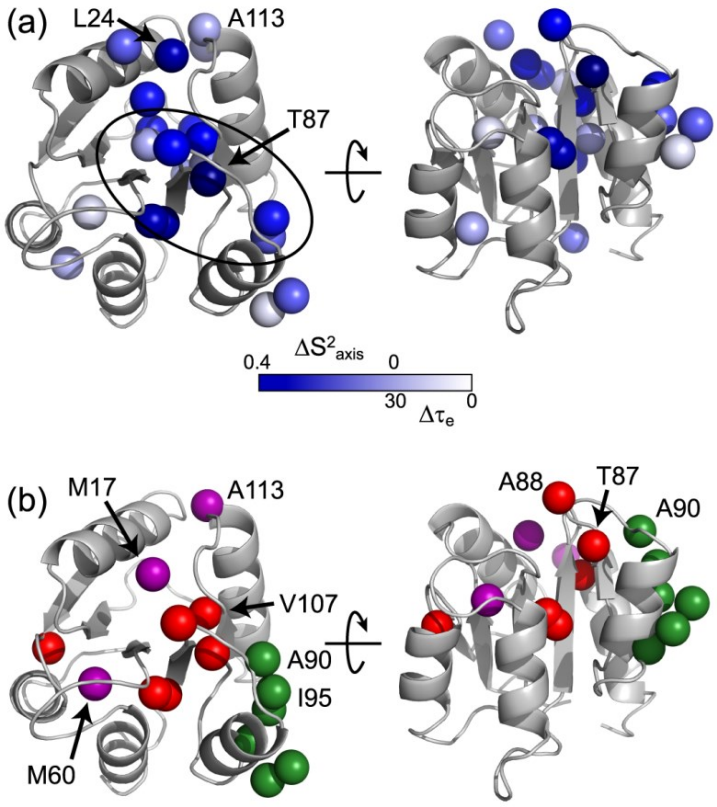

Figure 3.8. Largest changes in ps-ns dynamics localize to the region of allosteric conformational change. (a) Methyl groups with a change in ps-ns dynamics upon phosphorylation are shown as blue spheres. A gradient color scheme is used in which the largest ΔS^2_{axis} are darkest blue and lightest colors indicate a change in τ_e without a change in ΔS^2_{axis}. Residues with a change in both S^2_{axis} and τ_e are shown according to ΔS^2_{axis}. A region that contains many large changes in ΔS^2_{axis} and τ_e that corresponds to the allosteric conformational switch are enclosed by the oval. (b) The locations of residues active in the allosteric switch (red), FliM binding (green), or mutation (purple) have their methyl groups shown as spheres.

The remainder of the β4-α4 loop shows a mixture of rigidification and flexibility upon activation. Although the ^{2}H methyl relaxation experiments yield no information on side-chain dynamics of E89, a small but detectable increase in the backbone NH S^2 from 0.82 ± 0.02 to 0.87 ± 0.01 was observed for this residue (Figure 3.5), consistent with the formation of a hydrogen bond between the side-chain hydroxyl of Y106 and the backbone carbonyl of E89 upon activation[27]. Interestingly, the C^β S^2_{axis} of A90 is unusually low for both inactive and activated states, at a value of ~0.67 ± 0.01, compared to the CheY average

of 0.86 for alanine. No backbone S^2 values were obtained for A90 due to spectral overlap, but the low S^2_{axis}, as well as the low NH S^2 of 0.66 ± 0.01 for K91 (of the inactive state), suggest that A90 and K91 are quite flexible in the inactive state. Together, these data indicate that in general the β4-α4 loop is flexible, but rigidification of the backbone at E89 upon phosphorylation does not affect the flexibility of the A90 C^{β}.

3.3.4 Small significant changes in ps-ns side-chain dynamics are in distal regions associated with CheY function

Many methyl groups with a small, but significant change in methyl order parameter or a change in correlation time are near to the active site yet are not known to be involved in the allosteric switch or coordinating the Mg^{2+} or BeF_x. For example, M17 and M60 have a small increase in S^2_{axis} and a small change in τ_e, respectively. These residues are both near to the active site (Fig. 3.8b) but are not considered active site residues. In the CheY ^{15}N-^{1}H HSQC, M60 is a broad peak and has a large chemical shift change upon Mg^{2+} binding and subsequent BeF_x binding. Therefore, M60 reports on the binding of these two ligands. Since M17 has been shown to be intolerant of mutation, it was proposed to play a role in the propagation of signal after phosphorylation.[102] Furthermore, mutation of methionine to alanine at 17 produces significant changes in the chemical shift of Y106 and V107 more than 9 Å away (McDonald & Lee, unpublished), indicating its involvement in the allosteric pathway. Both M17 and M60 are not known to be directly involved in the allosteric signaling upon phosphorylation, but both seem to have functional importance. Their significant changes in side-chain dynamics on the fast timescale may be indicative of their involvement in the allosteric signaling.

Another methyl group that has only a change in τ_e without a change in S^2_{axis} is A113. A mutation of A113 to proline causes increased activity in CheY as measured by increased clockwise flagellar rotation and FliM binding affinity.[74] Alternatively, a mutation to asparagine at this position results in an increase of counterclockwise flagellar rotation. A113 is more than 17 Å from the bound BeF_x and 12 Å from the bound FliM peptide (using pdb 1F4V[34]). Mutations that affect CheY function at A113 are surprising since it is so far from the active site, FliM, and any residues involved in the allosteric transition. Therefore, it is especially interesting to observe a change in ps-ns dynamics upon phosphorylation in the methyl group of A113. Other nearby methyl groups also have perturbations to dynamics, such as I20, L24, I55, and L120 (all decrease in S^2_{axis}, Figure 3.7). All of these methyl groups localize to the pocket between the beta sheet and helices 1 and 5. The residues form a network between the active site and the FliM binding interface (Figure 3.8a). This suggests that the link between A113 and CheY function may be directly related to ps-ns dynamics associated with the side chains. To our knowledge, other than mutational studies of A113, this region of CheY or any RR has never been shown to be important for function.

3.3.5 Correlation of fast and slow motions in CheY

The relationship between the overall increase or decrease in flexibility of a protein on different timescales is not well understood. Here, by monitoring changes in both fast and slow dynamics upon phosphorylation, we hoped to shed light on this potentially complex relationship. Upon phosphorylation of CheY, we report an apparent decrease in slow dynamics with an overall slight increase in flexibility in the side chains on the fast timescale. However, we do observe an apparent increase in rigidity on both timescales in the active site.

This complex behavior in CheY demonstrates the difficulty in predicting the relationship between motions on different timescales.

Recent reports of changes in side-chain dynamics on the fast timescale link these changes to the function of the protein. These reports rely on the connection between fast dynamics and conformational entropy.[6-9] For calmodulin,[6] a PDZ domain,[13] and catabolite activator protein[14] changes in conformational entropy regulate the protein's binding activity. In these cases, changes in the dynamics were detected throughout the protein as opposed to being localized to the active site. This global redistribution of side-chain motions has an overall effect on the conformational entropy of the system to affect protein function. Here, we report the changes in ps-ns dynamics of CheY are largely localized to the active site and residues in the allosteric pathway. In CheY, at least for the case of phosphorylation, there is not a global effect on the motions of the methyl side chains on the fast timescale as seen in these other cases.

In addition to the spatial restriction of changes in fast side-chain dynamics in CheY, there is segregation of residues that become more rigid from those that become more flexible. The largest rigidifications to ps-ns side-chain dynamics are in the active site with residues that become more flexible distributed nearby (Figure 3.7c). This localization of rigidifying residues may be necessary for the allosteric conformational switch in CheY. 9 of 13 residues with a change in ps-ns dynamics become more flexible upon phosphorylation and this is likely to entropically compensate for the large rigidifications in the active site.[100, 101] Furthermore, CheY seems to be built for this kind of entropic compensation. All four methyl groups that become more rigid upon phosphorylation have low S^2_{axis} values in CheY-unP compared to the average values for that particular methyl group. Most interesting is T87 $C^{\gamma 2}$

which has the largest increase in S^2_{axis} and has an S^2_{axis} value of 0.50 ± 0.04 in CheY-unP where the average CheY values for Thr $C^{\gamma 2}$ is 0.69. In the unphosphorylated state of CheY, many methyl groups, especially T87 $C^{\gamma 2}$ seem "poised" for the change in ps-ns dynamics upon phosphorylation. Residues that become more flexible do not seem to be "poised" (3 of 9 have high S^2_{axis} values in CheY-unP), but nearly all (8 of 9) have less than average S^2_{axis} values in CheY-P. Together, this suggests the entropic compensation in CheY may be a necessary element of the allosteric switch.

While the entropic compensation may be necessary in CheY, changes in the ps-ns dynamics caused by phosphorylation seem to be restricted to locations near to the active site. Many distal regions of CheY are silent on the μs-ms timescale and have little or no change in fast dynamics upon phosphorylation. For proteins that have been similarly studied on multiple timescales[14, 103], there is a global impact on ps-ns dynamics upon perturbation. These proteins (in addition to others with reports of changes in ps-ns timescale dynamics upon perturbation[6, 13]) seem to readily spread changes in ps-ns dynamics throughout the protein. CheY's unique ability to subdue this propagation of ps-ns dynamics changes may reflect a distinct mechanism by which proteins utilize ps-ns dynamics for function.

Localization of changes in fast dynamics at regions of allosteric conformational change is not surprising. This is due to the conformational change which causes a change in the chemical environment of a methyl group and the very responsive ps-ns side-chain dynamics being affected. In CheY, residues A113, M60, and M17 are in regions without large conformational change and do not have measureable slow motions. Nevertheless, the presence of modest changes in ps-ns side-chain dynamics at these residues suggests changes

in ps-ns dynamics in CheY go beyond the simple explanation of a mere effect from conformational change.

CheY reveals a mechanism that utilizes segmental motions on the timescale of the conformational change[89] and colocalized changes in faster fluctuations upon that conformational change. This correlation of motions on different timescales in CheY sheds light on the importance of the relationship between multiple timescales of motion. The nature of the relationship and how it results in allosteric function is still poorly understood. Utilization of CheY mutants may yield additional information to better understand the relationship between timescales in an allosteric signaling protein.

CHAPTER 4

ACTIVATION MECHANISM OF ACTIVATING MUTANT A113P CORRELATES FAST AND SLOW DYNAMICS OF CHEY

4.1 Introduction

Allostery is a common mechanism for signal transduction and the regulation of cellular pathways. Dynamics occur over a range of timescales and are crucial to the allosteric function; however, it is not understood how the dynamics contribute to the allosteric mechanisms. Furthermore, dynamics occur over a range of timescales and the relationship between these dynamics and how they together affect protein function is unclear. Dynamics on a slow (μs-ms) timescale typically affect an allosteric protein's function by a conformational switch between an inactive (I) and an active (A) conformation. Additionally, fast fluctuations about a mean conformation have been shown to be important for function in a number of proteins.[6, 13, 14] Dynamics on different timescales are typically studied separately, yet there could be a link between them that is important for protein function and specifically for allosteric signaling. Therefore, there is a need for multi-timescale experimental dynamics data on allosteric proteins.

Escherichia coli CheY is an excellent protein for the study of the relationship of dynamics and allostery. As a response regulator (RR) receiver domain, CheY is a small well behaved protein that has been studied extensively for its role in chemotaxis regulation. CheY is composed of only a single domain and upon phosphorylation by its two-component system

partner, the histidine kinase CheA, binds to the flagellar motor. Binding of CheY to the flagellar motor protein FliM causes a change in the rotation of the flagella to clockwise.

Unphosphorylated CheY is in a dynamic equilibrium between inactive (and inactive-like; I) conformation(s) and active (and active-like; A) conformation(s). It was previously shown that this conformational change is not a simple two state switch, but occurs in a segmental manner (Chapter 2[89]). Furthermore, changes in the methyl dynamics on a fast timescale (ps-ns) upon phosphorylation correlate to the regions of conformational change (Chapter 3[104]). This indicates a possible connection between dynamics on multiple timescales is important in the allosteric mechanism in CheY.

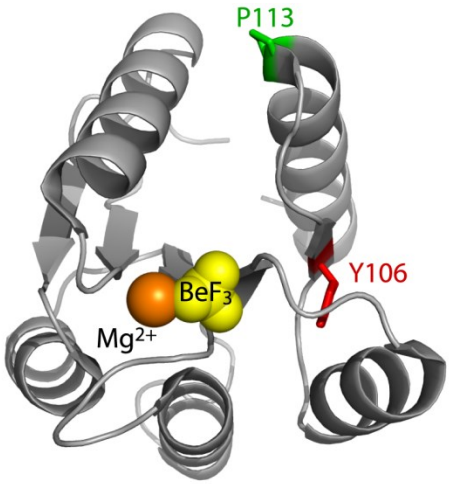

Figure 4.1. Location of P113 compared to the site of phosphorylation. The crystal structure of A113P CheY with the site of mutation (green), Y106 (red), phosphoryl mimic (BeF_x), and Mg^{2+} (orange) highlighted.

Mutation of alanine 113 to proline in CheY is an activating mutation based on non-chemotactic behavior resulting from increased clockwise rotation of flagella.[74] This behavior could be due to a number of changes in CheY and its interactions with CheA, CheZ and FliM. Bourret and coworkers suggest mutation of A113P causes the I-to-A equilibrium in CheY to be shifted toward the active conformation determined by an increased

autophosphorylation rate, increased binding to FliM, and increased binding to CheZ.[74] A113 is located at the start of α5 distal from the site of phosphorylation (Figure 4.1). It is unclear how a mutation in this location could cause a shift in the conformational equilibrium.

Here, we observe the dynamics of CheY A113P on a range of timescales to gain further insights into the allosteric mechanism of WT CheY. Determination of the activation mechanism of this mutant may lead to an increased understanding of the intramolecular interactions of the WT protein. Chemical shift perturbation and relaxation dispersion data of A113P support A113P's shift toward the active population. Changes in fast timescale dynamics upon mutation to A113P in the unphosphorylated state are significant for a number of methyl groups. Many of these changes occur in the same methyl groups in which changes were noted upon phosphorylation of WT CheY. This indicates, according to the fast dynamics of the protein, a similar activation process occurs whether the protein is activated by A113P mutation or BeF_x binding. Together, this is further validation of an important connection between dynamics on multiple timescales in the allosteric transition in CheY.

4.2 Materials and Methods

4.2.1 Protein Expression and Purification

Overexpression and purification of *E. coli* CheY was carried out as previously described (Section 2.2). The CheY plasmid was transformed into BL21 Star (DE3) cells (Invitrogen) and grown in minimal media utilizing the appropriate isotopes. $^{15}NH_4Cl$ [99%] and/or D-glucose [U-$^{13}C_6$-99%] were used to get the appropriate labeling. Additionally, samples were grown in partial $^2H_20$ to yield approximately 60% ^2H and >80% ^2H incorporation for ^2H relaxation and ^{15}N CPMG relaxation dispersion, respectively. Pure

CheY was concentrated and stored at 4 °C in NMR buffer (50 mM NaP_i, 10 mM $MgCl_2$, 0.02% NaN_3, and pH 7.0). The A113P mutant was made by site-directed mutagenesis and assigned with triple resonance experiments.

4.2.2 NMR Spectroscopy

All NMR experiments were collected on 1 mM protein with NMR buffer. Samples with BeF_x were made as previously described (Section 2.2). Relaxation dispersion experiments were collected at 15 °C while all others were at 25 °C. All NMR experiments were collected on Varian INOVA spectrometers equipped with room-temperature probes except for 600 MHz ^2H relaxation of A113P-unP which was collected on a Bruker Avance Spectrometer. All NMR data were processed with NMRpipe[62] and analyzed with nmrDraw and NMRView.[63]

4.2.3 ^{15}N CPMG relaxation dispersion

As previously described (Section 2.2), ^{15}N relaxation dispersion experiments were collected using relaxation-compensated CPMG experiments.[64] For unphosphorylated A113P (A113P-unP), relaxation dispersion experiments were collected at 500 and 700 MHz with a 40 ms total time and 13 unique τ_{cp} values, two duplicates and a reference experiment. Planes were collected interleaved and peak intensities were used to calculate $R_{2,eff}$.[65] For phosphorylated A113P (BeF_x bound A113P; A113P-P) relaxation dispersion experiments were collected for τ_{cp}= 10 ms and τ_{cp}= 0.556 ms and an approximate R_{ex} is calculated as previously described (section 2.2).

Relaxation dispersion analysis of A113P-unP was in the same manner as WT (section 2.2). A two-state model was assumed to fit using the Carver-Richards equation using the in house program exrate2.0.

4.2.4 ^{15}N backbone and ^{2}H methyl relaxation

Standard ^{15}N relaxation experiments (T_1, T_2, and $\{^1H\}$-^{15}N NOE) were used to measure the backbone ps-ns dynamics of A113P CheY at 500 MHz. For T_1 and T_2 experiments, 9 relaxation time points plus 3 duplicates were collected interleaved. A recycle delay was a 4.5 s saturation period plus a 100 ms pre-delay. For methyl side-chain ps-ns dynamics of A113P-unP, ^{2}H relaxation was collected by T_1 and $T_{1\rho}$ experiments[94] to measure IzCzDy and IzCzDz relaxation.[95] Nine relaxation time points plus three duplicates were collected at 500 MHz and collected interleaved at 600 MHz.

In-house programs were used to fit relaxation decay curves to single exponentials. The model-free formalism was used to characterize the dynamics on the ps-ns timescale. Global tumbling of A113P-unP was measured to be 7.9 ns which is very close to the WT value of 8.1 ns (reported in Chapter 3[104]). As described for WT above (Section 3.2), A113P backbone relaxation rates were fit to the standard model-free models and side-chain methyl dynamics were fit to reveal S^2_{axis} and τ_e parameters.

4.3 Results

4.3.1 A113P CheY provides evidence for a two-state equilibrium in CheY

In order to further understand the activation mechanism of the distal site mutant A113P, we analyzed the chemical shift perturbations upon mutation and BeF_x binding. As

discussed in Chapter 2[89], we found chemical shifts moved along a line for a number of residues (Figure 4.2). A protein in fast exchange between two states (I and A) will display a linear pattern of chemical shifts. Each peak will appear at the population weighted average of the two end states. Therefore, A113P-unP's shift towards the BeF_x-bound WT peak supports the conclusion that A113P-unP has an increased population of the active conformation compared to WT-unP. To confirm the increased population of the active conformation, we measured the binding affinity of A113P-unP to FliM using fluorescence spectroscopy revealing a K_d of 180 μM compared to WT-unP with FliM of 350 μM.

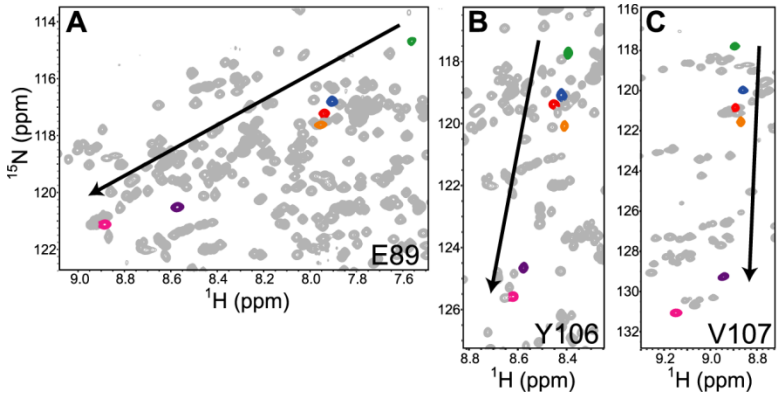

Figure 4.2. Linear chemical shift perturbations of A113P and WT CheY. ^{15}N HSQC overlay of CheY with a single peak highlighted from each spectra indicating E89 (A), Y106 (B), and V107 (C). Spectra are shown for the inactivating mutant T87I in 10 mM Mg^{2+} (green), WT-unP with 10 mM Mg^{2+} (blue), WT-unP with 1 mM EDTA (red), A113P-unP with 10 mM Mg^{2+} (orange), WT-P (purple), and A113P-P (pink). Previously shown as Figure 2.8.

The dynamics associated with the conformational change between I and A in CheY were measured with ^{15}N CPMG relaxation dispersion experiments. Full relaxation dispersion experiments were carried out on the unphosphorylated A113P. We found many of the same residues to have significant dynamics on this timescale for A113P-unP as were reported for WT-unP. As with WT, fitting to the Carver –Richards equation indicates CheY is switching in a more complex manner than a simple two state switch. However, upon inspection of R_{ex}

values calculated from these experiments, we found for nearly every residue there is a high R_{ex} in A113P-unP as for WT-unP (Figure 4.3, red and blue). An increase in R_{ex} could be due to a decrease in k_{ex}, an increase in $\Delta\omega$, or a shift in the populations. Therefore, if we assume our end states (I and A) and k_{ex} are unchanged, the increase in R_{ex} is consistent with an increase in the active population.

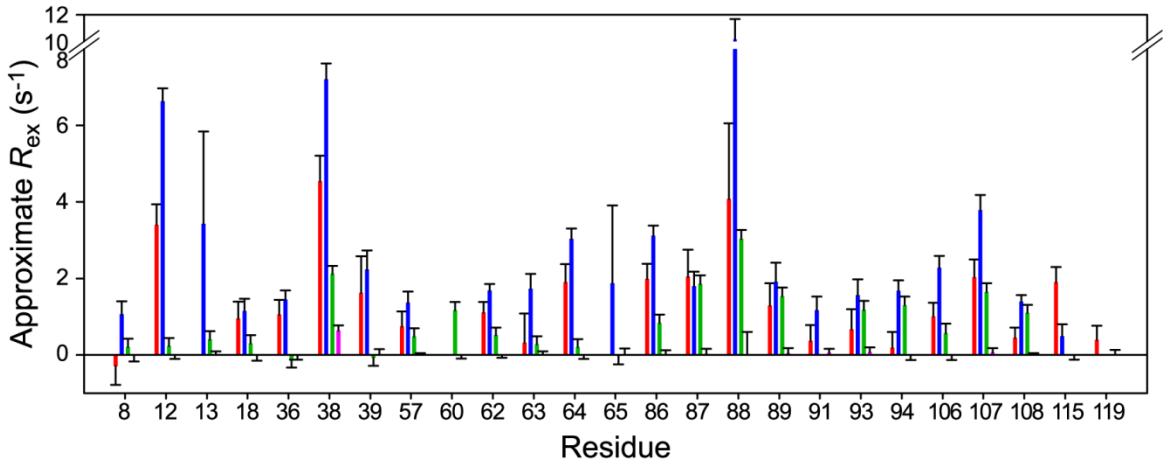

Figure 4.3. Approximate R_{ex} of A113P and WT CheY. Approximate R_{ex} was calculated from ^{15}N CPMG relaxation dispersion experiments of WT-unP (red), A113P-unP (blue), WT-P (green), and A113P-P (purple). Residues are shown for which $R_{ex} > 1\ s^{-1}$ for any of the four states. All data is at 500 MHz.

.

Not only does A113P-unP shift in a linear manner, A113P-P also lines up with WT-unP and WT-P (Figure 4.2). In proteins switching between an inactive and active state, when provoked to the active state such as by phosphorylation (or BeF_x binding), the protein is thought to switch completely to the active state. It is for this reason that CheY-P has been thought to be completely in the active conformation. By looking at the chemical shifts of A113P-P we find it is shifted further from the unphosphorylated CheY peaks. According to a two state equilibrium, this suggests A113P-P has a higher population of the active conformation than WT-P.

In Chapter 3[104], it was suggested that CheY-P was able to access the inactive conformation. Since the switch between inactive and active conformations, occurs on the μs-ms timescale, measurement of dynamics on this timescale in WT-P suggests a significant population of the inactive conformation. To probe whether A113P-P also has dynamics on this timescale, we measured ^{15}N CPMG relaxation dispersion planes to calculate the approximate relaxation due to exchange (R_{ex}). We found A113P-P to have decreased R_{ex} compared to WT-P (Figure 4.3, green and purple), supporting a decrease in the inactive conformation for A113P-P.

It is possible that A113P is switching between the inactive and active states accessed by WT, but the mutation could be causing a change in the end states of the equilibrium. Therefore, we used x-ray crystallography to determine the structure of A113P-P and took a closer look at the A113P-unP structure previously solved by Bourret and coworkers (PDB ID: 3OO1 & 3OO0). The crystals of CheY A113P in the presence of BeF_x and Mn diffracted to 2.10 Å resolution with a final R factor of 20.2%. The crystals are in the $p2_12_12_1$ space group and two molecules are in the asymmetric unit. The two molecules are extremely similar to one another with a backbone RMSD of 0.10 Å. The conformation is very similar to the WT-P (BeF_x & Mn bound; PDB ID: 1FQW) conformation with a backbone RMSD of 0.15 Å (Figure 4.4B). If a similar comparison is made to the WT-unP structure we calculate a backbone RMSD of 0.48 Å. Clearly, A113P-P is more similar to the phosphorylated conformation. A glance at the side chains reveals extremely similar packing. This suggests the active conformation for A113P is the same as WT. A similar comparison can be done for the unphosphorylated proteins showing A113P in the inactive state with Y106 in the "out" and "in" positions.

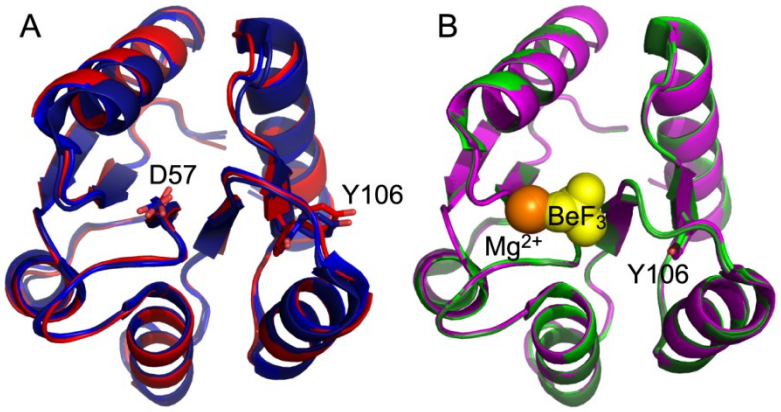

Figure 4.4 Crystal structures of A113P-unP and A113P-P. (A) An overlay of the two molecules of the asymmetric unit of A113P-unP (medium blue and dark blue) with WT-unP (red; PDB ID: 3CHY). (B) An overlay of the two molecules in the asymmetric unit of A113P-P (medium purple and dark purple) with the two molecules of WT-P (medium green and dark green; PDB ID: 1FQW).

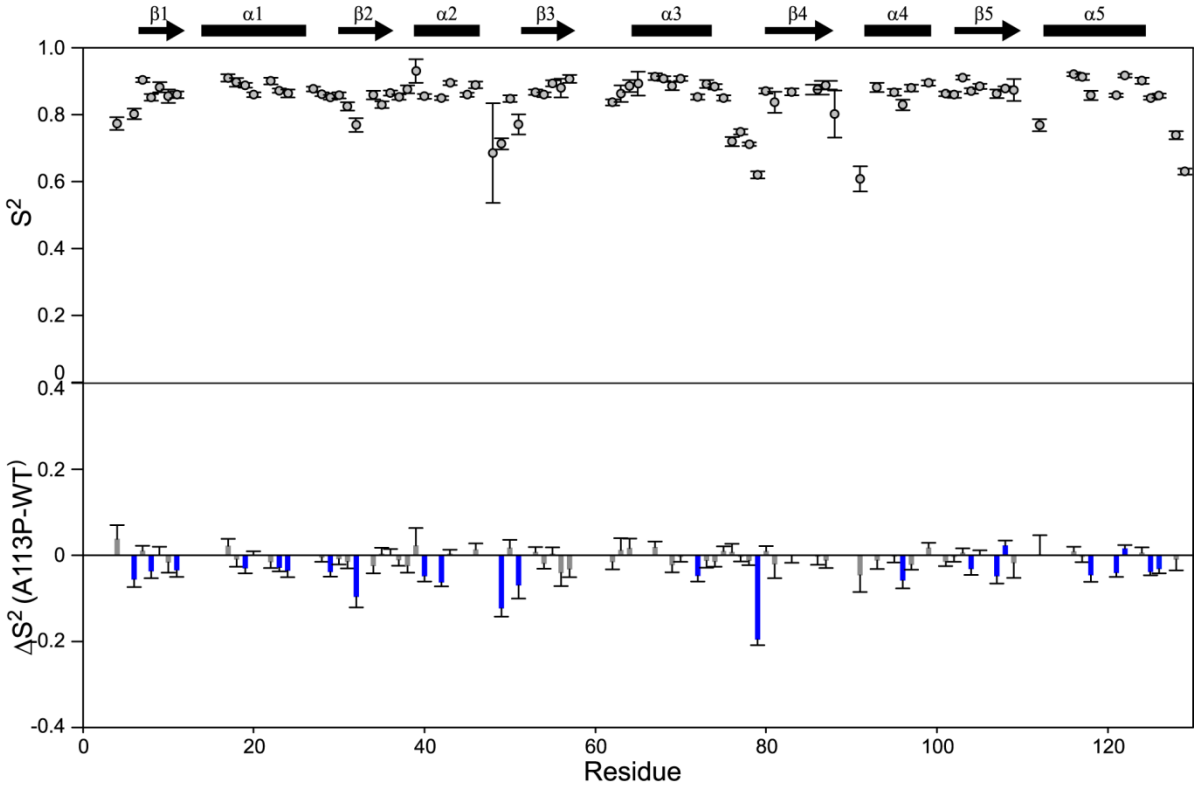

Figure 4.5. Backbone ps-ns dynamics of A113P-unP. ^{15}N relaxation of A113P-unP analyzed with model-free yields the order parameter, S^2 (top). Comparison of A113P-unP S^2 with WT-unP data showing significant ($\Delta S^2 > 2\sigma$) changes in blue (bottom).

4.3.2 A113P-unP dynamics on the ps-ns timescale

In order to further understand the activation mechanism of A113P CheY, we measured the ps-ns dynamics of the unphosphorylated protein. We collected ^{15}N relaxation experiments at 500 MHz to measure relaxation of T_1 and T_2 in addition to the $\{^1H\}$-^{15}N NOE. By way of the model-free formalism, we found parameters to describe the dynamics of amide bond vectors throughout the protein. The order parameters, S^2, which is a measure of the flexibility, was found on average to be 0.83 (Figure 4.5A) where 1 is completely rigid and 0 has no orientational preference. Comparison to the WT-unP order parameter shows small changes in dynamics of the backbone on the ps-ns timescale (Figure 4.5B, blue). For the most part, the extent of these changes is comparable to the changes upon phosphorylation of WT (Figure 4.5B, blue & Figure 3.5). However, for A113P-unP compared to WT-unP 7 amides have a $\Delta S^2 > 0.05$ with two of those (49 and 79) > 0.1 compared to 4 amides having a $\Delta S^2 > 0.05$ between WT-P and WT-unP. Furthermore, for A113P-unP – WT-unP, nearly every significant change is negative indicating an increase in flexibility upon mutation. Conversely the changes between WT-unP and WT-P are in both directions. Therefore, this data indicates an overall increase in flexibility of A113P with is not seen in the WT-P. Unfortunately data for A113P-unP was only collected at a single field. Therefore, it is important to collect data at second field to check the reliability of the data presented here, since a poorly determined τ_m or bad model selection could yield inaccurate S^2 values.

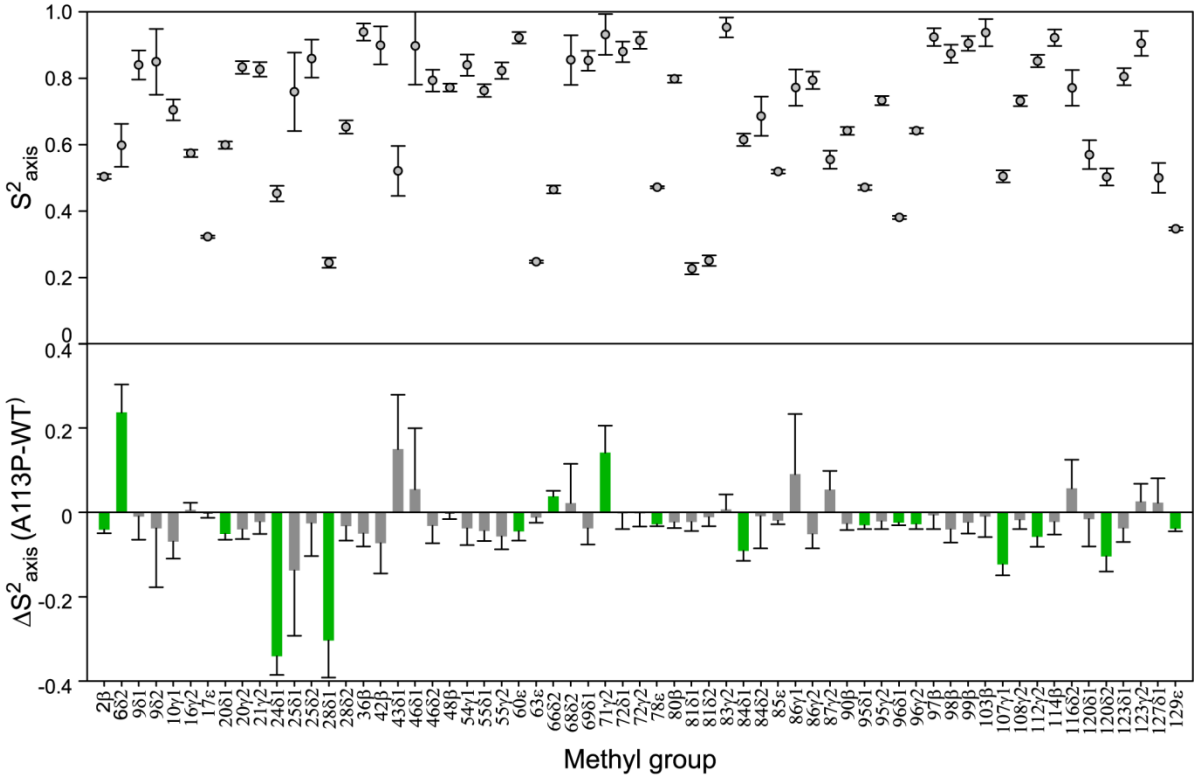

Figure 4.6. Methyl side-chain ps-ns dynamics of A113P-unP order parameter values. ^{2}H relaxation of A113P-unP analyzed with model-free yields the order parameter, S^2_{axis} (top). Comparison of A113P-unP S^2_{axis} with WT-unP data showing significant ($\Delta S^2_{axis} > 2\sigma$) changes in green (bottom). Methyl groups are shown for which data is available for both A113P-unP and WT-unP.

Side-chain dynamics are much more sensitive to perturbation and are more heterogeneous than the backbone. For, this reason, side-chain dynamics can reveal functional dynamics invisible to the backbone. ^{2}H relaxation experiments were collected on A113P-unP at 500 and 600 MHz to monitor the ps-ns dynamics of the methyl side chains. The average order parameter is 0.67 with a range of 0.22 to 0.93 (Figure 4.6A). A number of methyl groups have a significant increase in flexibility or increased rigidity when compared to WT-unP (Figure 4.6B). The changes in dynamics are much larger for the methyl side chains than for the backbone upon activation by mutation to A113P. Most methyl groups experience an increase in flexibility upon mutation to A113P just like in the backbone. Additionally, from

these experiments we learn the internal correlation time for the methyl symmetry axis, $\tau_{e,axis}$ (Figure 4.7A). There are significant increases and decreases in $\tau_{e,axis}$ throughout the protein upon mutation of A113P for the unphosphorylated CheY (Figure 4.7B). Interpretation of changes in $\tau_{e,axis}$ is not as straightforward as for S^2, but is significant to the dynamics of the protein.

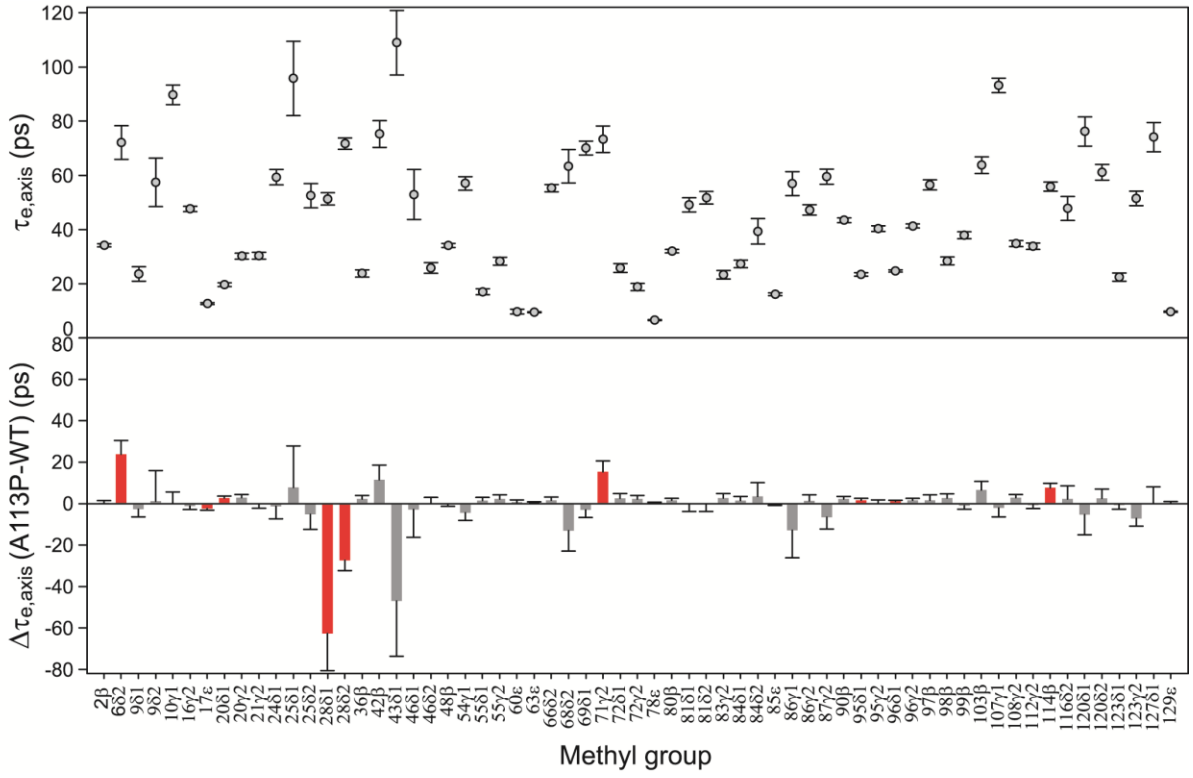

Figure 4.7. Methyl side-chain ps-ns dynamics of A113P-unP internal correlation time values. ^{2}H relaxation of A113P-unP analyzed with model-free yields $\tau_{e,axis}$(top). Comparison of A113P-unP $\tau_{e,axis}$ with WT-unP data showing significant ($\Delta\ \tau_{e,axis} > 2\sigma$) changes in red (bottom). Methyl groups are shown for which data is available for both A113P-unP and WT-unP.

4.4 Discussion and Conclusions

4.4.1 Reconciling segmental switching with the two-state shifted equilibrium in A113P

The allosteric conformational switch in wild-type CheY was previously monitored with ^{15}N CPMG relaxation dispersion (Chapter 2[89]). We found the conformational change

between inactive and activate conformations to not be a simple two-state switch. The conformational change is likely a segmental switch in which local sites can independently access the active conformation. The support and explanation for this is discussed at length in Chapter 2[89]. Here, we attempt to characterize the activation mechanism of the A113P mutation of CheY in order to gain an improved view of the allosteric switch in CheY. Assuming CheY is in a simple dynamic equilibrium between the inactive and active conformations, chemical shift analysis and approximate R_{ex} measurement both suggest A113P-unP has a population shift towards the active conformation. Furthermore, this data indicates WT-P is not completely in the active conformation but upon mutation (A113P-P) it is able to reach a more fully active state.

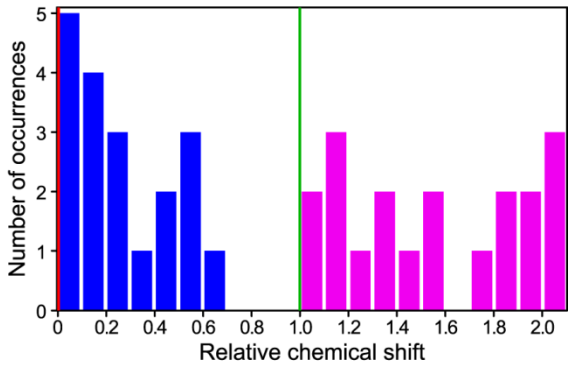

Figure 4.8. Relative chemical shift of A113P-unP and A113P-P compared to WT. With WT-unP (red) set to 0 and WT-P (green) set to 1, the relative chemical shift is the fraction A113P-unP (blue) and A113P-P (purple) are shifted along the line including all 4 peaks. Residues are only counted for which Δδ > 0.1 where $\Delta\delta = \sqrt{\Delta HN^2 + \left(\frac{\Delta N}{5}\right)^2}$ between WT-unP and A113P-P.

In order to resolve the paradox of the combination of the WT segmental switch and the A113P shift toward the active population, we take a closer look at the chemical shifts upon mutation to A113P. If A113P has a population shift toward the active conformation along a simple two state equilibrium, the whole protein would be in the new equilibrium between I and A. Therefore, every residue should have the same weight from the I and A

states to cause the chemical shift change. We would find every residue's chemical shift to be the same fraction along the linear path. However, for CheY, we did not find consistent fractions of chemical shifts for A113P. Figure 4.8 displays a histogram of the fraction A113P-unP (blue) is shifted from the inactive WT-unP chemical shift (red) toward the active WT-P (green) for each residue. Also displayed is how much A113P-P is shifted past WT-P (purple) relative to WT-unP. There is a large variety in the fraction shifted for both A113P-unP and A113P-P which indicates the whole protein is not simply shifted to a new equilibrium of I and A. Together with the linear nature of the shifts, this supports the theory of segmental switching in CheY in which each residue is in an individual equilibrium between I and A states.

4.4.2 Activation by A113P and BeF_x binding yield similar changes in ps-ns dynamics.

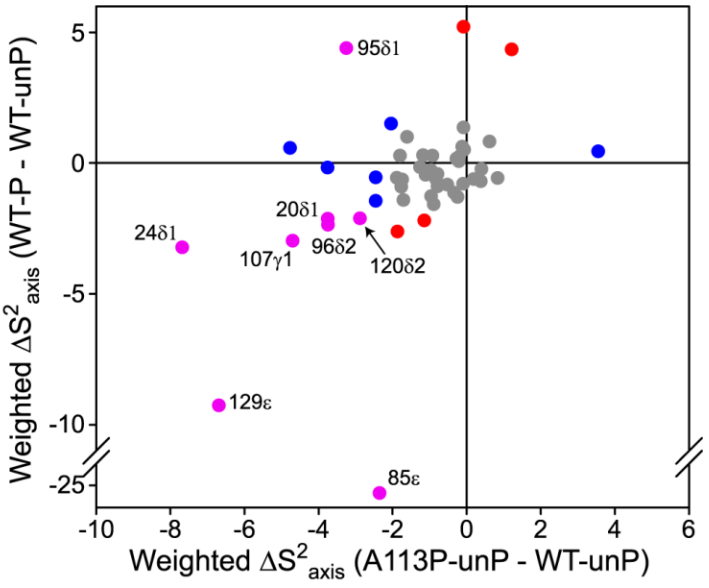

Figure 4.9. Comparison of ΔS^2_{axis} for A113P-unP – WT-unP and WT-P – WT-unP. The weighted ΔS^2_{axis} is calculated as the ΔS^2_{axis}/error to emphasize large ΔS^2_{axis} values with small error. The significant changes are highlighted for A113P-unP – WT-unP (blue), WT-unP – WT-P (red), and both (purple). Methyl groups are only shown for which data is available for A113P-unP, WT-unP and WT-P. Significant changes are $\Delta S^2_{axis} > 2\sigma$.

Changes in ps-ns dynamics of the methyl side chains upon mutation to A113P are located throughout the protein. Similarly changes in the side chain dynamics upon activation by BeF_x binding are located throughout the protein. Surprisingly many of the significant changes are in the same methyl groups (Figure 4.9). Of the methyl groups of which we have data in all three states (WT-unP, WT-P and A113P-unP), 4 have significant changes upon activation by BeF_x binding but not A113P mutation, 6 are significant for A113P mutation, but not BeF_x binding, 8 are significant in both cases and the remaining 31 do not change for either activation mechanism. A Fisher's exact test gives a P value of 0.0008 deeming this correlation extremely significant. Not only do 8 methyl groups have changes for both cases, 7 of the 8 change in the same direction where activation increases flexibility.

A113P is an activating mutation that has similar changes in ps-ns side-chain dynamics to the typical activation, by phosphorylation (BeF_x binding). Since both cause activation of CheY, this pattern of (mostly) increases of flexibility is likely a necessary step in the activation of CheY. This indicates an important relationship between the ps-ns dynamics in CheY and the protein's function. Typically proteins that undergo conformational changes are studied for their motions on that slow timescale. These results for CheY are a good indication that all timescales of motion could be at play to regulate a protein's function.

While both A113P and binding of BeF_x activate CheY, the extent of activation is very different. CheY-P is shifted nearly completely to the active (and active-like) states while A113P-unP still for the most part in the inactive conformation. Therefore, there is a disconnect between the conformational change and the change in the fast dynamics. In Chapter 3[104], we discussed at length the localization of changes in fast dynamics occur at regions of conformational change. Here, for A113P, we see similar change in ps-ns dynamics

without the large conformational shift to the active state (s) or the initial allosteric perturbation (BeF_x binding).

These results show that A113P-unP is similar to WT-P in fast dynamics yet more similar to WT-unP in conformational equilbria and slow timescale dynamics. This disconnect highlights the important role of the fast timescale dynamics in the activation of CheY. This suggests that ps-ns dynamic changes could be just as important as the conformational switch in readying CheY for binding to FliM. Additionally this leads to possibilities of ps-ns dynamics priming or causing the switch in conformations. In order to more fully understand the interaction of dynamics on multiple timescales in CheY, it would be beneficial to study additional mutants that affect CheY's function and dynamics in a variety of ways.

CHAPTER 5

HYDROGEN EXCHANGE USED TO SHOW LONG RANGE INTERACTIONS IN CHEY

5.1 Introduction

5.1.1 Long Range Interactions in Allosteric Proteins

Cellular regulation of protein activity is often achieved by means of an allosteric mechanism. At the root of allosteric signaling is the transduction of a signal from one site to a second distal site. This fundamental ability of an allosteric protein to communicate over a long distance is crucial to cellular regulation and signaling. Therefore, an increased understanding of how a signal is transduced across a protein is important in the overall understanding of allosteric mechanisms.

Two traditional models of allostery have been proposed, KNF and MWC, differing mainly in whether the activated conformation pre-exists (described in Chapter 1). Regardless of which mechanism of allostery is utilized, the protein must pass information from the initial perturbation site to the distally affected site. This long-range communication must occur through a pathway or network connecting the two sites. Therefore mapping of the interaction network is crucial to understanding the mechanisms of allostery. Numerous studies have been published utilizing MD simulations or other computational methods with little experimental results to define propagation networks within proteins.[105-107] In other words, distal sites communicate through intermediary residues which are not random, but evolutionarily chosen to propagate the signal.[108, 109] It is important to gain experimental

information on long-range interaction networks within proteins to accompany the computational studies. However, experimental determination of long-range thermodynamic couplings has been limited to double mutant cycles.

5.1.2 Hydrogen Exchange Theory for Local Free Energy Changes

Amide hydrogen exchange is an excellent tool to gain information about local free energy changes and to map these changes upon perturbation to a protein. Backbone amides exchange with solvent protons, but when in a protected ("closed") position in a protein exchange cannot occur. Only when the protein changes to an "open" state is it able to exchange with the solvent.[110, 111] Accordingly, the exchange reaction is resultant of a structural fluctuation. Typically these fluctuations occur in one of two categories: 1) global unfolding of the protein takes place and exchange occurs in the unstructured state and 2) within the native state ensemble, local fluctuations cause a switch to an "open" state in which exchange is able to occur.[110, 112] Once in an "open" state, exchange occurs at the rate for a random coil (k_{rc})[113] such that

$$closed \underset{k_{cl}}{\overset{k_{op}}{\rightleftarrows}} open \xrightarrow{k_{rc}} exchange \tag{5.1}$$

where k_{op} and k_{cl} are the rate constants for opening and closing. Therefore, the exchange rate constant, k_{ex}, for steady state conditions is

$$k_{ex} = \frac{k_{op}k_{rc}}{k_{op}+k_{cl}+k_{rc}} . \tag{5.2}$$

This equation can be simplified by making one of two assumptions. In the first, $k_{cl} << k_{rc}$ (EX1 limit) which leads to an exchange rate of

$$k_{ex} = k_{op} . \tag{5.3}$$

For the EX1 limit, every opening fluctuation leads to exchange. The second possible assumption is $k_{cl} >> k_{rc}$ (EX2 limit) which gives

$$k_{ex} = \left(\frac{k_{op}}{k_{cl}}\right) k_{rc} = K_{op} k_{rc} \tag{5.4}$$

where $K_{op} = k_{op}/k_{cl}$. The EX2 limit is common for stable proteins.[114] If we use the EX2 limit assumption, we are able to calculate local free energy using

$$\Delta G_{HX} = -RT \ln K_{op} = -RT \ln(k_{ex}/k_{rc}). \tag{5.5}$$

Upon confirming CheY exchanges in the EX2 limit and we are monitoring local fluctuations instead of global unfolding, we are able to calculate local free energy change for hydrogen exchange for each of these residues.

5.1.3 Determining Long Range Thermodynamic Couplings with Hydrogen Exchange

It is straightforward to calculate changes in ΔG_{HX} for each exchanging amide upon a perturbation to the system such as mutation:

$$\Delta\Delta G_{HX} = \Delta G_{HX}^{mut} - \Delta G_{HX}^{WT}. \tag{5.6}$$

In this manner we are able to calculate local changes in free energy throughout a protein upon a single site mutation. This type of analysis has been termed semi-mutant cycles[115] as it has a strong similarity to the traditional double mutant cycles (Figure 5.1).[116] In the familiar double mutant cycle, single site mutants and the corresponding double mutant are created to test for interaction between the two mutation sites (Figure 5.1A). If the effect from the sum of the two sites does not equal the effect from the double mutant this results as nonadditivity or coupling: $\Delta\Delta G(WT \rightarrow ij) \neq \Delta\Delta G(WT \rightarrow i) + \Delta\Delta G(WT \rightarrow j)$ where I and j are single site mutations. The sites are generally expected to be able to "sense" one another if close in space. However double mutant cycles are especially useful for probing long range

interactions where additivity is generally expected, but nonadditivity has been observed in many cases.[116-118]

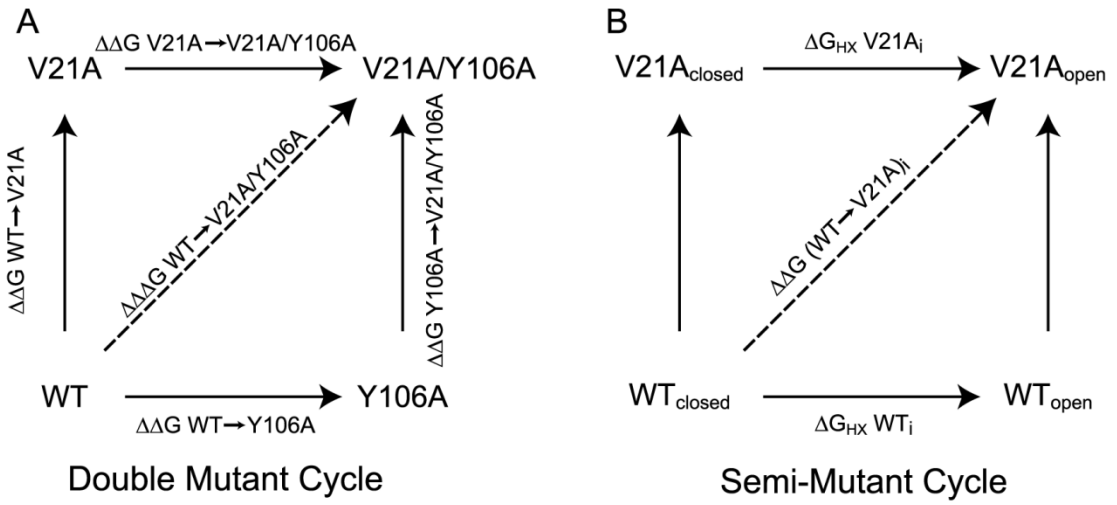

Figure 5.1. Comparison of double mutant and semi-mutant cycles. (A) A double mutant cycle with two example mutations, Y106A and V21A. These mutations could be made to probe potential long range interactions in CheY between these sites. ΔΔG values are the difference in ΔG upon mutation where ΔG is a globally determined value. (B) ΔG determined by site specific hydrogen exchange rates. The indice I represents every exchanging amide in the protein. Therefore, the difference in ΔG (ΔΔG) for the V21A mutation will be calculated for every i.

A major problem with double mutant cycles is the large number of mutants needed to map out interactions throughout a protein since each coupling requires a separate cycle. In a double mutant cycle, energetic changes are measured as changes in a global transition. The ability to locally probe changes in free energy would provide localized information of changes upon mutation. This allows the ability to probe multiple sites located throughout a protein with a single mutation. NMR-based hydrogen exchange is an excellent tool for residue level thermodynamic information. Local free energy differences (ΔG_{HX}) provide per-residue resolution to probe for multiple thermodynamic couplings from a single mutation. Therefore the difference in ΔG_{HX} between WT and a mutant will report a potential thermodynamics coupling for every exchanging amide (Figure 5.1B).

5.1.4 Long Range Thermodynamic Couplings of CheY

CheY is an excellent protein for measurement of long-range thermodynamic couplings. Not only is there a lot of information pertaining to CheY structure, phosphorylation, and FliM binding, we also know information about the dynamics on multiple timescales. The extent to which CheY is studied will allow easy correlation between allosteric pathways mapped here and previously determined functionally important residues.

Clearly, there is interest in residues directly between the site of phosphorylation and FliM binding interface such as T87 and the β4-α4 loop. However, a recent report described a set of residues (the D1 switch) well conserved throughout all Rossmann fold proteins which localize to α1 and β2.[119, 120] In CheY, the D1 switch residues have never indicated any involvement in the allosteric signaling mechanism. However, it is possible for residues to be a part of an allosteric network without being close in space to either the site of phosphorylation or the FliM binding site. NMR-based hydrogen exchange is an excellent tool to probe for this potential interaction network within CheY.

In this work, we present preliminary findings utilizing NMR to measure residue-level resolution thermodynamic couplings. We seek to measure the hydrogen exchange rate and therefore the ΔG_{HX} for CheY. The data reveals weak support for CheY being fully in the EX2 limit and only a small number of residues displaying local exchange behavior. The standard conditions selected were simply based on keeping consistent with all other NMR work on CheY. Therefore, optimization of conditions has a high possibility of improving the results and conclusions presented here.

5.2 Materials and Methods

5.2.1 Protein Expression and Purification

Escherichia coli CheY was overexpressed and purified as previously described (Section 2.2.1). The CheY plasmid was transformed into BL21 Star (DE3) cells (Invitrogen) and grown in minimal media supplemented with $^{15}NH_4Cl$ [99%] for isotopic labeling. Pure CheY was concentrated and stored at 4 °C in the appropriate NMR buffer to be used in the HX experiment where the standard buffer is 50 mM NaP_i, 10 mM $MgCl_2$, and 0.02% NaN_3, pH 7.0. Mutant CheYs were made by way of site-directed mutagenesis PCR.

5.2.2 NMR Spectroscopy

All NMR hydrogen exchange experiments were collected at 25 °C on a Varian INOVA 500 MHz with a room-temperature probe. The data were processed using NMRpipe[62] and visualized with NMRDraw and NMRView.[63] Assignments of wild-type CheY under standard conditions were previously determined (Section 2.2.2). For samples with a change in pH, addition of GdmCl, or mutation, assignments were determined by choosing the nearest peaks or following peak shifts upon increased change from the standard conditions.

5.2.3 Hydrogen Exchange

Protein in 100% H_2O NMR buffer were passed through a NAP-5 column packed with Sephadex G25 equilibrated with 90% D_2O NMR buffer. Under standard conditions, the NMR buffer is 50 mM NaP_i, 10 mM $MgCl_2$, and 0.02% NaN_3, pH (or $pD_{corrected}$) 7.0. In cases with an addition of GdmCl or a different pH from the standard conditions, both the 100% H_2O and 90% D_2O buffers reflect the change. Therefore, there will be no difference in

conditions upon exchange to the D_2O buffer. After completion of the experiment the pH was confirmed and corrected. Gentle pressure was applied to quickly pass the protein through the column and the samples were hurriedly transferred to an NMR tube and placed in the spectrometer. ^{1}H-^{15}N HSQC pseudo-3D spectra were acquired with a single plane acquisition requiring 5.9 minutes. Time points were collected for 30-45 hours. Peak intensities were extracted from each plane and fit to a simple three-parameter monoexponential. Peak intensity error was calculated from root mean square base plane noise for each plane. For free energy calculations for the mutational analysis, EX2 limit was assumed despite the weak support and the exchange rates and Molday factors were used. Therefore the changes upon mutation of the local free energy change (ΔG_{HX}) can be calculated as in equation 5.6.

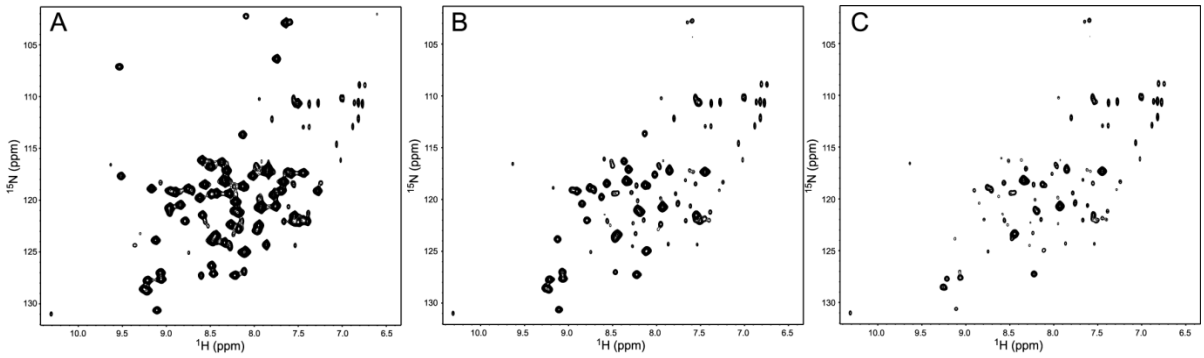

Figure 5.2. ^{1}H-^{15}N NMR spectra of CheY undergoing hydrogen exchange. Spectra collected under standard conditions after approximately 3 minutes (A), 11 hours (B), and 44.5 hours (C).

5.3 Results and Discussion

5.3.1 Hydrogen exchange under standard conditions

In an attempt to measure long range thermodynamic couplings, we collected NMR-based hydrogen exchange (HX) experiments of CheY. Successive ^{1}H-^{15}N HSQC spectra were recorded and decreasing peak intensity due to the amide exchange of H_2O to $^{2}H_2O$ followed (Figure 5.2). Under standard CheY NMR conditions[89] (10 mM $MgCl_2$, pH 7.0, and

25°C), 82 residues are not overlapped and of these 56 residues exchange slow enough to be fit (Figure 5.3).

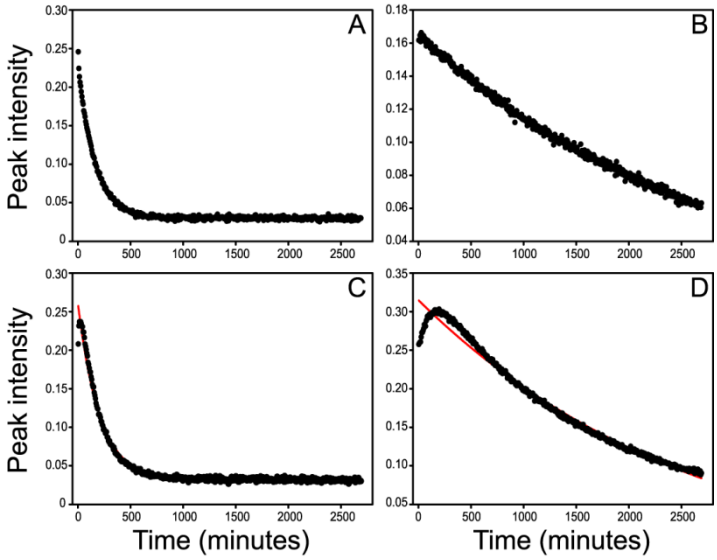

Figure 5.3. Peak intensity change over time during hydrogen exchange. Black dots represent the peak intensity for residue 107 (A), 11 (B), 40 (C), and 53 (D) in a single ^{1}H-^{15}N HSQC collected after the corresponding time has elapsed. Red lines are monoexponential fits to the data.

While many residues display exponential decays of intensity (Figure 5.3A & 5.3B), a number of residues have an increase in intensity at early time points (Figure 5.3C & 5.3D). This phenomenon is most prominent in data collected in the standard conditions for wild-type CheY. Mutation and the addition of GdmCl noticeably reduce the intensity increase. An additional variable that seems to have an effect is the starting concentration although a direct comparison is not available. It is hypothesized that this increase in intensity is somehow related to the high starting concentration of CheY (3-4 mM). In some way, interaction between CheY molecules causes slow tumbling and selective decreased peak intensity which is subsequently relieved upon dilution. All residues displaying an increase of peak intensity were fit to an exponential decay after all time point data were removed that displayed this phenomenon.

5.3.2 pH dependence of hydrogen exchange in CheY

In order for the exchange kinetics to be used to study the equilibrium between open and closed states, the protein must be in the EX2 limit ($k_{cl} >> k_{rc}$). In this limit, chemical exchange is the rate limiting step and the equation for the exchange can be simplified (Equation 5.4). We are then able to calculate the free energy of exchange (ΔG_{HX}, Equation 5.5) and therefore thermodynamic couplings (Equation 5.6). The ability to correlate the hydrogen exchange rate with free energy depends on the protein being in the EX2 limit.

The exchange behavior of CheY was determined by measuring the pH dependence of exchange rates of each amide in the protein.[121] For the EX2 limit, k_{ex} is proportional to the concentration of H^+. Therefore, we would expect a straight line with a slope of one and an intercept at the difference in pH when $\log(k_{ex})$ is plotted for each experiment (Figure 5.4).

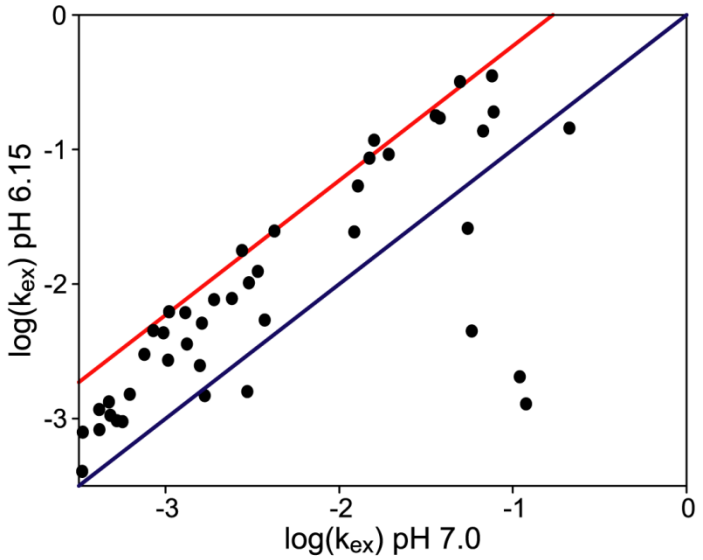

Figure 5.4. Dependence of hydrogen exchange rate on pH in CheY. Each dot represents a single residue in CheY. The blue line indicates pH independence and the EX1 limit while the red line is complete pH dependence and the EX2 limit.

HSQC-based hydrogen exchange experiments were collected for CheY under standard conditions (pH 7.0), pH 6.65 (not shown), and pH 6.15. A comparison of exchange rates for pH 7.0 and 6.15 reveals that nearly all measureable CheY residues have a pH dependence (Figure 5.4). However, a number of residues do not have a pH dependence or do not have the expected change for the EX2 limit. An additional troubling fact is that while most residues have a pH dependence, only a few residues have the change expected from a 0.85 pH change (red line in Figure 5.4). These data reveal that CheY is likely either in the EX2 regime but poor data yields a poor correlation, or CheY is not quite to the limit of $k_{cl} >> k_{rc}$. This means all further interpretation of data in these conditions may not be completely accurate since we are not able to completely propagate the free energy change from the exchange rates. However, we know that CheY is nearly to the EX2 limit and therefore we can make qualitative conclusions from further analysis of the data. Furthermore, these preliminary results indicate further testing would be useful since EX2 limit may be better realized at lower pH values.

5.3.3 GdmCl dependence of hydrogen exchange in CheY

In order to gain information about the thermodynamic couplings throughout CheY, we are interested in obtaining local perturbations to free energy. Therefore, it is crucial to distinguish between hydrogen exchange rates that are monitoring local fluctuations in protein structure and positions that are undergoing a global unfolding mechanism. Residues that undergo hydrogen exchange influenced by only local exchange have the simplest interpretation for determination of local free energy changes. These residues are determined by adding a destabilizing agent (guanidinium hydrochloride; GdmCl), and monitoring the

dependence of the hydrogen exchange rate. Amides that are dependent on GdmCl concentration are exchanging via a global mechanism where amides that are GdmCl independent at low GdmCl concentrations exchange via a local mechanism. All amide k_{ex} values are expected to be dependent on GdmCl at high GdmCl concentrations since the protein will begin to unfold.

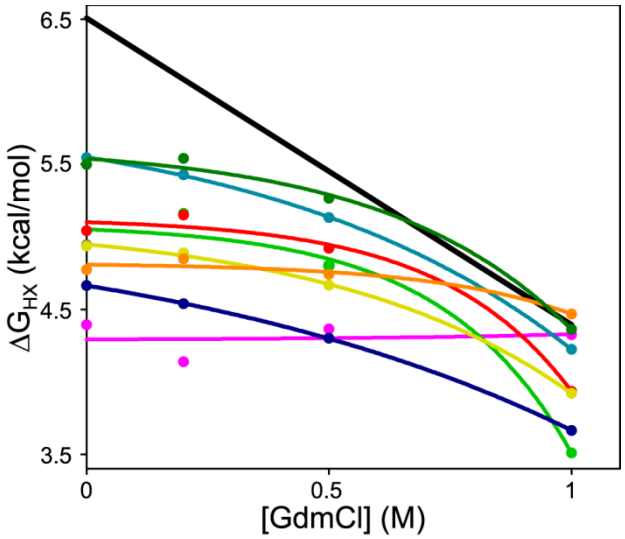

Figure 5.5. Free energy of hydrogen exchange dependence on GdmCl concentration. The black represents an average of residues with strong dependence on GdmCl concentration. Lines are fits to the equation $\Delta G_{HX}(GdmCl) = \Delta G_{HX}(0) - a \ln(1+b[GdmCl])$ where a is proportional to the number of denaturant binding sites and b is the denaturant binding constant.[110]

For CheY, HSQC-based hydrogen exchange experiments were collected at 0, 0.2, 0.5, and 1 M GdmCl (Figure 5.5). Most residues were highly dependent on the concentration of GdmCl even at the low concentration of 0.2 M indicated by the black line in Figure 5.4. However, a handful of residues indicate an independence from GdmCl at low concentrations. Similar to the comparison at multiple pH values, these data have a higher amount of variability than desired which limits the conclusions we can make. It is clear that a number of residues exchange at least partially through a local mechanism. However, there are only a small number of these residues, so this limits the locations throughout CheY that we are able

to monitor. It is possible that by varying the conditions we can find additional residues that yield a high amount of dependence on local rather than global fluctuations. Therefore, we conclude that this result is promising but optimization of conditions is necessary to yield results for quantitative comparison to mutant CheY.

5.3.4 Long range couplings probed by V21A and F8V CheY mutants

Despite a lack of a strong support for CheY being in the EX2 limit (Figure 5.4) and a small number of residues exchanging via a local mechanism (Figure 5.5), our overall goal is to use single site mutations to probe for long-range thermodynamic couplings. Specifically, we are interested in any linkage between the α1 helix (D1 switch) with the active site, FliM binding interface and known allosteric network residues (see further explanation above). We choose two mutants to test, V21A because it is in α1 and F8V which is in β1 and backs against α1. Both sites are part of the D1 switch with the conserved switch amino acid being valine for both 21 and 8.

We measured HSQC-based hydrogen exchange for V21A and F8V CheY under standard conditions. Despite all of the caveats covered above, we calculated the change in free energy upon mutation. For both mutants, we found in nearly every case there to be a decrease in ΔG_{ex} in the mutant compared to the same residue in the wild-type CheY with changes as large as 3 kcal/mol. This indicates these mutations are likely globally destabilizing to CheY and this destabilization is being reflected in the ΔG_{ex} values. It is difficult to make further conclusions with this data due to the large impact of the global fluctuations on the exchange rates of the protein.

5.4 Conclusions

In conclusion, preliminary results for measuring NMR-based amide hydrogen exchange rates in CheY are encouraging. Our initial conditions chosen did not yield data displaying strong pH dependence for the EX2 limit. Neither did it reveal a large number of residues with GdmCl independence at low concentrations indicating exchange via a local mechanism. Therefore, a search for ideal conditions is necessary for both realizing an EX2 limit and an increased number of dominantly locally exchanging residues. These results are a solid base for the promising investigation of long range interactions in CheY.

CHAPTER 6

SUMMARY AND FUTURE DIRECTIONS

The purpose of the work presented here is to increase the understanding of allosteric mechanisms in proteins by study of the model protein CheY. The focus is on interpretation of the dynamics and how they relate to the protein's structure and function. The study observes the dynamics of CheY on two timescales. First, ^{15}N CPMG relaxation dispersion experiments were used to monitor CheY dynamics on the μs-ms timescale which is the timescale of conformational change. Second, ^{15}N and ^{2}H relaxation experiments were used to monitor the dynamics on a fast timescale (ps-ns) related to bond librations and rotamer switching. Together, the data we have obtained on CheY in a variety of states (unphosphorylated, phosphorylated, and mutated) and on multiple timescales has led to an increased understanding in the allosteric mechanism of CheY.

6.1 Allosteric switch between inactive and active conformations

Chapter 2 focuses on the allosteric transition of CheY between inactive and active conformations. Until recently, CheY was thought to undergo a simple concerted switch between inactive and active states. Therefore, it was surprising when we found this not to be the case. The result that CheY switches in a segmental, asynchronous manner allows us to take a fundamental step towards understanding allosteric mechanism. Therefore, it is important to gain an even better understanding of the conformations and dynamics involved in CheY's transition between inactive and active states. In order to do this, collection of

relaxation data on additional nuclei to measure dynamics on this μs-ms timescale could be used in conjunction with the ^{15}N data to fit to more complex switching (3 state). Another way to probe the dynamics on this timescale would be analysis of mutants. A113P proved to be a valuable mutant due to its distal location. Additional mutants could be effective: Mutation at Y106 to F (inactivating) or W (activating) could be beneficial since they affect a large conformational change (Y106 "in" and "out" switching). These mutations could lead to localized changes in the exchange.

In Chapter 2, we introduce the idea of the allosteric signaling quartet which includes W58, M85, E89, and Y106. M85 and W58 were previously not identified to have particular importance to the allosteric switch. Therefore, to support their significance to the allosteric switch, it would be beneficial to probe their position in CheY such as by the M85A mutation. To my knowledge, the effect of mutation at position M85 has never been measured in any capacity. Therefore, measurement of CheY activity (assessed by FliM binding, autophosphorylation rate, and flagellar rotation) along with dynamics measurements could lead to valuable insights into the exact role of M85 along with W58.

Mg^{2+} binding to CheY has a unique effect on the dynamics at intermediate Mg^{2+} concentrations as described in Chapter 2. Metal binding is extremely important for the function for a number of proteins. So, it is possible that metal binding is a widespread tool used to regulate or fine tune allosteric dynamics. To further understand the effect of Mg^{2+} on CheY allostery, there are two possible directions for future experiments. First, full analysis of the dynamics at an intermediate Mg^{2+} concentration could lead to important insights obtained from the dispersion curves and fit exchange parameters. Furthermore, utilization of the increased R_{ex} by intermediate Mg^{2+} concentration would lead to a number of new residues

whose R_{ex} is high enough to be analyzed (> 2 s^{-1}). This could lead to a more complete picture of the dynamics occurring in CheY. Additionally, it is still not well understood how CheY is affected by the actual binding event of Mg^{2+}. A number of mutants could be used to probe this relationship. D13K is a mimic of the magnesium bound state. As stated in Chapter 2, A88 has a unique relationship with the Mg^{2+}, therefore a mutation at this location (such as A88V) could be used. Lastly, M17 is near to the site of Mg^{2+} binding and in Chapter 3 the interesting effect on chemical shifts of a M17A mutation is described. This site may be an important link between Mg^{2+}, phosphorylation and the allosteric signaling residues. Together, these mutants could serve as important tools for additional studies of the dynamics in CheY. These studies of the interaction of Mg^{2+} with CheY may lead to an increased understanding of the relationship between the Mg^{2+} binding and the transition between inactive and active conformations in CheY.

6.2 Relationship of fast timescale dynamics to CheY's allosteric function

In Chapters 3 and 4, we examined the dynamics of CheY on a fast (ps-ns) timescale which is the timescale of bond librations and rotameric interconversion. Dynamics on this timescale have been shown to be important for the function for a number of proteins.[6, 13, 14] The study reported here is atypical due to having data on the dynamics of CheY on both a fast and slow timescale; only a handful of studies have been reported with protein dynamics measured on both of these timescales. Furthermore, the discussion of the relationship between fast and slow timescale dynamics is nearly absent from the literature. Therefore, the publishing of Chapter 3 may lead to the increased dialogue of how multi-timescale dynamics

interrelate. Understanding this relationship is a crucial step in understanding how they together contribute to the function of the protein.

While the observations of dynamics in WT and A113P CheY lead to interesting insights, there are many questions that follow. It is clear that dynamics on both timescales are important for the allostery in CheY, but the nature of the relationship is unclear. Do the dynamics on one timescale or the other occur first and cause the change in the other? We could imagine two scenarios: the change in conformations induced by the slow timescale dynamics results in the change in fast dynamics or the change in fast timescale dynamics provokes the shift in populations of conformations. In order to start to answer these questions, utilization of additional CheY mutants could be beneficial. A mutant that may lead to separation of slow and fast timescale dynamics could be ideal. For instance, T87I CheY is an inactivating mutant yet is still able to be phosphorylated. This allows separation of the initial phosphorylation signal from the resulting output. Mutation at residue Y106 could lead to similar perturbation of the slow dynamics and fast dynamics.

6.3 Utilization of preliminary hydrogen exchange results

Preliminary results from NMR hydrogen exchange experiments for identification of long range communication are reported in Chapter 5. In performing these experiments, we encountered more problems than expected. However, improvement in the data collected is likely since no time was spent in identifying ideal conditions. Instead, conditions were used to be consistent with all of the other NMR data reported here. In continuing collection of hydrogen exchange experiments on CheY, the first step should be to identify the best

conditions for EX2 and local exchange. This could be done with a change in buffer conditions such as lower pH or addition of a stabilizing agent.

A limitation in performing hydrogen exchange experiments is in limiting the dead time between introduction of D_2O and data collection. A technique often used to minimize the dead time in hydrogen exchange experiments is lyophilization. This technique was not attempted with CheY since the low dead times of the data reported here (3-5 minutes) made attempting this unnecessary. Another limitation in these experiments is signal to noise and collection time. All of the data here was collected on a room temperature Inova 500 MHz spectrometer. Switching to a cryo probe will increase the sensitivity. Additionally a change in pulse program could lead to a decrease in experiment time.

6.4 Concluding Remarks

The results reported here focus on the dynamics of CheY on the μs-ms and ps-ns timescale in the unphosphorylated and phosphorylated states. However, there are a number of additional directions that could be helpful in understanding the allosteric transition in CheY. CheY interacts with a number of other proteins such as the flagellar motor protein FliM, the histidine kinase CheA and the phosphatase CheZ. The interactions between CheY and these proteins and how they affect the allosteric dynamics in CheY could be an important aspect in understand CheY's allosteric mechanism. The crystal structure of an intermediate conformation of CheY described in Chapter 2 contains unphosphorylated CheY bound to FliM.[44] This complex would be especially interesting to study. However, it would be a major challenge since the binding affinity of FliM to the unphosphorylated CheY is not very tight. Finding ideal conditions to study the complex by NMR may be difficult; however the result

may be very insightful. As NMR techniques have progressively improved, it is now possible to collect experiments in smaller and smaller time. Therefore, the ability to study the phosphorylated (actual phosphorylation, not BeF_x-binding) CheY may be possible. The fast autodephosphorylation rate of CheY (2.5 min^{-1} [32]) leads to a very short half-life of the phosphorylated protein. Measurement of phosphorylated CheY may be possible in the near future. Lastly, the work of numerous other scientists including the Bourret lab has given us a rich base of crystal structures and ever increasing knowledge of the phosphorylation and dephosphorylation process. Continued collaboration is important for the measurement of structural and functional information of the CheY mutants proposed above. This is a necessary component in order to understand the full picture of the allosteric mechanism present in CheY.

Understanding how dynamics relate to a protein's allosteric function is a more complex endeavor than simply measuring its two-state switch. The results presented here suggest a complex segmental switch between inactive and active conformations in CheY in which dynamics on the fast timescale are also important in the transition. These conclusions serve as a solid base for future experiments in order to further utilize CheY as a model system for the understanding of allostery.

REFERENCES

1. Koshland, D. E., Jr., Nemethy, G. & Filmer, D. (1966). Comparison of experimental binding data and theoretical models in proteins containing subunits. *Biochemistry* **5**, 365-85.

2. Monod, J., Wyman, J. & Changeux, J. P. (1965). On the Nature of Allosteric Transitions: A Plausible Model. *J Mol Biol* **12**, 88-118.

3. Kleckner, I. R., Gollnick, P. & Foster, M. P. (2012). Mechanisms of allosteric gene regulation by NMR quantification of microsecond-millisecond protein dynamics. *J Mol Biol* **415**, 372-81.

4. Makowski, L., Bardhan, J., Gore, D., Lal, J., Mandava, S., Park, S., Rodi, D. J., Ho, N. T., Ho, C. & Fischetti, R. F. (2011). WAXS studies of the structural diversity of hemoglobin in solution. *J Mol Biol* **408**, 909-21.

5. Bai, F., Branch, R. W., Nicolau, D. V., Jr., Pilizota, T., Steel, B. C., Maini, P. K. & Berry, R. M. (2010). Conformational spread as a mechanism for cooperativity in the bacterial flagellar switch. *Science* **327**, 685-9.

6. Frederick, K. K., Marlow, M. S., Valentine, K. G. & Wand, A. J. (2007). Conformational entropy in molecular recognition by proteins. *Nature* **448**, 325-9.

7. Akke, M., Bruschweiler, R. & Palmer, A. G. (1993). Nmr Order Parameters and Free-Energy - an Analytical Approach and Its Application to Cooperative Ca2+ Binding by Calbindin-D(9k). *Journal of the American Chemical Society* **115**, 9832-9833.

8. Yang, D. & Kay, L. E. (1996). Contributions to conformational entropy arising from bond vector fluctuations measured from NMR-derived order parameters: application to protein folding. *J Mol Biol* **263**, 369-82.

9. Li, Z., Raychaudhuri, S. & Wand, A. J. (1996). Insights into the local residual entropy of proteins provided by NMR relaxation. *Protein Sci* **5**, 2647-50.

10. Wand, A. J. (2013). The dark energy of proteins comes to light: conformational entropy and its role in protein function revealed by NMR relaxation. *Curr Opin Struct Biol* **23**, 75-81.

11. Henzler-Wildman, K. & Kern, D. (2007). Dynamic personalities of proteins. *Nature* **450**, 964-972.

12. Kleckner, I. R. & Foster, M. P. (2011). An introduction to NMR-based approaches for measuring protein dynamics. *Biochim Biophys Acta* **1814**, 942-68.

13. Petit, C. M., Zhang, J., Sapienza, P. J., Fuentes, E. J. & Lee, A. L. (2009). Hidden dynamic allostery in a PDZ domain. *Proc Natl Acad Sci U S A* **106**, 18249-54.

14. Tzeng, S. R. & Kalodimos, C. G. (2012). Protein activity regulation by conformational entropy. *Nature* **488**, 236-240.

15. Boehr, D. D., McElheny, D., Dyson, H. J. & Wright, P. E. (2006). The dynamic energy landscape of dihydrofolate reductase catalysis. *Science* **313**, 1638-1642.

16. Boehr, D. D., Dyson, H. J. & Wright, P. E. (2008). Conformational relaxation following hydride transfer plays a limiting role in dihydrofolate reductase catalysis. *Biochemistry* **47**, 9227-9233.

17. Mauldin, R. V., Carroll, M. J. & Lee, A. L. (2009). Dynamic dysfunction in dihydrofolate reductase results from antifolate drug binding: modulation of dynamics within a structural state. *Structure* **17**, 386-94.

18. Carroll, M. J., Gromova, A. V., Miller, K. R., Tang, H., Wang, X. S., Tripathy, A., Singleton, S. F., Collins, E. J. & Lee, A. L. (2011). Direct detection of structurally resolved dynamics in a multiconformation receptor-ligand complex. *J Am Chem Soc* **133**, 6422-8.

19. Tzeng, S. R. & Kalodimos, C. G. (2009). Dynamic activation of an allosteric regulatory protein. *Nature* **462**, 368-U139.

20. Bruschweiler, S., Schanda, P., Kloiber, K., Brutscher, B., Kontaxis, G., Konrat, R. & Tollinger, M. (2009). Direct observation of the dynamic process underlying allosteric signal transmission. *Journal of the American Chemical Society* **131**, 3063-8.

21. Farber, P. J. & Mittermaier, A. (2011). Concerted dynamics link allosteric sites in the PBX homeodomain. *Journal of Molecular Biology* **405**, 819-30.

22. Clegg, D. O. & Koshland, D. E., Jr. (1984). The role of a signaling protein in bacterial sensing: behavioral effects of increased gene expression. *Proc Natl Acad Sci U S A* **81**, 5056-60.

23. Matsumura, P., Rydel, J. J., Linzmeier, R. & Vacante, D. (1984). Overexpression and Sequence of the Escherichia-Coli Chey Gene and Biochemical Activities of the Chey Protein. *Journal of Bacteriology* **160**, 36-41.

24. Sanders, D. A., Gillece-Castro, B. L., Stock, A. M., Burlingame, A. L. & Koshland, D. E., Jr. (1989). Identification of the site of phosphorylation of the chemotaxis response regulator protein, CheY. *J Biol Chem* **264**, 21770-8.

25. Bourret, R. B. (2010). Receiver domain structure and function in response regulator proteins. *Current Opinion in Microbiology* **13**, 142-149.

26. Galperin, M. Y. (2010). Diversity of structure and function of response regulator output domains. *Current Opinion in Microbiology* **13**, 150-159.

27. Lee, S. Y., Cho, H. S., Pelton, J. G., Yan, D., Berry, E. A. & Wemmer, D. E. (2001). Crystal structure of activated CheY. Comparison with other activated receiver domains. *J Biol Chem* **276**, 16425-31.

28. Baker, M. D., Wolanin, P. M. & Stock, J. B. (2006). Signal transduction in bacterial chemotaxis. *Bioessays* **28**, 9-22.

29. Porter, S. L., Wadhams, G. H. & Armitage, J. P. (2011). Signal processing in complex chemotaxis pathways. *Nat Rev Microbiol* **9**, 153-65.

30. Sarkar, M. K., Paul, K. & Blair, D. (2010). Chemotaxis signaling protein CheY binds to the rotor protein FliN to control the direction of flagellar rotation in Escherichia coli. *Proc Natl Acad Sci U S A* **107**, 9370-5.

31. Dyer, C. M., Vartanian, A. S., Zhou, H. & Dahlquist, F. W. (2009). A molecular mechanism of bacterial flagellar motor switching. *J Mol Biol* **388**, 71-84.

32. Thomas, S. A., Brewster, J. A. & Bourret, R. B. (2008). Two variable active site residues modulate response regulator phosphoryl group stability. *Molecular Microbiology* **69**, 453-65.

33. Yan, D., Cho, H. S., Hastings, C. A., Igo, M. M., Lee, S. Y., Pelton, J. G., Stewart, V., Wemmer, D. E. & Kustu, S. (1999). Beryllofluoride mimics phosphorylation of NtrC and other bacterial response regulators. *Proceedings of the National Academy of Sciences of the United States of America* **96**, 14789-14794.

34. Lee, S. Y., Cho, H. S., Pelton, J. G., Yan, D., Henderson, R. K., King, D. S., Huang, L., Kustu, S., Berry, E. A. & Wemmer, D. E. (2001). Crystal structure of an activated response regulator bound to its target. *Nature Structural Biology* **8**, 52-6.

35. Cho, H. S., Lee, S. Y., Yan, D., Pan, X., Parkinson, J. S., Kustu, S., Wemmer, D. E. & Pelton, J. G. (2000). NMR structure of activated CheY. *J Mol Biol* **297**, 543-51.

36. Lukat, G. S., Stock, A. M. & Stock, J. B. (1990). Divalent metal ion binding to the CheY protein and its significance to phosphotransfer in bacterial chemotaxis. *Biochemistry* **29**, 5436-42.

37. Simonovic, M. & Volz, K. (2001). A distinct meta-active conformation in the 1.1-A resolution structure of wild-type ApoCheY. *Journal of Biological Chemistry* **276**, 28637-40.

38. Ma, L. & Cui, Q. (2007). Activation mechanism of a signaling protein at atomic resolution from advanced computations. *J Am Chem Soc* **129**, 10261-8.

39. Volkman, B. F., Lipson, D., Wemmer, D. E. & Kern, D. (2001). Two-state allosteric behavior in a single-domain signaling protein. *Science* **291**, 2429-2433.

40. Gardino, A. K., Villali, J., Kivenson, A., Lei, M., Liu, C. F., Steindel, P., Eisenmesser, E. Z., Labeikovsky, W., Wolf-Watz, M., Clarkson, M. W. & Kern, D. (2009). Transient Non-native Hydrogen Bonds Promote Activation of a Signaling Protein. *Cell* **139**, 1109-1118.

41. Barak, R. & Eisenbach, M. (1992). Correlation between phosphorylation of the chemotaxis protein CheY and its activity at the flagellar motor. *Biochemistry* **31**, 1821-6.

42. Volz, K. & Matsumura, P. (1991). Crystal structure of Escherichia coli CheY refined at 1.7-A resolution. *J Biol Chem* **266**, 15511-9.

43. Schuster, M., Silversmith, R. E. & Bourret, R. B. (2001). Conformational coupling in the chemotaxis response regulator CheY. *Proc Natl Acad Sci U S A* **98**, 6003-8.

44. Dyer, C. M. & Dahlquist, F. W. (2006). Switched or not?: the structure of unphosphorylated CheY bound to the N terminus of FliM. *J Bacteriol* **188**, 7354-63.

45. Guhaniyogi, J., Robinson, V. L. & Stock, A. M. (2006). Crystal structures of beryllium fluoride-free and beryllium fluoride-bound CheY in complex with the conserved C-terminal peptide of CheZ reveal dual binding modes specific to CheY conformation. *J Mol Biol* **359**, 624-45.

46. Lipari, G. & Szabo, A. (1982). Model-free approach to the interpretation of nuclear magnetic resonance relaxation in macromolecules.1. Theory and range of validity. *Journal of the American Chemical Society* **104**, 4546-4559.

47. Lipari, G. & Szabo, A. (1982). Model-free approach to the interpretation of nuclear magnetic resonance relaxation in macromolecules. 2. Analysis of experimental results. *Journal of the American Chemical Society* **104**, 4559-4570.

48. Palmer, A. G., Kroenke, C. D. & Loria, J. P. (2001). Nuclear magnetic resonance methods for quantifying microsecond-to-millisecond motions in biological macromolecules. *Nuclear Magnetic Resonance of Biological Macromolecules, Pt B* **339**, 204-238.

49. Okazaki, K. & Takada, S. (2008). Dynamic energy landscape view of coupled binding and protein conformational change: induced-fit versus population-shift mechanisms. *Proc Natl Acad Sci U S A* **105**, 11182-7.

50. Hammes, G. G., Chang, Y. C. & Oas, T. G. (2009). Conformational selection or induced fit: a flux description of reaction mechanism. *Proc Natl Acad Sci U S A* **106**, 13737-41.

51. Wlodarski, T. & Zagrovic, B. (2009). Conformational selection and induced fit mechanism underlie specificity in noncovalent interactions with ubiquitin. *Proc Natl Acad Sci U S A* **106**, 19346-51.

52. Zhou, H. X. (2010). From induced fit to conformational selection: a continuum of binding mechanism controlled by the timescale of conformational transitions. *Biophys J* **98**, L15-7.

53. Csermely, P., Palotai, R. & Nussinov, R. (2010). Induced fit, conformational selection and independent dynamic segments: an extended view of binding events. *Trends in Biochemical Sciences* **35**, 539-46.

54. Cui, Q. & Karplus, M. (2008). Allostery and cooperativity revisited. *Protein Sci* **17**, 1295-307.

55. Tsai, C. J., Del Sol, A. & Nussinov, R. (2009). Protein allostery, signal transmission and dynamics: a classification scheme of allosteric mechanisms. *Mol Biosyst* **5**, 207-16.

56. Gao, R., Mack, T. R. & Stock, A. M. (2007). Bacterial response regulators: versatile regulatory strategies from common domains. *Trends in Biochemical Sciences* **32**, 225-234.

57. Welch, M., Oosawa, K., Aizawa, S. & Eisenbach, M. (1993). Phosphorylation-dependent binding of a signal molecule to the flagellar switch of bacteria. *Proc Natl Acad Sci U S A* **90**, 8787-91.

58. Appleby, J. L. & Bourret, R. B. (1998). Proposed signal transduction role for conserved CheY residue Thr87, a member of the response regulator active-site quintet. *Journal of Bacteriology* **180**, 3563-9.

59. Feher, V. A. & Cavanagh, J. (1999). Millisecond-timescale motions contribute to the function of the bacterial response regulator protein Spo0F. *Nature* **400**, 289-93.

60. Silversmith, R. E., Smith, J. G., Guanga, G. P., Les, J. T. & Bourret, R. B. (2001). Alteration of a nonconserved active site residue in the chemotaxis response regulator CheY affects phosphorylation and interaction with CheZ. *J Biol Chem* **276**, 18478-84.

61. Moy, F. J., Lowry, D. F., Matsumura, P., Dahlquist, F. W., Krywko, J. E. & Domaille, P. J. (1994). Assignments, Secondary Structure, Global Fold, and Dynamics of Chemotaxis-Y Protein Using 3-Dimensional and 4-Dimensional Heteronuclear (C-13,N-15) Nmr-Spectroscopy. *Biochemistry* **33**, 10731-10742.

62. Delaglio, F., Grzesiek, S., Vuister, G. W., Zhu, G., Pfeifer, J. & Bax, A. (1995). NMRPipe: a multidimensional spectral processing system based on UNIX pipes. *J Biomol NMR* **6**, 277-93.

63. Johnson, B. A. (2004). Using NMRView to visualize and analyze the NMR spectra of macromolecules. *Methods Mol Biol* **278**, 313-52.

64. Loria, J. P., Rance, M. & Palmer, A. G. (1999). A relaxation-compensated Carr-Purcell-Meiboom-Gill sequence for characterizing chemical exchange by NMR spectroscopy. *Journal of the American Chemical Society* **121**, 2331-2332.

65. Mulder, F. A., Mittermaier, A., Hon, B., Dahlquist, F. W. & Kay, L. E. (2001). Studying excited states of proteins by NMR spectroscopy. *Nat Struct Biol* **8**, 932-5.

66. Skrynnikov, N. R., Dahlquist, F. W. & Kay, L. E. (2002). Reconstructing NMR spectra of "invisible" excited protein states using HSQC and HMQC experiments. *J Am Chem Soc* **124**, 12352-60.

67. Needham, J. V., Chen, T. Y. & Falke, J. J. (1993). Novel ion specificity of a carboxylate cluster Mg(II) binding site: strong charge selectivity and weak size selectivity. *Biochemistry* **32**, 3363-7.

68. Hubbard, J. A., MacLachlan, L. K., King, G. W., Jones, J. J. & Fosberry, A. P. (2003). Nuclear magnetic resonance spectroscopy reveals the functional state of the signalling protein CheY in vivo in Escherichia coli. *Mol Microbiol* **49**, 1191-200.

69. Bellsolell, L., Prieto, J., Serrano, L. & Coll, M. (1994). Magnesium binding to the bacterial chemotaxis protein CheY results in large conformational changes involving its functional surface. *J Mol Biol* **238**, 489-95.

70. Stock, A. M., Martinez-Hackert, E., Rasmussen, B. F., West, A. H., Stock, J. B., Ringe, D. & Petsko, G. A. (1993). Structure of the Mg(2+)-bound form of CheY and mechanism of phosphoryl transfer in bacterial chemotaxis. *Biochemistry* **32**, 13375-80.

71. Zhu, X. Y., Rebello, J., Matsumura, P. & Volz, K. (1997). Crystal structures of CheY mutants Y106W and T871/Y106W - CheY activation correlates with movement of residue 106. *Journal of Biological Chemistry* **272**, 5000-5006.

72. Alatossava, T., Jutte, H., Kuhn, A. & Kellenberger, E. (1985). Manipulation of intracellular magnesium content in polymyxin B nonapeptide-sensitized Escherichia coli by ionophore A23187. *Journal of Bacteriology* **162**, 413-9.

73. Ganguli, S., Wang, H., Matsumura, P. & Volz, K. (1995). Uncoupled Phosphorylation and Activation in Bacterial Chemotaxis - the 2.1-Angstrom Structure of a Threonine to Isoleucine Mutant at Position-87 of Chey. *Journal of Biological Chemistry* **270**, 17386-17393.

74. Smith, J. G., Latiolais, J. A., Guanga, G. P., Pennington, J. D., Silversmith, R. E. & Bourret, R. B. (2004). A search for amino acid substitutions that universally activate response regulators. *Molecular Microbiology* **51**, 887-901.

75. Birck, C., Mourey, L., Gouet, P., Fabry, B., Schumacher, J., Rousseau, P., Kahn, D. & Samama, J. P. (1999). Conformational changes induced by phosphorylation of the FixJ receiver domain. *Structure* **7**, 1505-15.

76. Neal, S., Nip, A. M., Zhang, H. Y. & Wishart, D. S. (2003). Rapid and accurate calculation of protein H-1, C-13 and N-15 chemical shifts. *J Biomol NMR* **26**, 215-240.

77. Bachhawat, P., Swapna, G. V. T., Montelione, G. T. & Stock, A. M. (2005). Mechanism of activation for transcription factor PhoB suggested by different modes of dimerization in the inactive and active states. *Structure* **13**, 1353-1363.

78. Sola, M., Gomis-Ruth, F. X., Serrano, L., Gonzalez, A. & Coll, M. (1999). Three-dimensional crystal structure of the transcription factor PhoB receiver domain. *J Mol Biol* **285**, 675-87.

79. Halkides, C. J., McEvoy, M. M., Casper, E., Matsumura, P., Volz, K. & Dahlquist, F. W. (2000). The 1.9 angstrom resolution crystal structure of phosphono-CheY, an analogue of the active form of the response regulator, CheY. *Biochemistry* **39**, 5280-5286.

80. Schuster, M., Zhao, R., Bourret, R. B. & Collins, E. J. (2000). Correlated switch binding and signaling in bacterial chemotaxis. *J Biol Chem* **275**, 19752-8.

81. Jiang, M., Bourret, R. B., Simon, M. I. & Volz, K. (1997). Uncoupled phosphorylation and activation in bacterial chemotaxis. The 2.3 A structure of an aspartate to lysine mutant at position 13 of CheY. *J Biol Chem* **272**, 11850-5.

82. Sola, M., Lopez-Hernandez, E., Cronet, P., Lacroix, E., Serrano, L., Coll, M. & Parraga, A. (2000). Towards understanding a molecular switch mechanism: thermodynamic and crystallographic studies of the signal transduction protein CheY. *J Mol Biol* **303**, 213-25.

83. McAdams, K., Casper, E. S., Matthew Haas, R., Santarsiero, B. D., Eggler, A. L., Mesecar, A. & Halkides, C. J. (2008). The structures of T87I phosphono-CheY and T87I/Y106W phosphono-CheY help to explain their binding affinities to the FliM and CheZ peptides. *Arch Biochem Biophys* **479**, 105-13.

84. Gouet, P., Chinardet, N., Welch, M., Guillet, V., Cabantous, S., Birck, C., Mourey, L. & Samama, J. P. (2001). Further insights into the mechanism of function of the response regulator CheY from crystallographic studies of the CheY--CheA(124--257) complex. *Acta Crystallogr D Biol Crystallogr* **57**, 44-51.

85. Kojetin, D. J., Thompson, R. J., Benson, L. M., Naylor, S., Waterman, J., Davies, K. G., Opperman, C. H., Stephenson, K., Hoch, J. A. & Cavanagh, J. (2005). Structural analysis of divalent metals binding to the Bacillus subtilis response regulator Spo0F: the possibility for in vitro metalloregulation in the initiation of sporulation. *Biometals* **18**, 449-66.

86. Manley, G. & Loria, J. P. (2012). NMR insights into protein allostery. *Arch Biochem Biophys* **519**, 223-31.

87. Henzler-Wildman, K. A., Lei, M., Thai, V., Kerns, S. J., Karplus, M. & Kern, D. (2007). A hierarchy of timescales in protein dynamics is linked to enzyme catalysis. *Nature* **450**, 913-U27.

88. Paul, K., Brunstetter, D., Titen, S. & Blair, D. F. (2011). A molecular mechanism of direction switching in the flagellar motor of Escherichia coli. *Proc Natl Acad Sci U S A* **108**, 17171-6.

89. McDonald, L. R., Boyer, J. A. & Lee, A. L. (2012). Segmental Motions, Not a Two-State Concerted Switch, Underlie Allostery in CheY. *Structure* **20**, 1363-1373.

90. Sheftic, S. R., Garcia, P. P., White, E., Robinson, V. L., Gage, D. J. & Alexandrescu, A. T. (2012). Nuclear magnetic resonance structure and dynamics of the response regulator Sma0114 from *Sinorhizobium meliloti*. *Biochemistry* **51**, 6932-41.

91. Uhrin, D., Uhrinova, S., Leadbeater, C., Nairn, J., Price, N. C. & Barlow, P. N. (2000). 3D HCCH(3)-TOCSY for resonance assignment of methyl-containing side chains in (13)C-labeled proteins. *J Magn Reson* **142**, 288-93.

92. Zwahlen, C., Gardner, K. H., Sarma, S. P., Horita, D. A., Byrd, R. A. & Kay, L. E. (1998). An NMR experiment for measuring methyl-methyl NOEs in C-13-labeled proteins with high resolution. *Journal of the American Chemical Society* **120**, 7617-7625.

93. Farrow, N. A., Muhandiram, R., Singer, A. U., Pascal, S. M., Kay, C. M., Gish, G., Shoelson, S. E., Pawson, T., Formankay, J. D. & Kay, L. E. (1994). Backbone Dynamics of a Free and a Phosphopeptide-Complexed Src Homology-2 Domain Studied by N-15 Nmr Relaxation. *Biochemistry* **33**, 5984-6003.

94. Muhandiram, D. R., Yamazaki, T., Sykes, B. D. & Kay, L. E. (1995). Measurement of H-2 T-1 and T-1p Relaxation-Times in Uniformly C-13-Labeled and Fractionally H-2-Labeled Proteins in Solution. *Journal of the American Chemical Society* **117**, 11536-11544.

95. Millet, O., Muhandiram, D. R., Skrynnikov, N. R. & Kay, L. E. (2002). Deuterium spin probes of side-chain dynamics in proteins. 1. Measurement of five relaxation rates per deuteron in (13)C-labeled and fractionally (2)H-enriched proteins in solution. *J Am Chem Soc* **124**, 6439-48.

96. d'Auvergne, E. J. & Gooley, P. R. (2003). The use of model selection in the model-free analysis of protein dynamics. *J Biomol NMR* **25**, 25-39.

97. Clarkson, M. W., Gilmore, S. A., Edgell, M. H. & Lee, A. L. (2006). Dynamic coupling and allosteric behavior in a nonallosteric protein. *Biochemistry* **45**, 7693-9.

98. Fuentes, E. J., Der, C. J. & Lee, A. L. (2004). Ligand-dependent dynamics and intramolecular signaling in a PDZ domain. *Journal of Molecular Biology* **335**, 1105-1115.

99. Igumenova, T. I., Frederick, K. K. & Wand, A. J. (2006). Characterization of the fast dynamics of protein amino acid side chains using NMR relaxation in solution. *Chem Rev* **106**, 1672-99.

100. Lee, A. L., Kinnear, S. A. & Wand, A. J. (2000). Redistribution and loss of side chain entropy upon formation of a calmodulin-peptide complex. *Nature Structural Biology* **7**, 72-77.

101. Loh, A. P., Pawley, N., Nicholson, L. K. & Oswald, R. E. (2001). An increase in side chain entropy facilitates effector binding: NMR characterization of the side chain methyl group dynamics is Cdc42Hs. *Biochemistry* **40**, 4590-4600.

102. Smith, J. G., Latiolais, J. A., Guanga, G. P., Citineni, S., Silversmith, R. E. & Bourret, R. B. (2003). Investigation of the role of electrostatic charge in activation of the Escherichia coli response regulator CheY. *Journal of Bacteriology* **185**, 6385-6391.

103. Schnell, J. R., Dyson, H. J. & Wright, P. E. (2004). Effect of cofactor binding and loop conformation on side chain methyl dynamics in dihydrofolate reductase. *Biochemistry* **43**, 374-83.

104. McDonald, L. R., Whitley, M. J., Boyer, J. A. & Lee, A. L. (2013). Colocalization of Fast and Slow Timescale Dynamics in the Allosteric Signaling Protein CheY. *J Mol Biol* **425**, 2372-81.

105. Bonchev, D. & Buck, G. A. (2007). From molecular to biological structure and back. *J Chem Inf Model* **47**, 909-17.

106. Vendruscolo, M., Dokholyan, N. V., Paci, E. & Karplus, M. (2002). Small-world view of the amino acids that play a key role in protein folding. *Phys Rev E Stat Nonlin Soft Matter Phys* **65**, 061910.

107. Atilgan, A. R., Akan, P. & Baysal, C. (2004). Small-world communication of residues and significance for protein dynamics. *Biophys J* **86**, 85-91.

108. Suel, G. M., Lockless, S. W., Wall, M. A. & Ranganathan, R. (2003). Evolutionarily conserved networks of residues mediate allosteric communication in proteins. *Nat Struct Biol* **10**, 59-69.

109. Lockless, S. W. & Ranganathan, R. (1999). Evolutionarily conserved pathways of energetic connectivity in protein families. *Science* **286**, 295-9.

110. Bai, Y., Milne, J. S., Mayne, L. & Englander, S. W. (1994). Protein stability parameters measured by hydrogen exchange. *Proteins* **20**, 4-14.

111. Mayo, S. L. & Baldwin, R. L. (1993). Guanidinium chloride induction of partial unfolding in amide proton exchange in RNase A. *Science* **262**, 873-6.

112. Qian, H., Mayo, S. L. & Morton, A. (1994). Protein hydrogen exchange in denaturant: quantitative analysis by a two-process model. *Biochemistry* **33**, 8167-71.

113. Bai, Y., Milne, J. S., Mayne, L. & Englander, S. W. (1993). Primary structure effects on peptide group hydrogen exchange. *Proteins* **17**, 75-86.

114. Hvidt, A. & Nielsen, S. O. (1966). Hydrogen exchange in proteins. *Adv Protein Chem* **21**, 287-386.

115. Boyer, J. A., Clay, C. J., Luce, K. S., Edgell, M. H. & Lee, A. L. (2010). Detection of native-state nonadditivity in double mutant cycles via hydrogen exchange. *J Am Chem Soc* **132**, 8010-9.

116. Horovitz, A. & Fersht, A. R. (1990). Strategy for analysing the co-operativity of intramolecular interactions in peptides and proteins. *J Mol Biol* **214**, 613-7.

117. Chen, J. & Stites, W. E. (2001). Energetics of side chain packing in staphylococcal nuclease assessed by systematic double mutant cycles. *Biochemistry* **40**, 14004-11.

118. Green, S. M. & Shortle, D. (1993). Patterns of Nonadditivity between Pairs of Stability Mutations in Staphylococcal Nuclease. *Biochemistry* **32**, 10131-10139.

119. Cammer, S. & Carter, C. W., Jr. (2010). Six Rossmannoid folds, including the Class I aminoacyl-tRNA synthetases, share a partial core with the anti-codon-binding domain of a Class II aminoacyl-tRNA synthetase. *Bioinformatics* **26**, 709-14.

120. Weinreb, V., Li, L. & Carter, C. W., Jr. (2012). A master switch couples Mg(2)(+)-assisted catalysis to domain motion in B. stearothermophilus tryptophanyl-tRNA Synthetase. *Structure* **20**, 128-38.

121. Neira, J. L., Itzhaki, L. S., Otzen, D. E., Davis, B. & Fersht, A. R. (1997). Hydrogen exchange in chymotrypsin inhibitor 2 probed by mutagenesis. *J Mol Biol* **270**, 99-110.